IN VIVO ROLES OF ENDOTHELIAL TRANSFORMING GROWTH FACTOR-β RECEPTORS IN VASCULAR DEVELOPMENT AND MALFORMATIONS

By

HA-LONG PHUOC NGUYEN

A DISSERTATION PRESENTED TO THE GRADUATE SCHOOL
OF THE UNIVERSITY OF FLORIDA IN PARTIAL FULFILLMENT
OF THE REQUIREMENTS FOR THE DEGREE OF
DOCTOR OF PHILOSOPHY

UNIVERSITY OF FLORIDA

2011

© 2011 Ha-Long Phuoc Nguyen

To my parents, Nguyen Phuoc Thanh and Nguyen Thi Kim-Truc

ACKNOWLEDGMENTS

I wish to acknowledge those that helped me throughout my graduate career. Firstly, I would like to thank my mentor Dr. Suk Paul Oh, for his encouragement and guidance over the course of my studies. I would also like to thank my committee members Drs. Jim Resnick, Peter Sayeski and Maria Grant for their time and comments during my studies. I am very thankful for Dr. Charles Wood for providing the NIH T32 training grant in Endocrine, Metabolic, and Pre-Natal Basis of Chronic Kidney Disease and Hypertension by which I was supported for two years. I would also like to acknowledge Dr. Helen Arthur at Newcastle University in Newcastle, UK, for providing the Endoglin-floxed mice.

I would like to express my gratitude to former and present Oh lab members. I would like to thank Dr. Young-Jae Lee for providing help in designing some cre primers and resolving various technical problems. I would like to acknowledge Naime Fleiss for her advice on immunohistochemistry and how she provided a friendly environment. I give thanks to Jairo Tabora for editing aid of writings, such as abstracts, and for his assistance in tissue preparation. I am indebted to Dr. Chastity Bradford for providing constructive criticism in writings and presentation preparation.

I am forever grateful to my parents, Nguyen Phuoc Thanh and Nguyen Thi Kim-Truc, for their support in all my endeavors and efforts to ensure I can focus on my career. I also appreciate my siblings (and nieces and nephews) and my friends for being my cheerleaders along the way and providing the laughter that always helped reduce stress.

TABLE OF CONTENTS

page

LIST OF TABLES

LIST OF FIGURES

LIST OF ABBREVIATIONS

ALK	Activin-Like Kinase Receptor
AVM	Arteriovenous malformation
cre	*cre* recombinase
cKO	Conditional knockout
EC	Endothelial Cell
ECM	Extracellular matrix
ENG	Endoglin
EPC	Endothelial Progenitor Cell
GI	Gastrointestinal
HHT	Hereditary Hemorrhagic Telangiectasia
iKO	Inducible Knockout
KO	Knockout
PECAM-1	Platelet Endothelial Cell Adhesion Molecule-1
RGD	Arginine-Glycine-Aspartic acid
SMA	Smooth muscle actin
SMC	Smooth Muscle Cell
TGF-β	Transforming Growth Factor-β
TGFBR2	Transforming Growth Factor-β Type II Receptor

Abstract of Dissertation Presented to the Graduate School
of the University of Florida in Partial Fulfillment of the
Requirements for the Degree of Doctor of Philosophy

IN VIVO ROLES OF ENDOTHELIAL TRANSFORMING GROWTH FACTOR-β RECEPTORS IN VASCULAR DEVELOPMENT AND MALFORMATIONS

By

Ha-Long Phuoc Nguyen

May 2011

Chair: Suk Paul Oh
Major: Medical Sciences – Physiology and Pharmacology

Haploinsufficiency of the TGF-β type I and type III receptors, Activin receptor-like kinase-1 (ALK1) and Endoglin (ENG), cause the autosomal dominantly-inherited vascular disorder Hereditary Hemorrhagic Telangiectasia (HHT), which is characterized by vascular lesions, such as telangiectases and visceral arteriovenous malformations (AVMs). Current treatment for HHT treat the symptoms, thus understanding the pathological mechanism is essential for creating more effective or preventative treatment. The central dogma of the HHT field is that *ALK1* and *ENG* work in concert to propagate TGF-β signals in a linear SMAD-dependent manner during angiogenesis and to maintain vascular integrity. Thus, AVMs form when either is disrupted; however, this relationship has not been clearly defined *in vivo*. Thus, two *Eng* conditional knockout (cKO) mouse models were generated and characterized using the same two cre-deleter lines (endothelial-specific L1cre and tamoxifen-inducible R26-Cre^{ER}, iKO) previously used against *Alk1*, in which mice consistently developed AVMs. Although, many of the same organs developed AVMs or displayed AV-shunting in *Eng* iKO and *Alk1* iKO models, phenotypes in *Eng* iKO mice varied widely in terms of development, severity

and location. The results indicate that there may be differing pathogenetic mechanisms underlying the two major types of HHT.

Additionally, there is still debate over what roles, if any, the TGF-β type II and TGF-β type I receptors (TGFBR2 and ALK5) play in endothelial cells (ECs). Contradictions in previous *in vivo* and *in vitro* data indicate that TGF-β superfamily members have spatial and temporal roles in ECs. Thus, *Alk5* and *Tgfbr2* were deleted specifically in ECs using a novel ALK1 cre-knockin deleter line ($Alk1^{GFPcre}$) at E9.5. $Alk1^{GFPcre};Alk5^{fl/fl}$ and $Alk1^{GFPcre};Tgfbr2^{fl/fl}$ mice were embryonic lethal by E13.5 and E14.5, respectively. Mice displayed specific cerebral hemorrhages at E11.5 as previously seen in knockout models of *αv* integrin, *αvβ8* and *Tgfb1/3*. Thus, it was suggested paracrine neuroepithelium-specific integrin-mediated activation of TGF-β signaling within ECs is essential for the midgestational establishment of the cerebrovasculature.Taken together, the data presented provide resourceful insight in the formation of vascular lesions *in vivo*. Our mouse models produced more consistent phenotypes than currently available mouse models and will be vital to future studies in HHT.

CHAPTER 1
BACKGROUND

The Vasculature and Endothelium

The Vasculature

There are three main types of blood vessels (the arteries, capillaries, and veins) that have distinct features, from their structure to specific factors expressed within each. Arteries and veins have three cellular layers: the innermost layer (intima) consists of a single layer of endothelial cells (ECs); the media consists of smooth muscle; and the tunica adventia is the outermost layer consisting primarily of fibroblasts. Arterial vascular walls are thicker and their tunica media have multiple layers of smooth muscle cells (SMCs), elastin, and extracellular matrix (ECM). This contributes to the high elasticity necessary for these vessels to withstand the high shear stress, pressure and pulsatile flow as a result of blood circulation. Veins have thinner smooth muscle layers and are not as flexible; consequently, veins have a low tolerance to high pressure and high blood flow [1]. Additionally, many veins have valves that prevent black flow of blood. Arteries and veins are connected via capillaries, with smaller arterioles and venules. Capillaries consist of a single layer of ECs occasionally surrounded by pericytes and ECM. This feature is essential for the exchange of oxygen, waste and nutrients between blood and tissues. Capillaries account for the majority of the circulation's surface area and possess the most phenotypic differences between vascular beds and highest adaptability to the local tissue [2, 3].

Formation and maintenance of the vasculature The vascular system is one of the first organs to form during embryogenesis. The vasculature is established and maintained mainly via two mechanisms: vasculogenesis and angiogenesis [4].

Vasculogenesis, the *de novo* establishment of the primary capillary plexus, is the initial process [5]. The process is initiated as Sonic and Indian hedgehog (SHH/IHH) proteins signal for endothelial progenitor cells (EPCs) within a population of mesodermal cells to differentiate into hemangioblasts, the common progenitor of endothelial cells and hempatopoietic stem cells (HSCs) [1, 6]. The hemangioblast becomes the angioblast, which pools into blood islands that fuse into the primary capillary plexus [7, 8]. Vasculogenesis is followed by angiogenesis, which is defined as the sprouting of new vessels from pre-existing ones, leading to branching and remodeling of vessels to form the basic vascular architecture of arteries, capillaries and veins [9]. It is not until the heart has developed and blood flow commences that a functional circulatory system is established.

Vasculogenesis mainly takes place during embryogenesis, however, studies with EPCs suggests that it may occur to a certain degree in adults [5, 10]. Angiogenesis continues after birth and over the lifetime of an organism to maintain the endothelium. It is tightly regulated during physiological conditions (wound healing, ovulation, and pregnancy) and aberrant angiogenesis is responsible for several pathological conditions (certain genetic vascular diseases, rheumatic arthritis, cancer, retinopathies) [9, 11, 12]. There are two phases of angiogenesis: the activation phase and resolution phase. The activation phase consists of the proliferation and migration of ECs. During this stage a group of ECs within the capillary bed, termed tip cells, begin to sprout. The tips cells then elongate and grow directionally by extending filipodia that sense attractive and repulsive cues within the microenvironment [13]. Lying behind the tip cells are proliferating and differentiating stalk cells. In the resolution phase, there is an arrest of

EC proliferation and migration, deposition of the extracellular matrix, recruitment of the smooth muscle cells, and the eventual stabilization of the nascent vessel. When the tip cells contact another tip cell or vessel, they fuse with and form a bridge at the cell-to-cell contact point. The vascular lumen is established by vacuole fusion in stalk cells or during tip cell fusion. The establishment of the lumen allows blood flow to begin, and consequently, leads to reduced pro-angiogenic factors and stabilization of the vessel, e.g. by recruitment of mural cells (pericytes and SMCs) [14].

More recently, it has been discovered that vascular growth can occur through other modes. Arteriogenesis is now recognized as a third phenomenon by which vessels can form that takes place in adult stages [15]. Mechanistically, it appears similar to angiogenesis in that it involves neovascularization from pre-existing vessels; however, it is more specifically the formation of a vessel from an arteriole to restore blood flow in response to an arterial occlusion. Another major distinction between the two is that angiogenesis is initiated by physiological circumstances, such as wound healing and hypoxia, while arteriogenesis results from a persistent state of inflammation and monocyte invasion. To a lesser degree in adult stages, bone marrow derived EPCs have been shown to either incorporate directly into the EC layer (thereby enlarging the vessel) or be recruited to active tip cells and participate in the angiogenic process [16].

Vascular anomalities Vascular anomalies in humans, which often appear congenitally, are localized pathological conditions that result from aberrant vasculogenesis or angiogenesis and phenotypically appear as focal increases of tortuous and enlarged vessels [17, 18]. Vascular anomalities often spontaneously appear, but several rare genetic diseases are associated with certain types [19]. These

are separated into two broad categories: vascular tumors and vascular malformations. The vascular tumors consist primarily of hemangiomas, which is an overgrowth of ECs typically seen as red lesions in small children. It is believed these arise as a result of hyperproliferation of progenitor cells, but the trigger for proliferation is unknown. Vascular malformations (VM) are further classified into the vessel type affected (e.g. venous, capillary, arteriovenous, and lymphatic), each possessing a particular characteristic and, in some cases, associated with a specific genetic mutation. As such, some insight in the mechanisms underlying pathological/physiological angiogenesis can be derived from the genetic diseases [20]. Some examples are familial venous malformations (mutations in TIE2), familial juvenile hemangioma (VEGFR2), and Hypotrichosis-lymphedema-telangiectasia/LM (SOX18). Interestingly, the inherited vascular malformations are typically autosomal dominantly-inherited, multifocal, systemic, begin small in size but enlarge over time, and manifestation severity vary among patients, even within the same family [17, 18]. The majority of the vascular malformations affects the EC layer of vessels (opposed to SMCs), and are associated with mutations in endothelial-specific factors.

The Endothelium

The endothelium is the innermost single layer of cells lining the circulatory and lymphatic systems [1, 21]. It is the intermediate barrier between blood and tissues and the location of many critical processes, such as the maintenance of blood homeostasis, vascular tone and delivery of necessary nutrients to the different organs [12]. The functionally adaptive endothelium is highly heterogenous and its vessel identity (e.g. artery vs. vein) is dependent upon expression of particular molecular surface markers. EC factors expressed by arteries include ephrinB2 (EPHB2), Jagged1, notch1, Delta-

like 4 (DII4), ALK1, endothelial PAS domain protein I (EPAS1), Hairy/enhancer-of-split related with YRPW motif protein (HEY)-1, HEY-2, neurophilin 1 (NRPI), and decidual protein induced by progesterone (DEPP). In veins, EphB4, NRP2, Chicken Ovalbumin Upstream-Promoter-Transcription Factor (COUP-TF)-II, and class III β-tubulin are expressed, although the last one is expressed only in the tip of venous valves. The lymphatics include vascular endothelial growth factor receptor (VEGFR)-3, lymphatic vessel endothelial hyaluronan receptor-1 (LYVE1), and Podoplanin [14, 22].

The determination of arterial/venous identity is seemingly pre-programmed as several endothelial factors are expressed even during vasculogenesis. At the hemangioblast stage, ECs expressing bone morphogenetic protein (BMP)4, VEGF120, and VEGF164 are influenced into becoming arteries, while VEGF160-expressing ECs to veins or lymphatic system. ECs destined for arterial specification express DII4 and the Notch1 receptor at the angioblast stage then HEY1 and HEY2 at the final stage, after the capillary plexus is established. Likewise, venous/lymphatic identity is determined by the expression of COUP-TFII. Furthermore, the lymphatic ECs, derived from jugular vein ECs, express of VEGF-C, Sox18 and Prox1 [6, 23].

The actions and function of the endothelium is the driving force of angiogenesis. There are two main states of ECs: active and quiescence [24]. The adult endothelium is largely quiescent, in which ECs appear to be anti-coagulant, anti-adhesive, and vasodilatory. When ECs are “active” they take on pro-coagulant/adhesive and vasoconstrictive roles [12]. Several signaling pathways are vital for maintaining this balance. EC dysfunction, the ECs inability to adapt to a pathophysiological stimulus, is the basis of many pathological diseases, either as the primary cause or secondary

response [12]. Among the most studied endothelial pathways are the vascular endothelial growth factor (VEGF) and angiopoietin/Tie signaling pathways [25-28]. Other pathways include the platelet-derived growth factor (PDGF), ephrin, and Notch pathways [22, 29, 30]. Not only are these involved in embryonic vascular development, they are also known to be involved in physiological and pathological angiogenesis after birth [12, 19]. Adding to the complexity of vascular signaling is the fact that expressions of certain molecules are restricted to certain tissues, cell types, or vessels and pathways may cross-talk. The Transforming Growth Factor (TGF-β) superfamily is of interest in this study.

Transforming Growth Factor-β (TGF-β) Signaling Pathway

The Transforming Growth Factor-beta (TGF-β) signaling pathway is involved in a wide range of physiological and pathological cellular processes, such as inflammation, proliferation, apoptosis, development, tumor progression, and cancer [31-34]. Cellular functions are dependent on the interaction between over 40 various highly conserved members of this superfamily, in mammals, including ligands, Type I and II Serine-Threonine (Ser-Thr) kinase receptors, and intracellular signaling transport molecules, mainly SMADs [35].

The classical mechanism of TGF-β signaling is deceptively simple. A ligand binds to dimeric Type II receptors, which in turn phosphorylate serine and threonine residues within corresponding dimeric Type I receptors. The activated Type I receptor then recruits intracellular receptor-activated (R-)SMADs to the membrane, where these form heteromeric complexes. The heteromeric SMAD complexes then interact with a common mediator SMAD4. The complex is now allowed to translocate to the nucleus where it can regulate gene transcription of various downstream targets [31-33, 36].

[Summarized in Figure 1-1, though showing those superfamily members pertaining to vascular cells]

TGF-β Ligands

Over 30 multifunctional TGF-β ligands have been identified in mammals. The ligands are categorized into five subfamilies that can be structurally distinguished by the number conserved cysteines within the C-terminus of the mature polypeptide [31]. The subfamilies are the 1) TGF-β; 2) bone morphogenetic proteins (BMPs); 3) growth and the differentiation factors (GDFs); 4) nodal, inhibins, and activins; and 5) anti-Müllerian hormone (AMH). Furthermore, the each subfamily of ligands may have multiple isoforms. There are three TGF-β isoforms (TGF-β1, -2, and -3); about nine BMPs (BMP2-7, 8A, 8B, 9, 10); eleven GDFs (GDF1, 3, 5-9, 9b, 10, 11); three nodals (Nodal, LEFTY1, LEFTY2); five activins and inhibins (inhibin α, inhibin-βA, -βB, -βC, -βE); and one AMH ligand [37].

Receptors for TGF-β Ligands

For the multitude of ligands, there have been only five TGF-β type II receptors and seven TGF-β type I receptors that have been identified, indicating redundancy and the promiscuity among the TGF-β superfamily members [38]. The type II receptors are: 1) TGF-β type II receptor (TGFBR2), 2) Activin type II receptor (ACVR2A), 3) BMP type II receptor (BMPR2), 4) Activin type II receptor (ACVR2B), and 5) AMH type II-receptor (AMHR2). The type I receptors are activin receptor-like kinases (ALK) 1 through 7) [31]. The type II and I receptors share high homology and have large intracellular domains, with the key feature of cytoplasmic kinase domains with strong Ser-Thr kinase activity. The TGF-β type II receptors are constitutively active and bind ligands with high affinity, but do not possess properties to further transduce signals [35].

Structurally, Type II and Type I receptors differ in that the Type I receptors lack a Ser-Thr-rich cytoplasmic tail. Additionally, TGF-β type I receptors include a 30-aa GS-domain that contains the Ser-Thr residues targeted by the type II receptor and a non-activating non-downregulating (NANDOR) box. An L45 loop sequence determines the types of downstream intracellular SMADs recruited to the Type I receptor [39].

TGF-β signaling can be divided into two major signaling pathways, based on the ligand and the L45 loop sequence in the Type I receptor, thus the SMADs involved [24, 40]. The TGF-β signaling cascade is activated by TGF-β1, -2, -3, nodal, inhibins-βA, -βB, and GDF-1,-3, -8 and -9 ligands and their subsequent interaction with any Type II receptor, excluding AMHRII, and the Type I receptors, ALK4, -5, and -7. Signals are propagated intracellularly via SMAD2/3 (Figure 1-1A). The BMP signaling pathway involves all other ligands and the Type I receptors in combination with any Type II receptor. The signal is further processed by SMAD1/5/8 (Figure 1-1B).

Signaling of the Type II-Type I receptor complexes can involve auxiliary type III receptors. There are two type III receptors, Endoglin/CD105 (ENG) and Betagylcan/TGFBR3 (β-glycan), which share highly similar sequences [41-43]. Structurally, the Type III receptors have large extracellular domains, but lack the kinase domain typical of the Type II and I receptors, thus Type III receptors can aid in enhancing or inhibiting TGF-β signaling, but cannot signal on their own. The receptors differ in that β-glycan is ubiquitously expressed and reportedly more involved in the TGF-β signaling pathway [41] (Figure 1-1A). Meanwhile, ENG is predominantly found in ECs and involved in both the TGF-β and BMP signaling cascades [44] (Figure 1-1A and B).

Intracellular Pathways

SMAD-dependent The dominant manner that TGF-β signals are propagated to the nucleus is via SMAD proteins. SMADs were initially discovered and studied in *C. elegans* and the *Drosophila* (*SMA* from *C. elegans* + *MAD* [Mother against Decapentaplegic] proteins from *Drosphila*) and are highly evolutionarily conserved. Eight SMAD subtypes are categorized into three classes: 1) receptor-activated, 2) co-mediator, and 3) inhibitory SMAD [45, 46]. There are five receptor-activated (R-) SMADs: SMADs -1, -2, -3, -5, and -8. When activated the R-SMADs are recruited to an activated type I receptor, specific R-SMADs group to form homo/heteromeric complexes, which form in any combination between SMAD2/3 or SMAD1/5/8 (Figure 1-1A and B). Co-mediator SMAD4 will then combines with the R-SMAD complex and aid in translocating the TGF-β signal into the nucleus. Once in the nucleus, the heterocomplex can control various transcriptional targets by interacting with specific-response elements, such as SMAD binding elements (SBEs) located within the targets' transcription regulatory regions [36, 46, 47] (Figure 1-1C).

SMAD signaling can be inhibited at various points in the signaling cascade [33, 48]. The Inhibitory (I-) SMADs [-6 or -7] may also prevent TGF-β intracellular propagation by competing with the R-SMADs for the binding site within the TGF-β type I receptor. I-SMADs quench the signal propagation by calling for the degradation of the type I receptor by recruiting ubiquitin ligases or inviting inactivating phosphatases (Figure 1-1D). A signal may also be inhibited if the R-SMADs are directly degraded by SMURF1 and SMURF2 within the cytoplasm [48].

SMAD-independent pathway TGF-β signaling can "cross-talk" with other signaling pathways, most notably components of the Mitogen Activated Protein Kinase

(MAPK), Rho-like GTP-ase, and phosphatidylinositol-3-kinase (PI3K)/Akt pathways. The cross-talk can be initiated at the membrane, with the Type II receptor, or intracellularly with the SMADs [49] (Figure 1-1E).

TGF-β Signaling Pathway in the Endothelium

Several TGF-β members are expressed within the vasculature, some specifically in the endothelium. These are the TGF-β1,–β3, BMP9 and BMP10 ligands, Type II receptors TGFBR2 and BMPR2, Type I receptors ALK1 and ALK5, and all SMADs [40, 50]. These were considered major players in the vasculature because there are several human cardiovascular diseases linked to certain genetic mutations and further confirmed in various *in vivo* models. Such examples are Marfan Syndrome (TGFBR2 mutations) and Loeys-Dietz Syndrome (ALK5 and TGFBR2) [51, 52]. Other members may be essential within the vasculature based on *in vitro* and *in vivo* studies, despite not being associated with human diseases. It was found that mice null for the TGF-β1 ligand, *Tgfbr2*, *Alk5*, *Eng* and *Smad5* were commonly embryonic lethal at midgestation (from E9.5-11.5) due to defective yolk sac vasculogenesis [53-59]. *Alk1* was also embryonic lethal at E10.5, but due to defective angiogenesis. Additionally, *Eng* knockout (KO) and *Alk5* KO mice presented cardiac defects and *Tgfb1 KOs* were affected with inflammation and autoimmunity.

There is debate over what roles the differing TGF-β signaling members play in the vasculature, and many *in vivo* and *in vitro* studies are contradictory. Both ALK1 and ALK5 are thought to be both expressed in EC. It is reported from *in vitro* studies that both propagated the TGF-β class of ligands via TGFBR2, but ALK5 signals via SMAD2/3 and ALK1 via SMAD1/5/8. Goumans et al. suggested that ALK5 kinase is essential for ALK1 activation and these may balance the other's function within ECs

[60]. The authors found that ECs deficient in ALK5 were defective in both TGF-β/ALK5 and TGF-β/ALK1 responses. Although, it is found that ALK5 and ALK1 induce opposing angiongenic responses. TGF-β/ALK1 seems to promote EC migration and proliferation (activation phase), while TGF-β/ALK5 promotes extracellular matrix deposition (ECM) and inhibits EC migration and proliferation [61]. However, another group performed a study in which ALK1 was constituitively activated in ECs. They found that ALK1 appeared in be involved in the resolution phase of angiogenesis [62].

Additionally, there is not a clear consensus as to which cell types the Type I receptors are expressed. It is accepted that ALK1 is expressed on ECs. Immunohistochemical expression experiments of human colon demonstrated that both ALK1 and ALK5 are expressed in ECs [60], but murine expression studies indicate that ALK5 is expressed only in SMCs, not ECs [63]. The murine finding was further supported in an *Alk5* cKO mouse model in which *Alk5* was specifically deleted in ECs using an *Alk1*-cre deleter line (L1cre). The *L1cre(+);Alk5*$^{fl/fl}$ mice were completely unaffected, while *Alk1* cKO mice using the same cre-deleter line consistently developed vascular malformations and died shortly after birth [64]. There has been debated over which pathway ALK1 may activate, having originally implicated in the TGF-β pathway based largely on *in vitro* data assuming the physiological ligand for ALK1 was TGF-β1. However, there is growing evidence that ALK1 is more of a BMP signaling member and that its natural ligands are BMP9 and BMP10 [65, 66].

Of the two signaling cascade, the BMP signaling pathway seemingly plays a larger role in the endothelium [24, 50]. The cross-talk with other signaling pathways, such as the Notch, Shh, and WNT, is essential for the regulation and function of this pathway. Of

the ligands, BMP2 and BMP4 are mediators of endothelial differentiation and function. Two other endothelial-specific ligands, BMP10 and BMP9, promote a quiescent endothelium [66, 67]. Targets of the quiescent factors include inhibitor of differentiation (ID)-1, ID2, interleukin-8, and ENG. Certain BMP-antagonists (including noggin, chordin, and BMPER) play critical roles in regulating the expression of the various BMP ligands, typically in a dose-dependent manner. For example, low concentrations of BMPER activate BMPs, while high concentrations have the opposite effect. Gremlin is another BMP antagonist that is induced in hypoxic conditions and works by preventing the BMP ligand from binding to the receptor [50].

The importance of TGF-β signaling within the endothelium is exemplified in the genetic vascular dysplasia Hereditary Hemorrhagic Telangiectasia because mutations in *Alk1*, *Eng* and *Smad4* cause the disease.

Hereditary Hemorrhagic Telangiectasia (HHT)

Hereditary Hemorrhagic Telangiectasia (HHT), or Rendu-Osler-Weber Syndrome, is an autosomal dominantly-inherited vascular disorder. Though still considered rare, it is one of the more common inherited diseases, affecting 1:5,000 to 10,000 people worldwide, with no clear preference to gender, geography or race [68, 69]. Clinical diagnosis of HHT is based on the following Curaçao Criteria: 1) an affected immediate family member, 2) epistaxis, 3) mucocutaneous telangiectasia, and 4) arteriovenous malformations (AVMs) within certain major organs [70]. A patient is a given a suspected diagnosis if there are only two of the four Criteria, but a confirmed diagnosis if he/she have at least three. The vascular malformations can leave the vessels quite fragile and prone to rupturing and hemorrhaging. HHT is a largely unpredictable disease in that the severity and location of symptoms varies amongst patients, even family members, and

symptoms often appear spontaneously. Interestingly, only predilection sites of vascular beds are frequently affected in a highly variable pattern. Age of onset of symptoms also varies, although there seems to be a degree of age-dependent prevalence, appearing more frequently in the older population, typically older than 40 years of age [71]. HHT is often diagnosed late or overlooked as the symptoms are very broad and many non-specialized physicians may not properly identify an HHT patient [68]. The level of concern caused by hemorrhaging depends upon bleeding severity, tissue location and environment. Acute hemorrhaging is of concern if it affects hemodynamics, occurs in a closed space (i.e. cerebral/spinal system), or compromises organ function (e.g. oxygen exchange in the lungs). Chronic hemorrhaging can lead to anemia; a small population of HHT patients (6-7%) may experience thromboemboli [72].

Genetics of HHT

HHT is caused by mutations that result in the haploinsufficiency of five genes, each of which correspond to a type of the disease (HHT1-4, JP-HHT); however, only three of the genes have been definitively identified. HHT type I (HHTI) is associated with mutations in ENG and HHT type II (HHT2) is due to ALK1 [73, 74]. HHT1 and HHT2 account for >80% of cases. SMAD4 is linked to a phenotypically combined syndrome of HHT and another autosomal dominantly-inherited disease called Juvenile Polyposis (JP-HHT) [75]. The JP-HHT patients (which comprise of only 1-2% of cases) experience the formation of polyps within the gastrointestinal (GI) tract and colon during childhood, hallmarks of JP, in addition to HHT phenotype. It is reported that a quarter of JP-HHT were results of *de novo* mutations [76]. HHT3 and HHT4 are reportedly due to mutations in regions within chromosomes 5 and 7p14, respectively, however, the specific genes are still unknown [77, 78]. A suggested candidate gene for HHT4 is

BMPER [78]. Based on recent fine mapping sequencing, genes that have been *excluded* for HHT3 are the angiogenic proteins vascular endothelial (VE)-cadherin, Sprouty4, and fibroblast growth factor (FGF)-1 [79]. The paucity of information of HHT3 and HHT4 indicate symptoms are milder compared to the other types of HHT [77, 79].

In general, it is largely believed that patients are heterozygous for the genetic mutations as there has not been a confirmed case of a homozygous mutated patient [71]. Also, conventional animal knockout models for each HHT gene are embryonic lethal, supporting the notion that patients may be heterozygous for the dysfunctional gene. Additionally, it has been accepted that the vascular malformations develop as a result of haploinsufficiency of the functioning gene [80, 81].

Clinical Aspects

The most common symptom (afflicting >90% of patients) is recurrent, spontaneous epistaxis, lasting from a few minutes up to hours. Though seldom life-threatening, it often leads to a reduced quality of life and is the most frequent reason a patient would seek treatment and possibly a diagnosis [82]. Many patients typically experience the first nosebleed by age 10 then their condition may worsen by which they may experience nosebleeds daily and multiple times a day [72].

In general, the bleeding seen in HHT patients is presumably a consequence of abnormalities in the vascular bed, with endothelial dysfunction being the most likely culprit. The nosebleeds are believed to result from the formation and subsequent rupturing of telangiectases within the nasal passage. Telangiectases, the second most common symptom (at 80% of cases), are focal lesions in which the postcapillary venules have dilated [83]. Consequently, the vessel wall is compromised and highly susceptible to rupturing. Telangiectases can appear as red spots if they are near the

surface of the skin. These are often visible within the tongue, oral cavity, lips, and surface of the skin (seen in ~75% cases), though they have also been found in visceral organs, like the liver and brains, and have been shown to cause arteriovenous (AV) shunting, a process when arterial blood flows directly in the veins. While telangeictases inside the nose or GI tract frequently bleed, they are seldom dangerous if these are superficially located on the skin or oral cavity [84]. However, facial lesions can be stigmatizing.

When telangiectases have progressed in size enough, the arteries will connect directly into the veins, an abnormality known as an arteriovenous malformation (AVM) [83, 85]. AVMs are the most problematic of the HHT symptoms especially if formed in major visceral organs, such as the lungs, liver, and brain. AVMs are treatable when found; however, in some cases the patient may be unaware of its existence. These visceral AVMs are akin to “time-bombs” in that these may be asymptomatic, even for years, then suddenly cause catastrophic complications. AVMs within the pulmonary and cerebral vasculature can cause severe neurological problems and are the leading cause of death if they are not detected and treated in a timely manner. When patients are screened for AVMs, it is for these two types of AVMs [86].

Interestingly, 80-90% of all reported pulmonary AVMs (PAVMs) are associated with HHT, although only 15-50% of HHT patients develop PAVMs. Most PAVMs develop later in life and more HHT1 patients over HHT2. Lung afflictions that may directly result from PAVMs include hypoxaemia, cyanosis, poor exercise tolerance/decompression illness and dyspnoea [87]. Secondary effects to the cerebral system include migraines, “transient ischemic attacks,” stroke, seizures and cerebral

abscesses due to paradoxic embolism [87]. In fact, 30-40% of patients with a PAVM develop strokes, seizures and cerebral abscesses. The size and number of the PAVMs plays a big factor in the severity of secondary symptoms. Rupturing of a PAVM and death from it can happen though rare, with only ~10% of patients experiencing hemothorax or hemoptysis [87].

Another commonly affected organ system is the GI tract, with 25-33% of HHT patients found with vascular malformations in areas such as the stomach, duodenum, jejunum and colon. Telangiectases are more often seen and bleeding can lead to severe, transfusion-dependent anemia and having patients undergo more frequent blood transfusions occur, particularly in patients older than 60-years-old [87]. Patients with SMAD4 mutations should additionally be screened for gastric polyps as these may progressively become malignant [76].

It is believed that 32.5-74% patients experience the hepatic manifestations [88]. Fortunately, most liver vascular malformations are not life-threatening and HHT patients typically remain asymptomatic because the heart can compensate for minor shunting. On the other hand, in very rare cases complications from the severe liver AVMs can be among the most dangerous and difficult to treat [89]. There are 3 categories of HHT liver disease: Garcia types 1-3. Garcia type 1 leads to heart failure (most common but treatable) and post capillary pulmonary hypertension; Garcia type 2 to portal hypertension (the most consistently difficult to manage); and Garcia type 3 to varietal biliary disease (with variable outcomes) [71]. Liver complications appear to affect more women than men, and those over the age of 40 experience heightened risk. Additionally, vascular lesions may also form in the bladder/ureter, conjunctiva,

pancreas, bowel or spleen, however, hemorrhaging at these sites are seldom of relevance [72].

Occurring in about 10-20% of HHT patients, one of the most critical types of AVM for HHT patients are the cerebral AVMs (CAVMs) because treatments are not standardized and can be high risk [72, 87]. HHT-related CAVMs can be classified into three types: micro AVMs (<1cm), small nidus AVMs (1-3 cm) and fistulous AV shunts, each with a prevalence of 40%, 30%, and 30%, respectively. Most CAVMs are superficial, rarely penetrating the white tissue matter. Symptoms from CAVMs are similar to the neurological affects of PAVMs mentioned previously. Interestingly, only 28% cases of the neurological complications are due directly from cerebral hemorrhaging from the CAVMs; instead 61% are indirectly from PAVM emboli [87]. Additionally, CAVMs can cause epilepsy and there are cases that CAVMs in children could lead to high output cardiac failure. Spinal AVMs are even rarer (>1%) and hemorrhaging from these can cause patients to be become paraplegics [72].

Women with HHT are typically capable of becoming pregnant and carrying the child to term if extra precautions are taken [71, 72, 84, 87]. PAVMs pose the biggest treat as these have a tendency to rapidly grow in size and consequently result in hemothorax or hemoptysis. Precutaneous embolotherapy is sometimes performed during the second trimester as a preventative measure. Additionally, antibiotics can be given before delivery to help prevent infections. If spinal AVMs are present, epidurals are largely avoided during delivery. Cases of major PAVMs hemorrhaging (1.3%) and major stroke (1%) is very rare. The chances of a miscarriage are increased if the mother is hypoxic.

A subset of HHT patients, predominantly HHT2, may also develop another rare but potentially fatal vascular disease called pulmonary arterial hypertension (PAH) [90]. PAH may result from maladaptive pulmonary vascular remodeling, including exaggerated proliferation and dysfunction of both ECs and vascular smooth muscle cells (vSMCs). This can lead to hypertrophied SMC layers in the pulmonary vascular system and cause increased vascular resistance. The consequent increase in pulmonary blood pressure leads to the PAH-characteristic mean pulmonary arterial pressure >25 mmHg at rest or >30mmHg during exercise [91]. There are multiple categories of PAH. Familial PAH (fPAH) occurs when the cause is genetic. Confirmed genetic cause of PAH are attributed to the TGF-β Type II receptor *BMPR2*. Secondary PAH arises in response to another disorder (e.g. scleroderma), and idiopathic (IPAH) PAH is when the cause is not known [91]. Symptoms of PAH which overlap with HHT include exercise intolerance, fatigue, dyspnea, and weakness [92].

Current Treatments

Current treatments for HHT alleviate the inconvenience of symptoms [86]. Recently, more focus has been on antiangiogenic targets. Clinical trials for drugs treating HHT patients include using anti-angiogenic agents such as beviacizumab (a neutralizing antibody against all VEGF-A isoforms), thalidomide and interferon α-2b in attempts to stop bleeds or the formation of AVMs [93-95]. In terms of treating epistaxis, it is believed that nasal humidification by topical ointments and sprays should be initially attempted [86]. Pharmacological treatments for epistaxis include the drugs mentioned above, antifibrinolytics (e.g. epsilon-aminocaproic acid and tranesamic acid), female sex hormones (e.g. estrogen) applied either systemically or topically or partial hormone antagonist distributed orally, such as tamoxifen or raloxifen [96, 97]. Surgical options

encompass coagulation of the endonasal telangiectases with electrical or laser cautery, the replacement of fragile respiratory nasal mucosa with skin grafts from the thigh or pedicled oral mucosa grafts as modifications of a septodermoplasty (first described by Sanders), and, in extreme cases, the nose may be surgically closed (via a modified Young's procedure) [98-100].

Preliminary attempts of gene therapy for HHT patients show promise. For one, a plasmid construct was created in which the endothelial specific gene *ICAM-2* and *Eng* were inserted upstream of human *Eng* cDNA. After injecting the expression vectors systemically or locally it was found that there was indeed ENG expression in the vessels of the lung, liver and skin [101]. Another method showing promise as therapy is the use of isolating blood outgrowth endothelial cells (BOECs) from the circulation, expanding them in culture then re-incorporating the cells *in vivo*. The initial reports of this were done in 2005 in which BOECs from HHT1 and HHT2 patients were collected and characterized. The matured ECs expressed the expected EC markers (e.g. PECAM-1-1, ENG, FLK1, ALK1, von Willebrand Factor), but there was a drastic decrease of ENG in both HHT1 and HHT2 derived cultures [102].

Significance

HHT is a systemic complex and unpredictable disease. For one, the vascular malformations seen in HHT appear as focal lesions, thus not all vascular beds are affected. Braverman et al. first describe the growth of a telangiectasia into an AVM in 1990. They described how the telangeictasia begins as a dilatation of the postcapillary venule. The SMC layer of the venule thickens and its diameter enlarges. Though there are still intervening capillaries conneting the growing venule to arterioles, eventually the arterioles begin to grow as well and the capillaries eventually disappear [83]. Because

the three known genes responsible for HHT are part of the TGF-β signaling family, and interestingly those expressed specifically on ECs, defective TGF-β signaling in which the EC is primarily affected appears to be a cause of the HHT lesions. Hence, examining TGF-β signaling in ECs to understand the underlying pathogenic mechanism is important for effective treatment. There are currently no treatments that genetically target the HHT genes, as the mechanisms of these are still not clearly understood.

To determine the *in vivo* role of *Eng* in physiological and pathologic angiogenesis and how the loss of *Eng* can lead to formation of vascular malformations, two *Eng* cKO (an endothelial-specific and a global KO) were generated and the phenotypes compared to *Alk1* cKO phenotypes (using the same cre deleter line). Then to clarify why EC-specific deletion of ALK5 and TGFBR2 did not result in vascular malformations, in our previous models [64], EC-specific *Alk5* and *Tgfbr2* ablation models were characterized using a novel cre-knockin line to determine whether TGF-β signaling superfamily members have spatiotemporal roles in ECs.

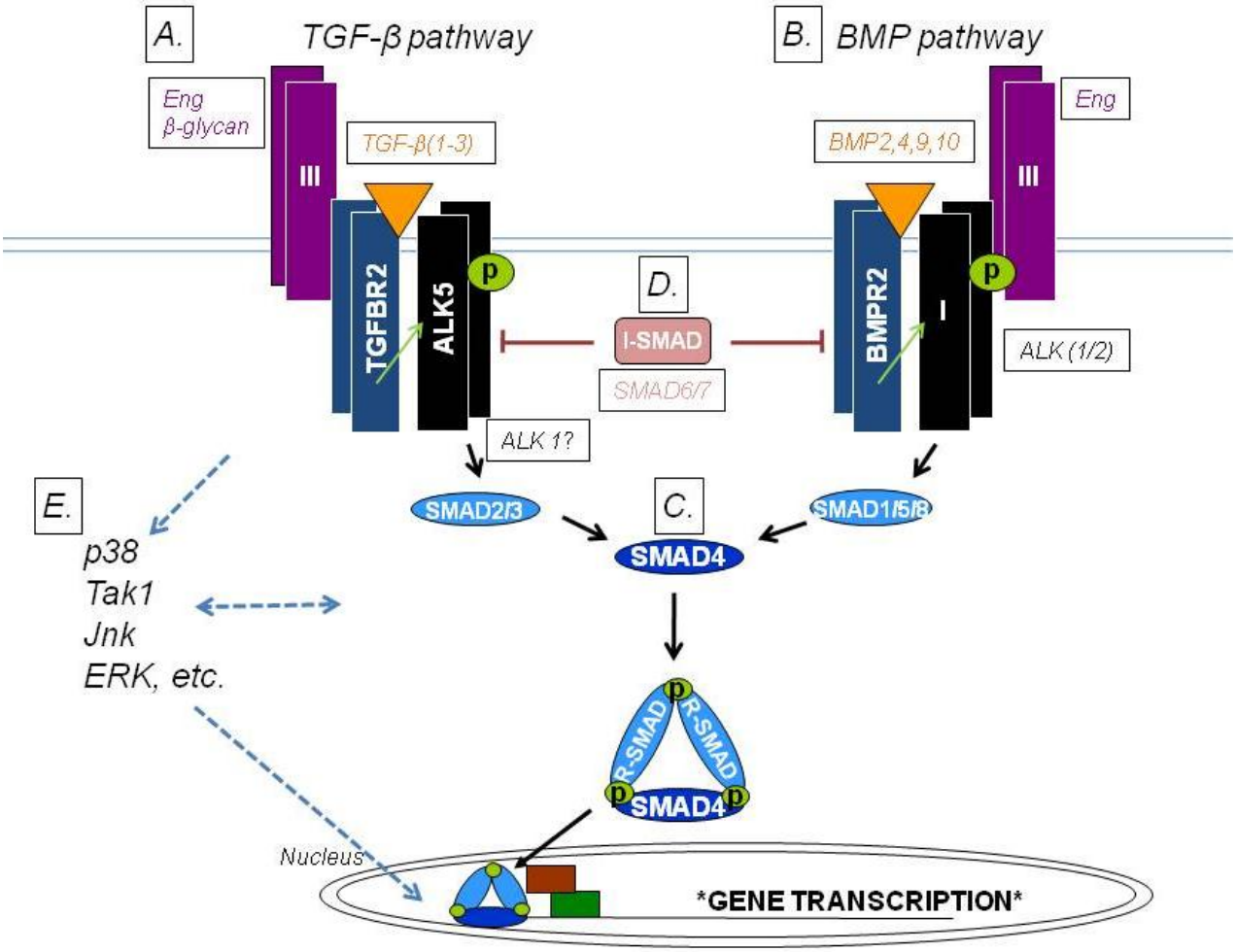

Figure 1-1. The two main TGF-β signaling pathways in vascular cells are the TGF-β and BMP pathways. A) In the TGF-β pathway, the TGF-β(1,-2,-3) ligands bind to TGFBR2, which phosphorylates a TGF-β type I receptor, predominantly ALK5. There is still debate whether ALK1 interacts or is involved in this pathway. Either the type III receptors β-glycan or ENG may aid in ligand binding. The TGF-β signal is propagated to the nucleus via R-SMADs 2/3. B) In the BMP signaling pathway, a BMP ligand (BMP2,-4,-9,-10) binds to the type II receptor BMPR2, which recruits and activates ALK1 or ALK2. ENG is the only type III receptor that is involved in this pathway. The signal is transduced intracellularly through SMAD1/5/8. C) The pathways converge as the pathway-corresponding R-SMADs complex with the co-mediator SMAD4. The heterocomplex translocates into the nucleus and regulate transcription of downstream targets. D) Signal transduction can be interfered by I-SMAD6 or -7, which can compete with R-SMADs to bind the activated type I receptor or recruit ligases that degrade the type I receptor or signal. E) Additionally, either pathway can cross-talk with other signaling pathways throughout the intracellular cascade, most notably TAK, JNK, and notch signaling. These can interact directly with the activated type I receptor, with the SMADs, or intercept and transduce the signal to the nucleus.

CHAPTER 2
METHODS AND MATERIALS

Transgenic Murine Models

Mouse Breeding

All procedures performed on animals were reviewed and approved by the University of Florida Institutional Animal Care and Use Committee. The generation of transgenic mouse lines: L1cre, bi-floxed Endoglin (*Eng*$^{2f/2f}$), floxed *Tgfbr2* (*Tgfbr2*$^{fl/fl}$), and floxed *Alk5* (*Alk5*$^{fl/fl}$) were previously described [55, 64, 103, 104]. R26-Cre^{ER} was purchased from Jackson Laboratories. To generate *L1cre(+);Eng*$^{2f/2f}$ mice, *Eng*$^{+/2f}$ mice were mated to *L1cre(+)* mice, resulting in litters heterozygous for the floxed *Eng* allele. *L1cre(+);Eng*$^{+/2f}$ were crossed with *Eng*$^{+/2f}$ mice. Eventually *Eng*$^{2f/2f}$ were selected to mate with *L1cre(+);Eng*$^{+/2f}$ to maintain colonies. Mice were on a mixed breed background of C57BL6 and 129Sv.

To generate R26-Cre$^{ER(+)}$*;Eng* mice, R26-Cre$^{ER(+)}$*;Eng*$^{2f/2f}$ mice were mated with *Eng*$^{2f/2f}$ mice to generated offspring that were either R26-Cre$^{ER(+)}$*;Eng*$^{2f/2f}$ or *Eng*$^{2f/2f}$. R26-Cre^{ER} activity was induced by an intraperitoneal (IP injection) of tamoxifen (TM), dissolved in corn oil, in adult mice (older than 2-months of age). Concentrations and number of injections used were at 2.5mg TM/25 g mouse body weight either once, twice or thrice, or at 2.5mg TM/40 g body weight either two or three times.

Timed Matings

Tgfbr2$^{fl/fl}$ and *Alk5*$^{fl/fl}$ mice were mated with respective *Alk1*^{GFPcre}*;Tgfbr2*$^{+/fl}$ and *Alk1*^{GFPcre}*;Alk5*$^{+/fl}$ mice, then the female was checked for a copulation plugs the next morning. The presence of a plug was designated embryonic day (E)0.5. At the embryonic day of desire the pregnant female was euthanized by exposure to 100%

isoflurane (Sun Surgical) followed by cervical dislocation. The embryos were removed and collected into cold 1X phosphate buffered saline (PBS). For E10.5-13.5 embryos, the heads were detached from the body then the embryos and corresponding placentas were collected. For E15.5 and older embryos, whole organs were removed and collected. Embryonic tissues were fixed in 4% Paraformaldehyde (PFA) in 1X PBS (pH 7.0) for 2-12 hrs at 4°C, with shaking.

Polymerase Chain Reaction (PCR) Analysis

Two-mm tail biopsies were collected from mice at three weeks of age or older; for embryos, the yolk sac was collected. Tissues were digested in Lysis buffer [50 mM Tris (pH 8.0), 0.5% Triton-X] with 1 mg/ml proteinase K (EMD Biosciences) for 8-16 hr at 55°C. The tissues were centrifuged for 10 min at 12000 rpm, 2 µl of the supernatant was added to the following PCR reaction: 5X PCR Buffer (Promega), 25 mM $MgCl_2$ (Promega), 25 pM dNTP, 0.5 µl of 25 pmol primers (Integrated DNA Technologies), volume to 25 µl with sterile ddH_2O. To avoid evaporation, a layer of mineral oil (Sigma) was added. A “Hot Start” was done in which the reaction was heated to 95°C for 10 min, then to 72°C during which *Taq* polymerase (Promega) was added. The reaction was allowed to undergo 36 cycles of: 95°C for 45 sec, 60°C for 45 sec, and 72°C for 1 min; followed by an additional 72°C elongation for 10 min. The products were run in a 2% agarose (Lorenza) and visualized by a ultraviolet (UV) transilluminator. See Table 2-1 for the list of PCR primers used.

X-Gal Staining

1-2-mm fragments of various organs were collected into 1X PBS. Tissues were incubated in X-gal fixative solution [1% formaldehyde, 0.2% glutaraldehyde, 2 mM $MgCl_2$, 5 mM EGTA, 0.02% NP-40) for 15 min at room temperature (RT), with rocking.

Tissues were rinsed twice with ddH_2O for 5 min each, with rocking. After washing the tissues were incubated in X-gal staining solution [5 mM $K_3Ke(CN)_6$, 5 mM $K_4Ke(CN)_6$, 2 mM $MgCl_2$, 0.01% Sodium Deoxycholate, 0.5 mg/ml X-gal], X-gal (Fisher Scientific)] for 6-16 hrs at 37°C in the dark, with rocking. The stained specimens were then washed in 1X PBS at RT then analyzed using a light microscope. Afterwards, these were prepped for histology.

Histology and Immunohistochemistry

Tissue Preparation

Embryos or 1-5 mm biopsies from various organs from adult mice (1.5 months or older) were collected into cold 1X PBS. The left lobe of adult mice was inflated for better resolution of the vessels. First, the lungs were flushed with 1 ml 10U/ml heparin (1:10 in 1X PBS,100U/ml; Abbott Laboratories) by injection into the right ventricle of the heart with a 26-G needle (BD Precision). The whole heart and lungs were collected into 1X PBS, then lung left lobe and the connected portion of the primary bronchi to the trachea branching point were excised. A blunted 25-mm gauge (G) butterfly needle was inserted into the bronchi and tightly tied with a suture. The lung was inflated with 1X PBS for 7 min following by 4% paraformaldehyde (PFA) for an additional 7 min, both via gravity flow, in which the fluid level was 20-cm higher than the lung. The inflated lung was pulled off the needle, immediately and completely ligated at the bronchi, then fixed with 4% PFA.

For paraffin-embedding of tissue**,** adult organs, the whole or at least 2 to 5-mm biopsies were collected into 1X PBS and fixed in 10% buffered Formalin (Fisher Scientific) or 4% PFA overnight (O/N) at RT, with shaking. For embryos, whole embryos were collected in cold 1X PBS, decapitated and fixed in 4% PFA O/N at 4°, with

shaking. All fixed tissues were then washed in 1X PBS then dehydrated in a graded series of ethanol (for adult organs: 2x70% to 2x95% to 3x100%; for embryos: 1x25% to 1x50% to 2x70% to1x80 to 2x95% then 3x100%), followed by clearing in CitriSolV (Fisher Scientific). The tissues were incubated in twice paraffin at 60°C then once at 60°C with vacuum pressure and finally embedded in paraffin wax. Using a microtome, tissues were cut into 5 µm thick sections onto positively-charged slides (Fisherbrand SuperfrostPlus) and heated for at least 20 min to fix the tissue onto the slide. For further histological processing, paraffin-embedded sections were cleared and rehydrated in CitriSolV (Fisher Scientific), a degraded ethanol series (100% to 95%) and ddH_2O.

For frozen embedding of tissue, whole organs or 2 to 5-mm biopsies were fixed in 4% PFA overnight at 4°C, with shaking. Fixed tissues were briefly washed in 1X PBS and ddH_2O, and incubated in 15% sucrose (Sigma) for 3-6 hrs then 30% sucrose O/N at 4°C, with shaking. Tissues were soaked in a 1:1 mix of OCT:30% sucrose for 2 hrs, then embedded in OCT (Tissue-Tek), then stored at -80°C until needed. Tissues were cut into 8µm sections onto positively-charged slides (Fisherbrand SuperfrostPlus) using a cryostat.

Hematoxylin and Eosin (H&E) Staining

Tissues were incubated in filtered hematoxylin (Richard-Allan Scientific) for 1.5 to 2 min, rinsed in ddH_2O, rinsed in clearing solution for 8 secs, bluing solution for 15 sec, then 95% ethanol for 1 min. Slides were placed in eosin (Y with phloxine; Richard-Allan Scientific) for 15-25 sec, dehydrated/cleared in 95% and 100% ethanol then CitriSolV and mounted with Permount (Fisher Scientific).

Immunohistochemistry (IHC)

After rehydration, tissues were blocked in 3% hydrogen peroxide (30%; Fisher). For staining of smooth muscle, tissues were stained using the Vector Mouse on Mouse (M.O.M) Peroxidase Kit (Vector Laboratories) according to the manufacturer's protocol. The primary antibody used was a mouse monoclonal α-SMA (1:800; Clone 1A; Sigma) and visualization was carried out using the DAB Substrate kit (Vector Laboratories). For staining of endothelial cells, tissues were digested using trypsin (Carezyme I; BioCare Medical) followed by blocked with Rodent Block M (BioCare Medical) then incubated in the primary antibody, α-PECAM-1/CD31 (1:100; BioCare Medical), diluted in Da Vinci Green diluent (BioCare Medical) O/N at 4°C. The protocol continued using the Rat on Mouse AP-Polymer kit (BioCare Medical), with 20 min incubation in both solutions. Chromogen reaction was carried out using the Vulcan Fast Red chromogen (BioCare Medical). Slides were counterstained in hematoxylin, dehydrated and cleared, then mounted with Permount.

For ENG staining, frozen sections were air-dried and fixed in cold acetone. Tissues were blocked with 5% Normal donkey serum (CalBioChem) then incubated in rat anti-mouse α-ENG (1:100; Clone MJ7/18; eBioscience) O/N at 4°C. This was followed by incubation in AlexaFluor 594 donkey anti-rat IgG (1:500; Molecular Probes). Sections were doubled stained with PECAM-1, re-fixing tissue in 4% PFA, blocking in 5% normal goat serum and incubating tissues with a PECAM-1 FITC-conjugated mouse monoclonal (1:250; Clone 390; Millipore) O/N at 4°C. Tissues were mounted using Vectashield mounting medium with DAPI (Vector Laboratories) diluted 1:1 in 1X PBS. Staining was visualized by a Leica confocal microscope.

Wound Induction in Endoglin (*Eng)* iKO models

On the last day of TM injection, mice were anesthetized with 5% isoflurane/95% O_2 then maintained under 1-3% isoflurane/O_2 delivered via nose cone connected to an anesthetization machine. A 2-mm hole was induced in the untagged ear with a 2-mm biopsy punch. For the dorsal skin wound, the dorsal fur was shaved off with an electric razor and the area briefly sprayed with alcohol. A 5-7-mm wound was induced and the wound immediately treated with an antiseptic, such as betadine.

Latex Vascular Casting

To visualize potential AVMs, a latex dye vascular casting was done in which latex was injected into the arterial circulation. Because latex is a thick liquid, it cannot travel completely through the fine capillary beds thus in normal conditions remains solely in the arteries. However, if there is AV shunting, the latex can be seen in the veins (often as a lighter shade of blue than the arteries).

Mice were anesthetized with a mix of 100 mg ketamine and 10 mg xylazine per kg body weight, injected intraperitoneally. A sagittal incision was made from the abdominal to the neck and the chest was opened to reveal the heart. For visualization of the systemic circulation, a 25 G butterfly needle (BD Precision) was inserted into the left ventricle. The circulation was perfused with a succession of three solutions (10 ml each) at a rate of 120 ml/hr using a KD Scientific syringe pump: 1) Heparin (20U/ml; Sigma) to unclot blood; 2) freshly-prepared vasodilator solution [10U/ml Heparin (Sigma), 0.4 mg/ml Papaverine, 100 µM sodium nitroprusside in 1X PBS] to dilate vessels; and 3) 10% buffered formalin (Fisher Scientific). 400-700 µl of blue latex (Connecticut Valley Biological Supply) was immediately injected using a 26G 3/8 syringe (BD Precision) inserted into the same injection site. For latex injection of the pulmonary circulation,

latex was injected into the right ventricle of the heart and the left atrium was nicked to allow dye to flow out. The injected mouse was washed of excess dye and fixed O/N in 10% buffered formalin. To better visualize vessels, the lungs, skin and ears were further process by dehydration in a graded methanol/ddH_2O series (50% to 70% to 90% to 100%) followed by clearing in an organic solvent solution (1:1 benzyl alcohol:benzyl benzoate).

Southern Blot Analysis

For the southern blot probe, a 760-bp PCR product was generated using conditions mentioned previously. The isolated PCR product was then labeled with DIG using either Roche's DNA labeling and detection kit or High Prime PCR-labeling kit, then following the manufacturer's protocol. 2-3-mm tissue biopsies were harvested and genomic DNA (gDNA) was isolated using QIAGEN Tissue and Blood kit, according to the manufacturer's instructions. gDNA DNA concentrations were measured using a Beckman Coulter spectrophotometer. 10 µg of gDNA was digested with 5U/µg BamHI restriction enzyme (NEB) for at least 16 hrs at 37°C. If total volume of digestion reaction was ≤ 25 µl, samples were loaded directly into the 1% agarose gel. If total volumes were > 25µl, sample volumes were to brought up to 100 µl by the addition of ddH_2O. Samples were precipitated by adding 2X sample volume and 10% sample volume of 100% ethanol and 3M sodium acetate, pH 5.2, respectively, then incubating at -20°C for at least 20 min. Samples were centrifuged at RT for 25 min, washed with 3X original sample volume of 70% ethanol, centrifuged for another 10 min at RT, the pellet air-dried, then resuspended in 20 µl autoclaved ddH_2O. 1 µl of 6X DNA loading dye was added to all samples. 1% agarose gels were loaded with a DIG-labeled molecular marker, with a well skipped between the marker and experimental samples. The

digested gDNA was slowly run in the gel at 35-35V until the dye has migrated at least 7 cm in the gel, indicating sufficient separation or gDNA.

After electrophoresis, the gel was incubated in depruination solution (250mM HCl), a denaturation solution (NaOH, NaCl) then neutralization solution (Tris base, NaCl). The gDNA was transferred onto a positively charged nylon membrane (Roche) via capillary action for at least 12 hrs, using 20X SSC (NaCl, Sodium citrate, pH 7.0) as a transfer buffer. Post-transfer, gDNA was fixed onto the membrane by UV-crossing by exposure to low UV wavelengths of a UV transilluminator for 5 min. The membrane was rinsed briefly in ddH_2O then preincubated in Roche's DIG Easy Hyb solution at 42°C. The DIG-labeled probe was allowed to hybridize to target gDNA for at least 16 hrs in a 42°C water bath, with shaking. Next, the membrane was washed in low stringency buffer (2X SSC, 0.1% SDS) at RT and high stringency buffer (0.1X SSC, 0.1% SDS) at 68°C, blocked in 1X blocking solution, then incubated with a α-DIG-AP-conjugated secondary antibody (1:10,000 in 1X blocking solution; Roche). Chemiluminescent bands were visualized using CDP-Star (Roche), then exposing the membrane to autoradiography film (GeneMate). Quantification of the southern blots was performed with ImageJ software (NIH, Besthesda).

Hemoglobin Measurement

To monitor potential internal hemorrhaging within cKO mice, the hemoglobin levels of tamoxifen treated mice were measured. Two-mm of the tip of the mouse tail was cut off and the first drop of blood was discarded. A second drop of blood was extracted, collected into a microcuvette (HemoPoint H2 n*x*t microcuvette, Stanbio Laboratories), then placed into a HemoPoint H2 Hemoglobin Photometer (Stanbio Laboratories). The

normal hemoglobin levels for mice is 10-20 g/dL, thus levels below would be indicative of hemorrhaging (http://www.fauvet.fau.edu/oacm/VetData/Handouts/mouseHO.htm).

Table 2-1. Conditional transgenic mouse lines used

Mouse line	Description
Eng^{2f}	*loxP* site flank exons 5&6, which code the extracellular domain
Tgfbr2^{fl}	*loxP* site flank exon 2, which contains the transmembrane domain
Alk5^{fl}	*loxP* site flank exon 3, which contains the transmembrane domain
R26R	Reporter gene used to visualize cre activity after X-gal staining
Alk1^{2f}	*loxP* site flank exons 4-6 of *Alk1* gene, which includes the transmembrane domain
Alk1^{3f}	*loxP* site flank exons 4-6; an additional neomycin resistant cassette and *loxP* site is inserted in intron 6

Table 2-2. Transgenic cre-deleter mouse lines used

Cre line	Time of cre activation	Mechanism	Cell type affected
L1cre	Beginning at E13.5	Cre driven by 9.2-kb region of *Alk1* promoter	ECs of lungs, GI tract, brain, reproductive organs, eye; NOT skin, liver, kidneys
R26-Cre^{ER}	Adult mice (aged >2months)	Cre activated by IP injection of tamoxifen	Ubiquitously expressed
Alk1^{GFPcre}	Beginning at E9.5	A GFPcre construct inserted into intron 3 of *Alk1* gene	ECs

Table 2-3. Mating schemes for cKO models

cKO genotype	Mating schemes
L1cre(+);*Eng*$^{2f/2f}$; R26R(+)	L1cre(+);*Eng*$^{+/2f}$; R26R(+) X *Eng*$^{2f/2f}$
R26-Cre$^{ER(+)}$;*Eng*$^{2f/2f}$	R26-Cre$^{ER(+)}$;*Eng*$^{2f/2f}$ X *Eng*$^{2f/2f}$
Alk1^{GFPcre};*Tgfbr2*$^{fl/fl}$	*Alk1*^{GFPcre};*Tgfbr2*$^{+/fl}$ X *Tgfbr2*$^{fl/fl}$
Alk1^{GFPcre};*Alk5*$^{fl/fl}$	*Alk1*^{GFPcre};*Alk5*$^{+/fl}$ X *Alk5*$^{fl/fl}$
L1cre(+);*Alk1*$^{2f/2f}$; *R26R(+)*	L1cre(+);*Alk1*$^{+/2f}$; R26R(+) X *Alk1*$^{2f/2f}$
R26-Cre$^{ER(+)}$;*Alk1*$^{3f/3f}$	R26-Cre$^{ER(+)}$;*Alk1*$^{3f/3f}$ X *Alk1*$^{3f/3f}$
R26-Cre$^{ER(+)}$;*Alk1*$^{2f/2f}$	R26-Cre$^{ER(+)}$;*Alk1*$^{2f/2f}$ X *Alk1*$^{2f/2f}$

Table 2-4. Primers used for PCR reactions

Primer	Forward (5' → 3')	Reverse (5' → 3')
Cre	GCTAAACATGCTTCATCGTCGGTC	CAGATTACGTATATCCTGGCAGCG
R26R	GTCGTTTTACAACGTCGTGACT	GATGGGCGCATCGTAACCGTGC
L1cre	GTTTTCCTTTGAAAAACACGATGA	ATCAGGTTCTTGCGAACCTCATCA
CreER	CATGAACTATATCCGTAACCTGGA	CATCCAACAAGGCACTGACCATCT
GFPcre	CGAGAAGCGCGATCACATGGTCCT	TTGCATCGACCGGTAATGCAGGCA
Endoglin, 2f allele	CCATTCTCATCCTGCATGGTCC	CCACGCCTTTGACCTTGCTTCC
Endoglin, 1f allele	CAGCCAGTCTAGCCAAGTCTTC	CCACGCCTTTGACCTTGCTTCC
Tgfbr2, floxed allele	TAAACAAGGTCCGGAGCCCA	ACTTCTGCAAGAGGTCCCCT
Tgfbr2, null allele	TAAACAAGGTCCGGAGCCCA	AGAGTGAAGCCGTGGTAGGTGAGCTT
Alk5, floxed allele	ACTCACATGTTGGCTCTCACTGTC	AGTCATAGAGCATGTGTTAGAGTC
Alk5, null allele	ATTTCTTCTGCTATAATCCTGCAG	AGTCATAGAGCATGTGTTAGAGTC
Eng, southern probe	GTCTTGATGGGCCAGGGAATCCGT	TTACTGCCTGGGCTGGGCCCCTGA
m*Eng*, RT-PCR	TGCACTCTGGTACATCTATTC	TGGATTGGGCAGTTCTGTAAA
mActin, RT-PCR	CCTGAACCCTAAGGCCAACCG	GCTCATAGCTCTTCTCCAGGG

CHAPTER 3
CHARACTERIZATION OF CONDITIONAL ENDOTHELIAL-SPECIFIC AND GLOBAL ENDOGLIN MURINE KNOCKOUT MODELS

Hereditary Hemorrhagic Telangiectasia (HHT): HHT1 vs. HHT2

The majority of HHT cases are attributed to mutations in *Eng* (HHT1) and *Alk1* (HHT2). *Eng* was the first identified HHT gene, reported by two independent groups in 1994 [73, 74]; however, even within one of the reports it was suspected that more than one gene may be responsible. It took another two years, in 1996, for *Alk1* to be identified by the Marchuk group [105]. Interestingly, it would take another ten years for other HHT causative genes to be found, although two have still not been definitively identified [75, 77, 78]. The different types of HHT are clinically indistinguishable, but geographically, there are reportedly higher incidences of HHT2 around the Mediterranean (e.g., Italy, France and Spain) and HHT1 is more prevalent in North America and northern Europe [106-110].

Adding to the complexity of understanding this disorder is the fact there is not one specific mutation responsible for causing the disease. Each reported HHT family has a unique mutation and *de novo* mutations have also been discovered, though rare. Thus far, there have been almost 330 and about 270 distinct ENG and ALK1, respectively, mutations reported (hhtmutation.org). Genotype:phenotype correlation studies (mostly performed on HHT1 and HHT2 patients) suggests that certain symptoms and visceral AVMs occur more frequently in HHT1 over HHT2, and vice versa. For instance, more HHT1 patients develop PAVMs and CAVMs, while HHT2 patients develop more hepatic and pancreatic AVMs and have a higher risk for PAH. Additionally, HHT2 patients seem to develop mucocutaneous telangiectases at an earlier age [72,111].

Fervent attempts have been made in understanding the functions and expression of both ALK1 and ENG in physiology and the HHT pathological states, with the overall goal of creating efficient treatment for the disease. ENG and ALK1 are unique compared to TGF-β superfamily members because their expression is almost exclusive to ECs. Furthermore, ALK1 is expressed specifically in arterial endothelial cells [112].

Endoglin (ENG)

Endoglin/CD105 is a homodimeric disulphide-linked plasma membrane receptor located on the human chromosome 9q34 [113] and chromosome 2 in mice [114]. Structurally, *Eng* consists of 15 exons and has a large extracellular domain. ENG has five glycosylation sites within its N-terminus and an O-glycan domain rich in serine and threonine residues near the transmembrane domain [115, 116]. ENG is conserved among higher mammals; however, one feature that is found only in human ENG is an Arginine-Glycine-Aspartate (RGD) motif that serves as a binding site for adhesion molecules in the extracellular matrix (ECM) [117]. The short cytoplasmic domain acts as a target for the TGF-β type I and II receptors [41].

There are two splice forms of ENG: long (L-) and short (S-ENG) forms, which differ in 33 amino acids (aa) in size [118]. L-ENG is a 658-aa long polypeptide, with a 47-aa long cytoplasmic tail. The L-ENG gene contains 15 exons, numbered 1-9a, 9b, 10-14. S-ENG involves the inclusion of an additional 135 nucleotides between exon 13 and exon 14 (effectively called exon 13A), introducing a premature stop codon that leads to a shortened 625-aa protein product with a 14-aa cytoplasmic tail [119]. The four domains of ENG are domains: a short 25-aa signal peptide domain (part of exon 1), a large extracellular domain (part of exon 1 through exon 13), a small 25-aa transmembrane domain (part of exon 13) and a 14- or 47-aa long cytoplasmic domain

(exons 13-14). There is also a third albeit soluble form of ENG (sENG) that lacks the transmembrane domain.

ENG is predominantly expressed in all vascular endothelial cells, but has also been found in erythroid precursors and stromal cells of the fetal and adult bone marrow, syncytiotrophoblasts, hematopoietic stem cells, very low levels in smooth muscle cells, and monocytes [120-122]. ENG expression is high during development and is expressed at basal levels in quiescent ECs [123]. ENG expression is increased again when ECs are activated, such as in angiogenesis, inflammation, wound healing and vascular injury [124-126]. ENG is first expressed at E6.5 in the extraembryonic ectoderm, and seen at E8.5 on primitive ECs of the yolk sac. By E9.5 ENG expression is on all ECs (particularly in endocardium but not myocardium). By E12.5 the strongest expression is within capillaries, but weak in veins and intermediate arteries [126].

The L-ENG isoform is the dominant form within the vasculature and the form that is the most studied in the literature. The functional differences between L-ENG and S-ENG have not been extensively studied. Interesting, it appears that the two lesser forms, S-ENG and sENG, have the same opposing/antiangiogenic response to L-ENG. Many studies focusing on S-ENG have been performed *in vitro*. The S-ENG expression is increased in cultured senescent human ECs and older mice, suggesting S-ENG is more active within the aged vasculature [127, 128]. An *in vivo* model by Perez-Gomez and colleagues, in which $Eng^{+/-}$ mice overexpressed S-ENG ($Eng^{+/-};S\text{-}Eng^{+}$) via adenovirus, was previously characterized. It was found that the two membrane-bound ENG isoforms were highly co-expressed in the lungs, heart and liver. Also, overabundance of S-ENG could not rescue the *Eng*-null mice, as no surviving $Eng^{-/-}$; S-

Eng^{+} were found. Further supporting opposing functions between L-ENG and S-ENG, when injected with Lewis Lung Carcinoma cell, S-*Eng*$^{+}$ mice developed tumors that were 35% smaller in weight and contained 65% less hemoglobin than control littermates [129].

ENG has received more attention lately as excessive sENG is linked to another pathology, preeclampsia [130]. Preeclampsia is a serious complication in 3-5% pregnancies and is characterized by hypertension, proteinurea, and edema [40, 131]. The disproportionate ratio of angiogenic and anti-angiogenic circulating factors is believed to be the major cause of preeclampsia [132, 133]. Sera taken from preeclampsic women have elevated levels of the anti-angiogenic circulating soluble fms-like tyrosine kinase (sFlt1) and sENG, but reduced pro-angiogenic factors like placental growth factor (PIGF) and VEGF [134, 135]. Additionally, the levels of sENG predict the severity of the disease [136-138]. A rat model of preeclampsia was created by injecting rats with adenovirus expression of sENG [138]. Additionally, elevated sENG levels are also found in cancer, atherosclerotic lesions, coronary artery disease, hepatitis, diabetes, biliary atresia, and sickle cell anemia [119, 139, 140].

Functionally, ENG has been found to interact directly with either Type II or Type I receptors. It is believed that ENG interacts with the two different TGF-β Type I receptors, ALK1 and ALK5, and induces opposing angiogenic responses. ENG preferentially interacts and activates the pro-angiogenic response via the ALK1/SMAD1/5/8 signaling. Conversely, it can stimulate an anti-angiogenic response by inducing ALK5/SMAD2/3 signaling [141-143]. During embryogenesis, ENG

expression overlaps with ALK1 (especially at E6.5-13.5), TGF-β1 and TGFBR2, but not with ALK5, TGF-β2, nor TGF-β3 [126, 144].

Many *in vitro* HHT studies have been performed using human umbilical vein endothelial cells (HUVECs) derived from HHT patients [145, 146]. Indeed, HUVECs from newborn HHT1 overall showed reduced ENG surface expression. Further studies also showed reduced ENG levels in the activated monoctyes and HUVECs collected from HHT1 patients. When cells were transfected with a mutated transcript of ENG, surface ENG expression was not detectable (due to a truncated protein or unstable mRNA transcript) [111,147].

There had been three independent *Eng* conventional mouse knockout (KO) models, with similar phenotypes: embryonic lethality at E10-11.5, defective yolk sac angiogenesis and heart development [56, 57, 148]. Analysis of the $Eng^{-/-}$ mice at E9.5 revealed the KOs had abnormal vasculature and yolk sac anemia. $Eng^{-/-}$ embryos were capable of forming highly vascularized primary plexuses, but with retarded vessel branching. Thus, the models revealed that ENG plays a role in angiogenesis, but apparently not vasculogenesis. The *in vivo* finding corroborated with embryonic stem cells studies derived from one of the $Eng^{-/-}$ models. Perlingeiro found that $Eng^{+/+}$ and $Eng^{-/-}$ embryonic stem cells expressed the same amounts of the vascular precursors (VE-Cadherin/FLK-1 and VE-Cadherin/TIE2), indicating vasculogenesis is not affected in $Eng^{-/-}$. In addition, ENG expression is essential within the early hemangioblast and in promoting HSC specification [149].

Other *in vivo* approaches in deleting *Eng* in mice take advantage of the cre-loxP system. Recently, Mancini et al. executed complementary studies in which ENG

function was activated specifically within ECs or SMCs [150]. The authors created an expression strain of *Eng* (TgEng^{fl}) by which *Eng* activity would be "turned on" where cre recombinase is located as it will remove a stop codon flanked by *loxP* sites within the construct. In order to express *Eng* specifically in ECs or SMCs, they used the *Tie2*-cre and *Sm22α*-cre deleter lines, respectively, and bred them into an *Eng*$^{-/-}$ background. Thus, *Tie2*-cre;TgEngNull expressed ENG only within ECs and *Sm22α*-cre;TgEngnull expressed ENG only in VSMCs. Both models saw a rescue of VSMC recruitment to the vessels, though the Sm22αcre;TgEngNull mice formed a thicker layer of smooth muscle layers. The study provided evidence that ENG plays a valuable role in recruitment of smooth muscle cells. Interestingly, activation of *Eng* within either cell type was not sufficient to rescue the *Eng*$^{-/-}$ embryos, indicating that ENG may be required earlier in vascular development, namely in the angioblast progenitor population. One possible function may be in arteriovenous identity.

A conditional bi-floxed *Eng* mouse was first described in 2007 by the Arthur lab and brought promise of specifically deleting *Eng* in different cells and tissues temporally [103]. However, it is now too early to report any findings although several approaches are currently being attempted, including the projects within this chapter. The only published report so far of an *Eng* conditional (cKO) mouse is by the Arthur lab by which *Eng* was specifically ablated within ECs using a tamoxifen-inducible Cdh5(PAC)-Cre^{ERT2} deleter line [151]. The Cdh5(PAC)-Cre^{ERT2};*Eng*$^{2f/2f}$ mice were created at postnatal day (PN)2 (examined at PN7) and adult mice. The Cdh5(PAC)-Cre^{ERT2};*Eng*$^{2f/2f}$ mice failed to develop gross AVMs or consistent HHT-like phenotypes. Though, closer examination revealed reduced angiogenic potential and venomegaly in adult mice. Retina

angiogenesis studies in the postnatal mice showed Cdh5(PAC)-Cre^{ERT2};*Eng*$^{2f/2f}$ mice had delayed vascular remodeling of capillary plexus, increased proliferation, localized AVMs, and areas of AV-shunts underwent muscularization, which may have resulted from the increased blood flow.

Activin-Like Kinase Receptor-1 (ALK1)

ALK1/ACVRL1 (Activin receptor-like kinase-1) is located on the human chromosome 12q11-q14. ALK1 is a TGF-β type I receptor. The *Alk1* gene consists of ten exons (1-10), although only 9 represent the actual coding sequence as exon 1 is noncoding. Because it has two transcriptional start sites, there are two mRNA isoforms. Structurally, ALK1 has six domains: a 21-aa leader peptide (exon 2), extracellular (exons 2-4), transmembrane (exon 4), GS-rich (exons 4-5), serine-threonine kinase (exons 5-10), and a NANDOR box (within exon 10) [147, 152].

Characterization of HUVECs and monocytes collected from HHT2 patients revealed that missense mutations in ALK1 that lead to amino acid substitutions account for about 60% of HHT2 cases [145, 153]. Interestingly, three of the *in vitro* HUVEC and transfection studies demonstrated that not only was ALK1 still expressed on the cell surface, but in two ALK1 was behaving in a dominant-negative manner. However, two of the three HUVEC lines were derived from families at risk for developing HHT-associated PAH, which could complicate the study and affect results. The drawback from the commonly used HUVECs in HHT research are the limited supplies collected from the newborns and that these cells are collected before any phenotypes have the chance to manifest. Another fundamental problem is that cell culture conditions vary among groups of investigators.

As with the *Eng*$^{-/-}$ mice, *Alk1*$^{-/-}$ are embryonic lethal at midgestation due to defects in angiogenesis [154, 155]. Supporting its importance in angiogenesis, a zebrafish model, in which *Alk1* ortholog *violet beauregard* was suppressed, resulted in the formation of arteriovenous malformations (AVMs) [156]. Additional murine studies targeting the expression of arterial marker EphrinB2 showed that *Alk1*$^{-/-}$ mice lost this expression within the dorsal aorta. Interestingly, *Eng*$^{-/-}$ mice do not demonstrate this phenotype [154, 157].

Mouse Models for HHT

One of the most striking findings from the *Eng* and *Alk1* null mouse models was that 30-70% of heterozygous mice (*Eng*$^{+/-}$ *and Alk*$^{+/-}$) faithfully phenocopied the human disease [57, 158]. Unfortunately, the appearance of HHT-like phenotypes in mice is as variable and unpredictable as the human disease. Nonetheless, most labs studying HHT still utilize heterozygous mice. It has been suggested that the variability in phenotypes may be influenced by modifier genes [159]. Bourdeau and colleagues showed that there were strain-dependent penetrance in *Eng*$^{+/-}$ mice, as 30%, 50% and 70% of *Eng*$^{+/-}$ mice on pure C57BL/6, mixed, and pure 129/Ola (respectively) strain background developed HHT-like symptoms [160].

The *Alk1* conditional mouse was generated by the Oh lab and first described in 2008 [64]. Simultaneously, the novel endothelial-specific cre-deleter line L1cre, in which cre recombinase was driven by a 9.2-kb region of the *Alk1* promoter [161], was introduced [64]. This line is unique in that cre is active beginning late in gestation, at E13.5 with spotty EC-specific X-gal staining. By E15.5 there is very strong X-gal staining of ECs. This delay in cre is essential as it by bypasses the midgestation lethality of many conventional knockout models. Another unique characteristic of L1cre

is activity is restricted to the brain, intestine, yolk sac, and strongly in the lungs. It was previously reported that L1cre(+);*Alk1*$^{3f/3f}$ and L1cre(+);*Alk1*$^{2f/2f}$ mice consistently developed dilated, disorganized and tortuous vessels in the lungs, GI tract and brain starting at E15.5 or E17.5, respectively, and death during late gestation (by E18.5) or shortly after birth, at PN5, respectively (Figure 3-1). Pulmonary vessels displayed irregular SMC layers. When the L1cre line was used to delete *Tgfbr2*$^{fl/fl}$ and *Alk5*$^{fl/fl}$, the cKO mice were unaffected, suggesting that ALK1 signals independently of TGFBR2 and ALK5. It further supports that ALK1 may actually signal via the BMP-driven signaling pathway [64].

Further studies were done with the *Alk1* conditional mice that provided more ALK1 signaling insight. *Alk1* was deleted globally in adult mice using a tamoxifen-inducible R26-Cre^{ER} line (*Alk1* iKO) [162]. Adult mice consistently showed pulmonary and GI bleeding. Latex vascular casting revealed evidence of AV-shunting in the lungs, with AVMs found in uterine vessels, in the peyer's patch of the intestine, and within *Alk1*$^{3f/3f}$ iKO mouse livers (Figure 3-2). When acute wounds were given in the ears and dorsal skin of *Alk1* iKO mice, *de novo* AVMs formed, suggesting that a second environmental injury, in addition to the genetic deficiency, is sufficient to inflict AVMs (Figure 3-2).

The underlying pathological mechanism underlying HHT is still largely unknown. Interestingly, the genes responsible for HHT are known, their physiological functions have not been clearly defined. Based on *in vitro* and some *in vivo* studies, it is assumed that ENG and ALK1 work in concert in a linear TGF-β/SMAD-dependent manner within ECs to induce angiogenesis and maintain vascular tone so reduced function of either receptor can lead to the vascular defects seen in HHT. However, this has not been

tested directly *in vivo*, thus we attempted to accomplish this goal by generating *Eng* cKO mouse models.

Although, the heterozygous models recapitulate HHT-like phenotype, the vascular malformations are highly variable in formulation, location, and severity. The L1cre(+);*Alk1* cKO and *Alk1* iKO mice our lab previously characterized are the first murine models that displayed highly consistent AVMs in specific organs (among those, the lungs, GI tract, and brain). This affords the opportunity to test the ENG/ALK1 signaling hypothesis by generating *Eng* cKO mice using the same cre-deleter lines. The expectation is that if these, indeed, signal in a linear fashion, the *Eng* cKO and *Eng* iKO mice would produce the same or overlapping phenotypes.

Results

Generation of Conditional (cKO) and Tamoxifen-Inducible (iKO) Eng *Knockout Mice*

Eng-bifloxed mice were previously generated by and obtained through the Arthur lab. In this conditional murine model, *LoxP* sites flank exons 5 and 6, which are part of the extracellular domain of the *Eng* gene (Figure 3-3A). When cre recombinase is present, homologous recombination between the *loxP* site leads to the removal of these exons ($Eng^{\Delta 5\text{-}6}$). Consequently, $Eng^{\Delta 5\text{-}6}$ results in a frameshift in the sequence that introduces a premature stop codon in exon 7 when translated into protein. The truncated protein (consisting of the extracellular domain from exons 1-4 and part of exon 7) is too short be functional and assumed to not even reach the plasma membrane, thus is a null allele [103]. Mice were genotyped via PCR for the floxed allele using primers 5+6 (Figure 3-3B). There was approximately 80-bp nucleotides introduced

into introns 4 and 6 associated with the *loxP* sites, however, these did not interfere with normal function of the gene.

Endothelial-Specific Deletion of Vascular Eng *(L1cre(+);*$\mathbf{Eng^{2f/2f}}$*) were Viable*

The first *Eng* cKO model generated was an endothelial-specific ablation, utilizing the L1cre line. It was surprising that all *Eng* cKO (hereby designated cKO) mice were viable and without signs of reduced longevity or exhibiting any outward health problems, compared to control mice (littermates that were cre negative). Immunostaining of the endothelial layer with PECAM-1 (red) and the SMC layer (brown) of the vessels of the uterus, intestine, kidney, and liver revealed Eng cKO mice were developmentally indistinguishable (Figure 3-4).

As L1cre is most active in the lungs and L1cre(+);$Alk1^{3f/3f,}$ displayed abnormal pulmonary vasculature in a highly consistent manner, the pulmonary vessel development was compared between control and *Eng* cKO mice at E15.5, E18.5 and adult (aged 2-months or older) stages (Figure 3-5). The *Eng* cKO mice were developmentally indistinguishable from control littermates (Figure 3-5A-D'). There were no indications of hemorrhaging or dilated vessels at any stage (Figure 3-5). In adult lungs, neither the arteriole vessels no arteries exhibited any evidence of vessel dilation (Figure 3-5E,G,F,H). Additionally, *Eng* cKO pulmonary vessels developed uniform smooth muscle layers similar to Controls (Figure 3-5E',G',F',H').

In a population of mice aged 4 to 15 months, hemoglobin (Hgb) levels were measured to indicate whether any Eng cKO mice may be bleeding internally. Surprisingly, almost all the Eng cKO had Hgb levels that were normal for mice (10-20 g/dL) and to Control littermates (Figure 3-6A). Eventually, only two *Eng* cKO mice, at an older age of 15-month, displayed any visceral phenotype. Latex vascular casting of

lungs taken from mice aged 1.5 years showed *Eng* cKO mice developed proper pulmonary vessels (Figure 3-6B), with no signs of AVMs as in L1cre(+);*Alk1*$^{2f/2f}$ (Figure 3-1J). It should be noted that one of the two mice that measured below 10 g/dL is the hemorrhagic mouse. Interestingly, the two *Eng* cKO mice both displayed abnormal livers, despite L1cre not being active in the liver. In one mouse, the liver was regressed and some vessels were visibly infused with latex (Figure 3-4C). In control mice, the latex dye is not normally visible. In the second *Eng* cKO mouse, the liver developed normally, but there were five AVMs present, exemplified in Figure 3-4C'. A magnified view (Figure 3-4C', inset), revealed a cluster of enlarged, dilated vessels. Only one *Eng* cKO mouse aged 15-months (one of the two mice in Figure 3-6A with Hgb levels below 10 g/dL) exhibited local hemorrhaging at two sites in the intestine (Figure 3-6D). There was mild AV-shunting in few vascular beds, evidenced by incomplete penetration of the latex into the vein, but one telangiectasia in one hemorrhage site (Figure 3-6D', inset). In Figure 3-6E, PCR analysis for the null allele was performed using the indicated primer set 4+6 (Figure 3-1A) on DNA extracted from various organs from control and *Eng* cKO mice. The results show that L1cre was active and exons 5 and 6 were deleted in the expected organs of *Eng* cKO mice, such as the lungs, heart, intestine, appendix, and uterus, but not in the liver or kidney and in any of the control organs. Reverse-transcriptase (RT)-PCR was also done, but results were not as clear because mRNA was collected from whole tissues, thus the true reduction of mEng in vascular ECs may be difficult to detect.

X-gal and Immunohistochemistry Confirmed Cre was Active in ECs of Expected Organs

The *Eng* cKO model also possesses the ROSA26 locus, which allows visualization of cre activity by X-gal staining. It was confirmed that cre was active in the *Eng* cKO lungs, heart, eye, brain, intestine and female reproductive organs, indicated by the blue X-gal precipitate (Figure 3-7I, J, M, N, O, P/P', respectively). The *Eng* cKO liver and kidney and all Control samples were not stained blue proving cre was not active in these locales (Figure 3-7K-L, A-H'). Also, shown as an additional control is that lung and brain from L1cre(+);$Eng^{+/2f}$ mice were also stained blue, but not the liver or kidney (Figure 3-5Q,R and S,T, respectively), further establishing cre is active and restricted to certain organs.

Histological analysis of X-gal stained Eng cKO lung (Figure 3-8A,A',D) shows the strongest cre activity. However, because the lung used for X-gal staining was not inflated and the X-gal staining is so strong, it was difficult to prove in the pulmonary microvasculature that the EC-staining was EC-specific (compared to SMC-specific) (Figure 3-8A/A', D). Co-staining of X-gal positive cells in the uterus, and intestine with either PECAM-1 or SMA (Figure 3-8/B/B',E,C/C',F respectively), indicate cre was active in ECs.

Confirmed Loss of Vascular Endothelial **Eng** *did not Affect Vascular Development*

Immunofluorescence (IF) staining of ENG in Control and Eng cKO lungs reveal that ENG was overall reduced (Figure 3-9A,E). An arterial vessel was selected from each sample (Figure 3-9B,F) and the colocalization of ENG and PECAM-1 show that the number of *ENG*-expressing cells were reduced in *Eng* cKO mice compared to control (Figure 3-9C,G). Quantification of the colocalization rate confirmed there was a

~50% decrease the numbers of ECs expressing ENG in the Eng cKO mice (Figure 3-9D,H,I). Thus, the data from the *Eng* cKO model surprisingly suggests that *Eng* cKO mice were largely unaffected by the late gestational loss of *Eng* in vascular ECs.

Eng *iKO Mice Displayed Variable Phenotypes*

The second knockout model was a global silencing of *Eng* in adult mice using the tamoxifen (TM)-inducible cre line, R26-Cre^{ER}. In this line, cre is fused with a mutated form of the estrogen receptor and remains inactive until TM is introduced and binds to the mutated estrogen receptor, activating it. Furthermore, the construct is inserted into the ubiquitous ROSA26 locus, thus induction of cre is a global event. The *Alk1* iKO model was created to determine what effects the loss of ALK1 in adult tissues would occur. A single IP injection of 2.5mg TM per 25g mouse body weight in R26-Cre$^{ER(+)}$;*Alk1*$^{2f/2f}$ (*Alk1* iKO) was sufficient to induce the aforementioned AVMs and hemorrhaging (Figure 3-2) within 7 days of TM treatment, with death as early as 9 days, but 100% fatality by 21 days after TM [162]. Thus, the same dose of TM was first given to the R26-Cre$^{ER(+)}$;*Eng*$^{2f/2f}$ (*Eng* iKO-TM1) mice that were at least 2-months of age. Control mice were *Eng*$^{2f/2f}$ littermates, which were R26-Cre^{ER}-negative, and injected with the same dose of TM. Surprisingly, the *Eng* iKO-TM1 mice were completely viable and did not seem affected by the loss of *Eng*. *Eng* iKO-TM1 were able to survive over 12 month after TM injection, without overt health concerns (Figure 3-14A). The only noticeable outward phenotype was the appearance of abnormal vasculature in the ear tissue surrounding the ear identification (ID) tag commonly given to mice at the time of weaning (age 21 days) (Figure 3-10A). The appearance of AVMs was confirmed by vascular (blue) latex casting of the systemic vasculature system. The ear phenotype, which was seen in all *Eng* iKO-TM1 mice, was slow to progress as dilated vessels were

not noticeable until 1.5 to 2 months after TM treatment (Figure 3-10G) and worsened over time, as seen at 6-months (Figure 3-10E, compared to control, C).

When further studies with the *Alk1* iKO mice were done in which 2-mm holes were induced within the ear and dorsal skin, *Alk1* iKO mice developed *de novo* AVMs in the tissue surrounding the injury site, indicating a "second-hit," e.g. injury, environment change, in addition to genetic loss of *Alk1* can cause AVMs (Figure 3-2G-I). However, when 2-mm holes were induced within the ID tag-free ear and dorsal skin of the *Eng* iKO-TM1 mice, AVMs never formed (Figure 3-10,D,F).

In support of the slow progression of phenotype (as seen in the ID tagged ear), autopsies of *Eng* iKO-TM1 mice 1- or 2-month after TM did not reveal any abnormalities (data not shown). However, autopsies of 5- and 6-month post-TM *Eng* iKO-TM1 mice revealed grossly tortuous, disorganized vessels in the ovaries and appendix, but the phenotype appearance was not in a consistent manner. Two females were hemorrhaging and possessed abnormal ovarian vessels (Figure 3-10I and I'). In a 6-month *Eng* iKO-TM1 case, the ovarian vessels appear to connect to the intestine (Figure 3-I'). In 2/6 mice the appendix show specific clusters of abnormal vasculature, as demonstrate in Figure 3-10J. Besides the ID-tag associated phenotype, the other consistent phenotype seen in mice was mild AV-shunting in the intestine, particularly in the large intestine (Figure 3-10K). Mice displayed cardiomegaly, shown here 5-months after TM (Figure 3-10L), beginning at 2-months post-TM. However, hemorrhages were not found as in *Alk1* iKO mice. Lung hemorrhaging, often seen in *Alk1* iKO mice, was absent in *Eng* iKO-TM1. Additionally, some *Eng* iKO-TM1/high dose mice excreted red

feces, indicative of blood in the feces. This would suggest internal bleeding; however, it was surprising that no hemorrhages were found during the necropsy.

A question of whether the single dose of TM was sufficient to use in the *Eng* iKO-TM1 was raised. Compared to other literature utilizing TM-inducible CreER lines, the *Alk1* iKO was unique in that a single injection was enough to lead to a phentotype. However, the typical number and dose of injections average three to five times at 2mg TM [151, 163]. Thus, two to three injections of the same concentration of TM was administered (*Eng* iKO-TM2 or 3/high dose). *Eng* iKO-TM2 or 3/high dose had high mortality rates (Figure 3-14A), with mice very sickly or close to death at an average of 7 days after the first TM injection. *Eng* iKO-TM2 or 3/high dose mice became hunched, lethargic and had scruffy fur, compared to control littermates (Figure 3-11A). Dilated vessels in tissue surrounding the ID tag were noticeable at 4 days after the first TM treatment but AVMs did not form (Data not shown), probably because death occurred too soon. Cardiomegaly and lung hemorrhaging were not seen in *Eng* iKO-TM2 or 3/high dose mice for the same reasons (not shown). There was 3/17 mice that had an abnormally small liver (Figure 3-11B). The GI tract appeared to be the most affected in the *Eng* iKO-TM2 or 3/high dose mice. 6/17 mice exhibited a distended GI-tract, however only 3 had major general intestinal hemorrhages. All mice have AV-shunting in the intestines and appendix (Figure 3-11C-E). A small AVM was found in the intestine of one *Eng* iKO-TM2 or 3/high dose mouse (Figure 311-E), however, global vascular defects as seen in *Alk1* iKO mice was not found.

The rapid death of *Eng* iKO-TM2/3, but survival of *Eng* iKO-TM1 mice with a slow phenotype progression, suggests that multiple injections of TM at 2.5 mg/25 g mouse

BW can lead to complete ablation of *Eng* in all cells, not just the vasculature, which have detrimental effects on *Eng* iKO mice. Though TM can be toxic at high doses and 2.5 mg TM/25 g BW is high compared to what is typically used, TM toxicity seems unlikely to be the cause of death as control mice do not die.

Multiple Lower Doses of Tamoxifen (2.5mg/40g BW) Leads to More Consistent Appearances of Phenotypes

A lower dose (2.5 mg TM/40 g body weight) was then used, with two or three TM injections given to mice (*Eng* iKO-TM2 or 3/low *dose*). Overall, there was an about 75% survival rate for either *Eng* iKO-TM2 or 3/low dose, with 25% dying at three weeks after the first TM injection (Figure 3-14A).

As consistently seen in *Eng* iKO-TM1/high dose mice, the vessels in the ear tissue around the ear ID tag became dilated and disorganized. The progression of the phenotype occurred sooner, with the appearance of possible telangiectases at 12-days post-TM (Figure 3-12B). AVMs were clearly visible if left for longer periods, as seen at 52 days after TM treatment (Figure 3-12C). In the wound induction studies, AVMs did not form around induced wounds in the *Eng* iKO-TM2/low dose ear, 12 days after (Figure 3-12E). Even at 52 days after TM treatment and 50 days after the ear punch, AVMs did not form; although, vessels were more disorganized and in the there may have been telangiectases but it was not clear (Figure 3-12F). It should be noted that the images represented is the most extreme case of the induced ear wound. Other *Eng* iKO-TM2 or 3/low dose ear punch mice were similar to controls.

AVMs were never seen in wounds induced in the dorsal skin, seen here 12 days after wounds induction (Figure 3-12E,F). Wounds were capable of healing in the *Eng* iKO-TM3/low dose dorsal skin. A fresh wound was given 42 days later and latex

injection was performed 10 days later, but there were still no AVMs present. Instead there was an increase of microvessels around the fresh wound (Figure 3-12I). The highly consistent ear ID tag-associated AVMs among all the treatments in the *Eng* iKO mice mirrors the *de novo* AVMs that form in the wounds in *Alk1* iKO mice; however, this phenotype arises from opposing stimuli. The ear ID tag could be considered a chronic stimulus and the wound can be an acute stimulus. Interestingly, as the *Eng* iKO mice did not form AVMs around the induced wounds, the *Alk1* iKO mice did not form AVMs in the ear tag (Figure 3-2J).

A necropsy revealed *Eng* iKO-TM3/low dose mice kept longer than 1.5 months after TM-treatment experienced cardiomegaly (Figure 3-13AB), which is more likely a secondary affect to internal hemorrhaging or possible hepatic vascular malformation. Assessment of vascular malformations by latex injection shows that that, as seen in the *Eng* iKO at all TM doses, the GI tract was affected. The appendix also shows mild AV-shunting in all *Eng* iKO/low dose mice (Figure 3-13D and E), and 1/17 *Eng* iKO-TM3 mouse developing an AVM in the appendix three months after TM (Figure 3-13E). The liver of *Eng* cKO was largely similar to control mice (Figure 3-13F&G), however, 2/17 *Eng* iKO-TM3/low dose mice had a regressed liver (Figure 3-13H). There was varying degrees of, though consistent, AV-shunting within intestinal vessels compared to control mice (Figure 3-13J&K,I, respectively); of note, not all vascular beds were affected. 1/6 of *Eng* iKO-TM2/low dose and 4/17 of *Eng* iKO-TM3/low dose had hemorrhages in the intestine (Figure 3-13J&K). Two *Eng* iKO-TM3/low dose mouse developed AVMs specifically in the peyer's patch of the intestine (Figure 3-13J'). Interestingly, this is a similar finding as in the *Alk1* iKO model. *Eng* iKO-TM2 or 3/low dose female mice

consistently hemorrhaged and developed AVMs specifically in ovarian vessels, but not in uterine vessels (as seen in *Alk1* iKO mice) (Figure 3-13M). Interestingly, two *Eng* iKO-TM3/low dose males had visibly enlarged scrotums with bloody feces (Figure 3-13O, compared to control N). The necropsy revealed the appendix had been moved in the scrotal area, and there was no vascular defects in the male reproductive organs, nor was there ever found in either *Eng* cKO model. As was found in the *Eng* iKO-TM1/high dose mice, there was not intestinal bleeding. However, AVMs in the rectum were discovered (Figure 3-13O' magnified view in yellow box), which could account for blood in the feces without any signs obvious internal hemorrhaging.

Lastly, as the vessels of the head are often affected in HHT patients, we decided to look the head vasculature of the *Eng* iKO mice. Examination revealed that abnormally dilated vessels in the turbinate of *Eng* iKO mice (Figure 3-13R). In two mice (one treated 3 times, the other 2 times of TM) telangiectases were present in the gums of the front two lower teeth (Figure 3-13S). Using multiple injections of the lower (2.5 mg TM/40 g BW) dose seems the most appropriate dose, with three times injection the best. Though, the appearance of vascular malformations in common organs were much more consistent in the *Eng* iKO/low dose mice, the phenotype is still heterogenous in terms of severity and location of AVM formation.

Hgb measurements were taken of *Eng* iKO-TM2 or 3/low dose mice to test for possible internal bleeding two to four months after TM treatment (Figure 3-14B). It was found that more *Eng* iKO-TM3/low dose (>50%) mice gave measurements around 10%, indicating internal hemorrhaging. In two of the mice, the feces were bright red in color, suggestive of blood in the feces. However, despite these findings the mice with the low

hgb did not display any signs of reduced health quality compared to controls or *Eng* iKO-TM2 or 3/low dose mice with hgb values within the normal range.

The 2f-to-1f Allelic Conversion Efficiency at the Different Doses Contributed to the Observed Variable Phenotypes

To test whether the variability in the *Eng* iKO phenotype is a true phenotype or a technical issue concerning the use of tamoxifen, the conversion of the conditional (2f) to null (1f) allele genomic copy of each allele was quantified by genomic southern blot (Schematic in Figure 3-15A). An *Alk1* iKO southern blot was also performed to show the 2f to 1f allele conversion in the *Alk1* iKO lungs and liver to act as a comparison for the *Eng* iKO samples. There was >95% conversion in the *Alk1* iKO lungs. However, the liver samples taken from the same mouse varied. One mouse had complete conversion to the null allele but the other showed ~90% conversion (Figure 3-15B). However, due to the high background in the former sample on the blot, this may not reflect a true measurement. More *Alk1* iKO southern blots will need to be run.

The single high dose of TM appeared to have the same conversion rate in the liver samples as the *Alk1* iKO mice (Figure 3-15D). There was a general trend in that there was more efficient 2f to 1f allele conversion in *Eng* iKO mice given increasing numbers of TM injections. The high dose of TM effective deleted *Eng*, there was >75% of the 2f to 1f allele in all *Eng* iKO mice. In the triple injected mice, there was 100% conversion, indicating deletion of *Eng* in the mice (Figure 3-15D). *Eng* iKO lung samples will have to be repeated to confirm this trend, but there is indications that complete ablation of *Eng* has detrimental consequences. Organ-specific differences in TM efficiency are seen as gDNA from the liver has more complete 2f to 1f conversion at the equivalent dose compared to the lungs (Figure 3-15D,F). There a low 2f to 1f conversion rate in the

lungs of *Eng* iKO mice given the lower TM dose, which may account for the lack of vascular phenotype in the lungs of *Eng* iKO/low dose mice (Figure 3-15D). However, there was >50% conversion in the livers of the same mice, with >80% deletion in the triple injected mice (Figure 3-15F).

Discussion

ALK1 and ENG are assumed to work in a linear, canonical BMP-driven signaling pathway during angiogenesis and in maintenance of the endothelium because both receptors are restricted to ECs, mutations in *Alk1*, *Eng* and *Smad4* are related to HHT, and mice heterozygous for either gene can develop HHT-like symptoms [57, 73, 75, 105, 158, 164]. Thus, it was very surprising that the confirmed loss of *Eng* in ECs expressing ALK1 had no obvious developmental impact on Eng cKO mice. In fact, any vascular anomalities seen in *Eng* cKO mice were slow to progress as only two mice, aged ≥15-months, presented mild vascular anomalities in the intestine and liver. Interestingly, despite L1cre not being expressed in the liver, both mice display abnormal livers. Additionally, one mouse exhibited two intestinal hemorrhages with a few vascular beds showing AV-shunting at each site and only one visible telangiectasia in one site. This contrasts with the *Alk1* cKO mice as all vascular beds are affected.

It was even more surprising that global deletion of *Eng* under the same conditions as the *Alk1* iKO model did not severely impact the *Eng* iKO mice. A majority (75% of iKO mice injected thrice with the low dose of TM) survived without any many health concerns. Though testing varying tamoxifen dosage and the number of injections in addition to the genomic southern blot quantification of the genomic copy of the null allele implies technical hindrances influenced the variability in the appearance of vascular abnormalities in the *Eng* iKO, the organs affected and the type of phenotype

seen were consistent. Additionally, though rare, similar pathologies were seen in the *Eng* cKO mice. This suggests the AV-shunting, GI hemorrhages, and AVMs that formed are legitimate phenotypes resulting from the loss of *Eng*.

Several organs (the ear, GI tract, female reproductive system, heart, liver) were commonly affected in the *Alk1* and *Eng* iKO models. There were only few cases where overlap seen. For example, two *Eng* iKO mice developed AVMs in the peyer's patch of the intestine, a structure in which *Alk1* iKO mice commonly form AVMs. However, in many cases the phenotype seen differed in severity, location, and in response to a stimulus. In the ear, AVMs formed in the tissue surrounding the ear ID tag, but not when a wound was given in the untagged ear (nor dorsal skin); *Alk1* iKO mice formed *de novo* AVMs around the wound site. In the female reproduction system, it is quite curious that the ovary and uterus is specifically affected in the *Eng* iKO and *Alk1* iKO model, respectively. The $Alk1^{3f/3f}$ iKO liver often exhibits AVMs however *Eng* iKO livers did not consistently form the hepatic abnormalities. These discrepancies indicate there may be disparate pathological mechanisms underlying HHT1 and HHT2.

One possible contributing factor to the difference in phenotypes in the *Alk1* and *Eng* iKO models is in the expression of ALK1 vs. ENG. ALK1 is more specifically expressed on arterial ECs while ENG is on all vascular ECs and in circulating endothelial cells (CECs), such as EPCs and HSCs. Additionally, it was previously reported in expression studies that in the pulmonary vasculature, ALK1 and ENG overlap only in the distal arterioles, venules and capillary bed [165]. In the L1cre line cre is active in arterial ECs, but as *Eng* is also expressed on vein ECs, loss of arterial *Eng* may not have as a severe affect as *Alk1* loss. Also, the milder phenotype in *Eng* cKO

mice may be CECs expressing ENG may be compensating for the loss of vascular *Eng* *[166]*.

The variable phenotypes seen support the finding that genetic loss alone of either *Eng* or *Alk1* is not always sufficient for the formation of AVMs. In the previous studies utilizing heterozygous mice, local treatment with VEGF, induction of repeated mechanical stress with magnets, and induced inflammation have lead to the formation of AV-shunting and abnormal vessels [167-170]. The preferential formation of AVMs in response to chronic vs. acute stimulus (the ear ID tag vs. induced wound) in the *Eng* and *Alk1* iKO models, respectively, strongly indicate *Eng*-deficient ECs may form AVMs in response to an increase in local inflammation at the injury site, while AVMs in *Alk1*-deficient ECs may form in response to an increase in pro-angiogenic factors/angiogenesis at the site of injury. The finding that inflammation may contribute to AVMs is supported by previous findings in that vascular lesions often form at sites of inflammation in $Eng^{+/-}$ mice (both secondary to spontaneous bleeding in the GI tract, eye or ear and induced by dextran sulfate in the intestine [169, 171]. It is believed that monocyte infiltration at the site of injury and the presence of certain cytokines, such as tumor necrosis factor-α (TNF-α), may help induced AVMs, possibly by removing vascular ENG [151]. Additionally, the Letarte group proposed that *Eng* is important in regulating endothelial nitric oxide synthase (eNOS) and that loss of *Eng* leads to increased superoxide production, instead of nitric oxide [172]. This inflammatory response has not been tested or confirmed in $Alk1^{+/-}$ mice. There is evidence that the activation of angiogenesis in *Alk1*-deficent conditions may is sufficient to lead to AVM formation. It was seen that treatment of $Alk1^{+/-}$ brains with VEGF was sufficient to cause

dysplasia [167]. In comparing to HHT patients, there has been no study focusing on how specific or equivalent stimuli in humans, e.g. piercings, affect HHT patients. Although, there is a mention that a volleyball player had a large number of telangiectases on the tips of their fingers, indicating repetitive stress leads to telangiectasia formation, but a clear relationship to genotype has not been determined [100].

The organs affected in the murine models are the same organs affected in HHT patients (discussed in detail in Chapter 1), establishing the importance ALK1 and ENG within the vasculature of these organs. One of the most striking findings is the lack of any phenotypes in the lungs in either *Eng* ablation models, even though *Alk1* cKO models consistently do and there are higher incidences of PAVMs found in HHT1 patients [64, 162]. The lack of phenotype in the pulmonary vasculature was also seen in another, albeit endothelial-specific (using Cdh5(PAC)-Cre^{ERT2}), *Eng* iKO. This may be explained, in part, from the genomic southern results in that there was low 2f to 1f conversion in Eng iKO/low dose mice. However, there is lack of any reported evidence of PAVMs in any *Eng* or *Alk1* heterozygous mice. The main reported pulmonary phenotype in adult *Eng*$^{+/-}$ mice was truncated pulmonary vasculature. It was previously suggested that this may due to the shorter pulmonary branches in mice [165], thus indicating a limitation in using mice as true model for HHT.

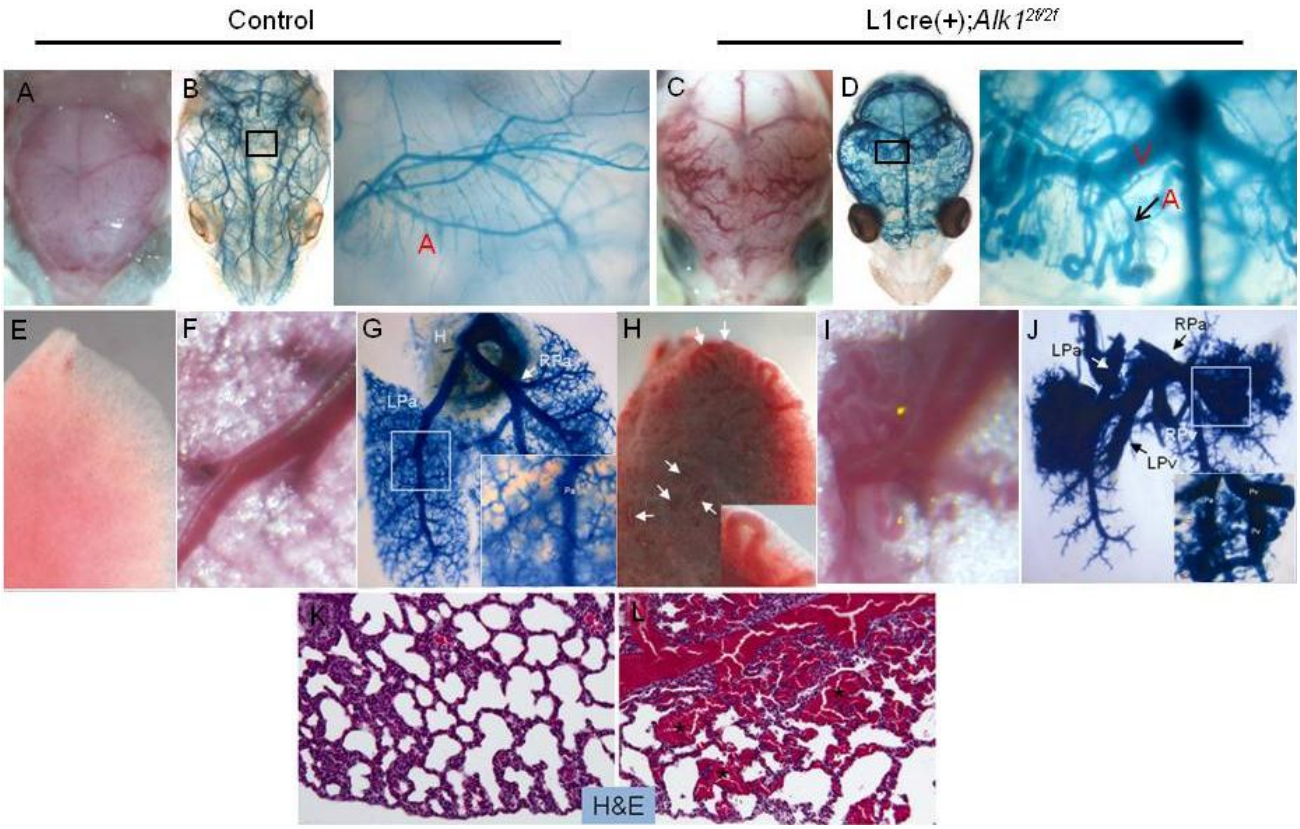

Figure 3-1. L1cre(+);*Alk1*$^{2f/2f}$ mice developed AVMs in the brain and lungs and were lethal by PN5. A) Overview of control brain vessels at PN5. B) Overview of PN5 control brain vessels after latex vascular casting. In the adjacent panel, a magnified view shows very fine microvessels in which the latex remained within arterial vessels. C) Overview of PN5 mutant shows grossly dilated vessels in the brain. D) Latex vascular casting revealed AV shunting and formation of AVMs in cerebral vessels, as evidenced with latex within the veins. E) Control PN5 lung. F) Magnified view of PN5 control pulmonary artery and vein. G) Latex vascular casting shows proper pulmonary vascular development and fine branching of vessels. H) PN5 *Alk1* cKO lungs were hemorrhagic and showed obvious vascular defects throughout the lung (exemplified by white arrows). I) Close-up up a dilated and disorganized PN5 *Alk1* cKO pulmonary artery and vein. J) Latex vascular casting revealed improper vascular branching of pulmonary vessels and large area AVMs (magnified in inset). K) Histological view of PN5 control lung. L) Histological view of PN5 *Alk1* cKO lung revealed blood cells throughout the tissue, not properly contained in vessels (denoted by asterisks). A, artery; V, vein; H, heart; LPa, left pulmonary artery, RPa, right pulmonary artery; LPv, left pulmonary vein.

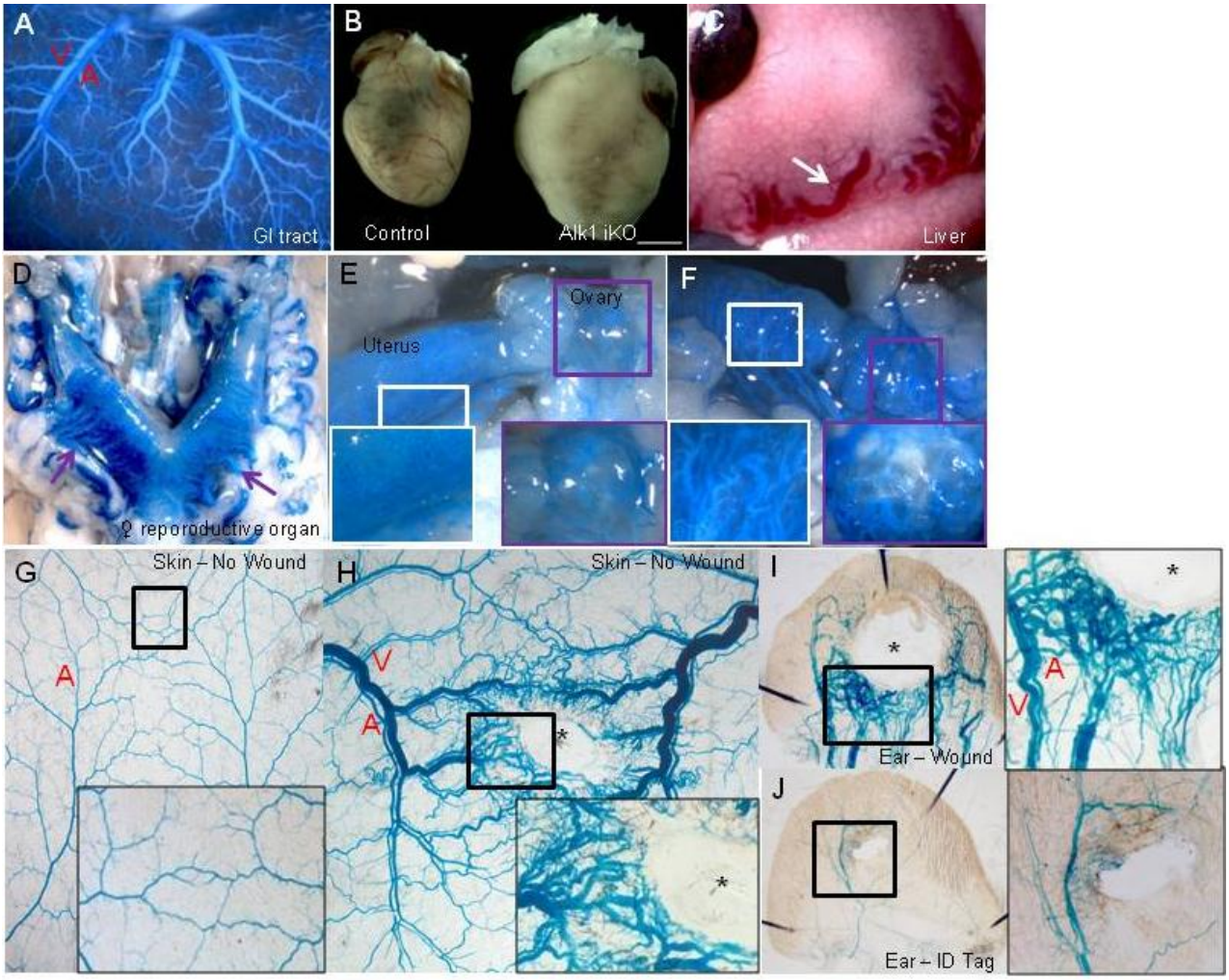

Figure 3-2. Global deletion of *Alk1*in adult mice resulted in phenotypes in the lungs, liver, heart, uterus, and in areas surrounding induced wounds, and death within 21 days after Tamoxifen introduction. A) *Alk1* iKO mice GI tracts were hemorrhagic. Latex vascular casting showed signs of AV shunting. B) *Alk1* iKO mice developed cardiomegaly. C) *Alk1*$^{3f/3f}$ iKO mice, hepatic AVMs developed (denoted by white arrow). D) The uterine vessels (purple arrows) were severely impacted in *Alk1* iKO females. E) Interestingly, the vascular malformations were restricted to uterine vessels. (white box) magnified view of uterine wall shows AV-shunting and dilated vessels in all vascular beds. (purple box) However, the ovarian vessels are not affected. F) A second example of the *Alk1* iKO female reveals the generalized uterine vascular malformations are consistent (white box). (Purple box) Though it appears the ovarian vessels appear affected, a magnified view shows that AVMs are present on the ovarian bursa, not within the ovary itself. G) Latex vascular casting of unwounded *Alk1* iKO dorsal shows no AVMs developed; however, *de novo* AVMs did arise after wound induction (H). I) AVMs formed in wound-induced ears of *Alk1* iKO mice. J) AVMs did not form in *Alk1* iKO ear tissue surrounding the ear ID tag. Scale bar denotes 3 mm. A, artery; V, vein.

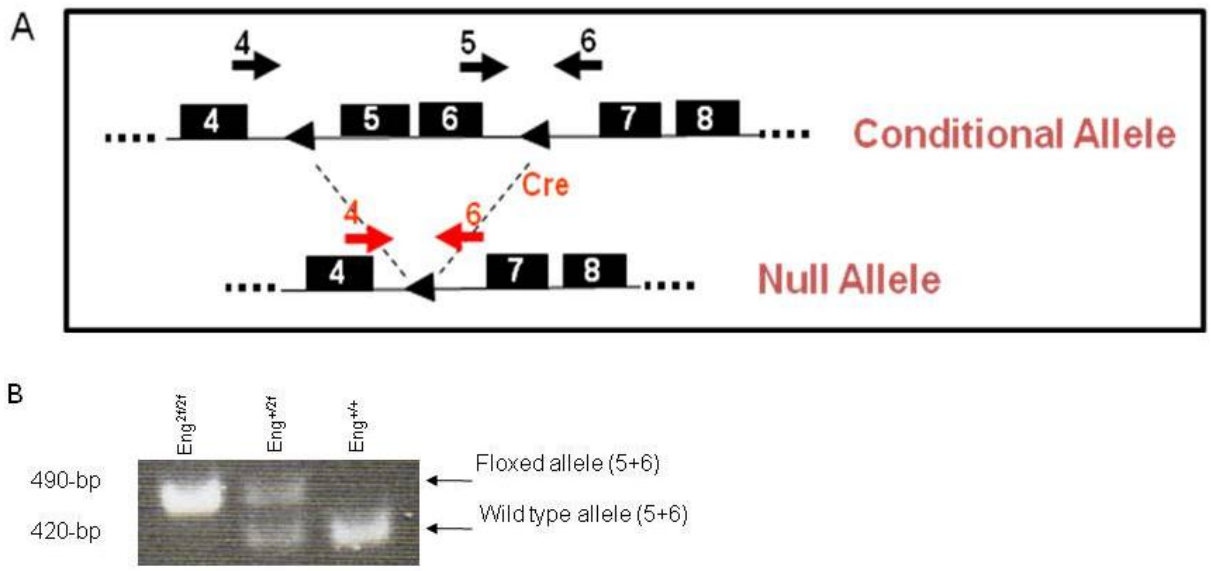

Figure 3-3. Schematic diagram of the *Eng*^{2f} conditional allele and subsequent deletion of exons 5-6 in the presence of cre. A) When in the presence of cre recombinase, homologous recombination between the *loxP* sites results in the loss of exons 5 and 6. Consequently, the null allele would be translated into a truncated, nonfunctional protein because a frameshift in the sequence in exon 7 would lead to a premature stop codon. B) Mice were PCR genotyped for the presence of the bifloxed allele using the primers 5+6. If the loxP site was present, PCR produced a product 490-bp. Otherwise the wild-type allele would have a 420-bp product.

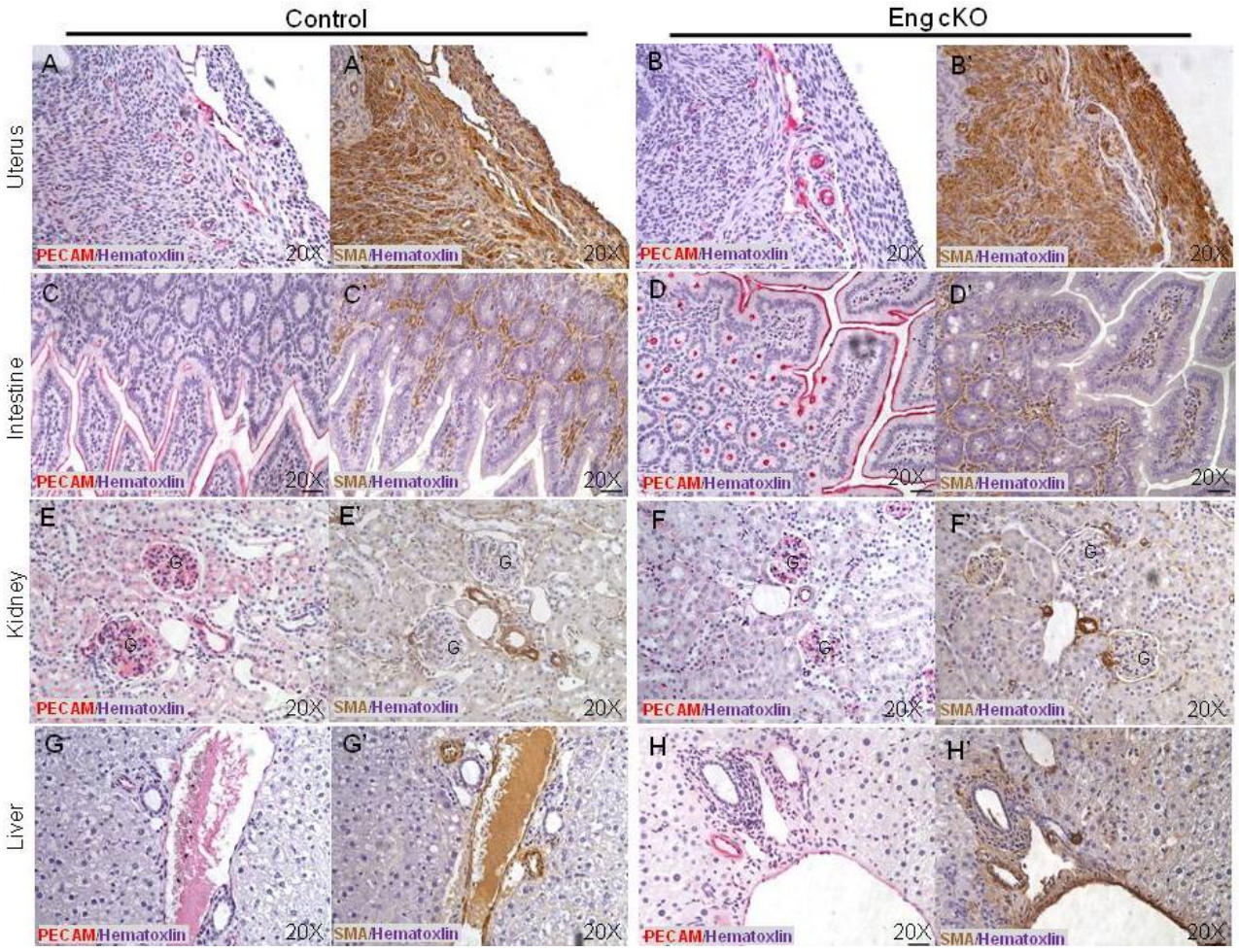

Figure 3-4. L1cre(+);*Eng*$^{2f/2f}$ (*Eng* cKO) mice were viable and vasculature in various organs were comparable to controls. Immunostaining of the endothelial layer with αPECAM-1 (red) and smooth muscle layer with αSMA (brown) of adult (aged 2-months) *Eng* cKO mice were capable was developing proper vessels. A) PECAM-1 staining of Control uterine vessels. A') SMA stain of Control uterine vessels. B, B') Eng cKO uterine vessels. C,C') Control uterine vessels. D, D') *Eng* cKO intestine. E, E') Control kidney. F, F') *Eng* cKO kidney. G, G') Control liver. H, H') *Eng* cKO liver. G, glomerulus.

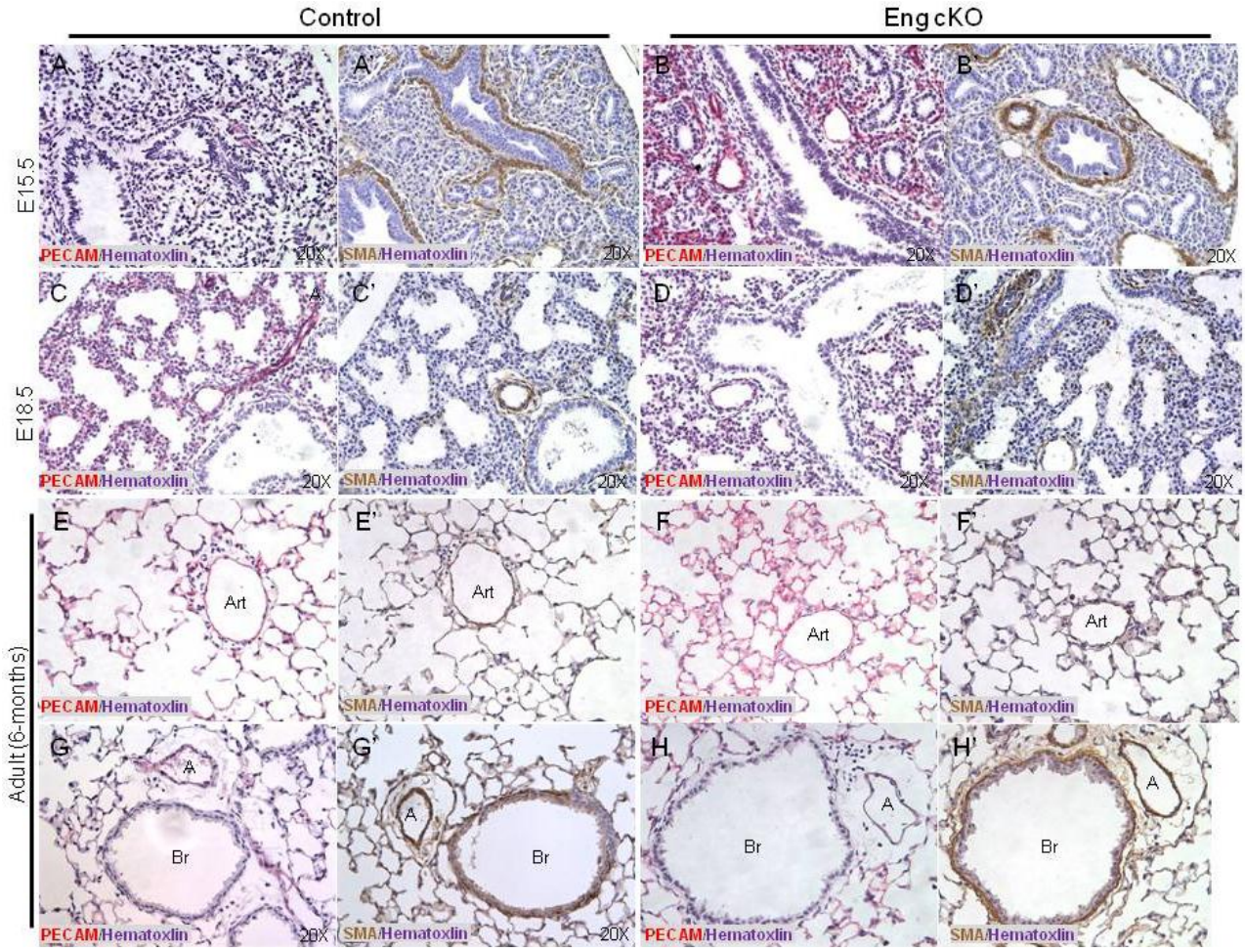

Figure 3-5. *Eng* cKO lung vasculature was comparable to controls at various stages of development and adult mice. L1cre is highly active in the lungs so more attention was given to this organ. αPECAM-1 and αSMA revealed comparable pulmonary vasculature in *Eng* cKO mice to Control littermates. A, A') E15.5 Control lungs. B,B') E15.5 *Eng* cKO lungs. C,C') E18.5 Control lungs. D,D') E18.5 *Eng* cKO lungs. E,E') Examination of the alveolar region of the adult Control lung. F,F') Alveolar region of adult *Eng* cKO lungs. G) Control lung bronchiole and artery. H) *Eng* cKO pulmonary bronchiole and artery. Art, arteriole; A, artery; Br, bronchiole.

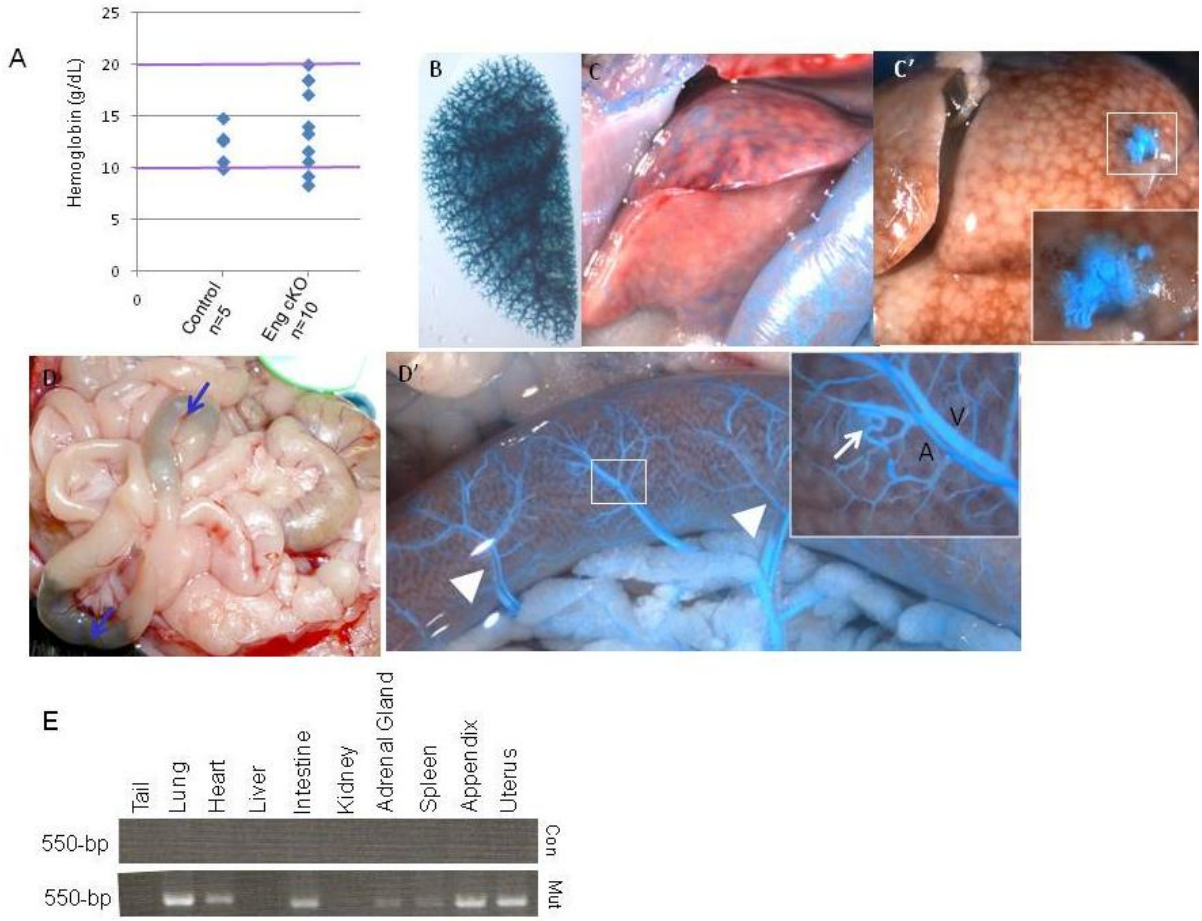

Figure 3-6. Only two old (15-month) *Eng* cKO mice displayed any vascular phenotype. A) Hemoglobin (Hgb) levels measured in adult mice (>4-months) show the majority of *Eng* cKO mice had Hgb levels within the normal range, thus not experiencing internal hemorrhaging. One of the *Eng* cKO below 10 g/dL Hgb is the mouse represented in (D). B) Latex vascular casting of 15-month old *Eng* cKO mouse revealed properly formed pulmonary vasculature, with no signs of hemorrhaging or AVMs. C) The lobe of one *Eng* cKO liver was regressed and the visibility of the blue latex suggests vascular malformations; however, this has yet to be confirmed. C') The second *Eng* cKO liver developed normally overall. However, 5 AVMs were found, exemplified by the white arrow. D) One *Eng* cKO mouse exhibited two focal hemorrhages in the GI tract (purple arrows). D') Latex vascular casting revealed mild AV-shunting in a few, not all vascular beds. (inset) One clear AVM was found that may have been the source of one hemorrhage site. E) PCR for the null allele using primers 4+6 produce a 550-bp product if the null allele was produced. Otherwise the PCR would be too large and unstable to produce. Testing for the null allele in various organs confirmed *Eng* was deleted in the lung, heart, intestine, adrenal gland, spleen, appendix and uterus, but not in the liver and kidney of *Eng* cKO mice. Control mice, which lack L1cre, did not produce any bands, indicating the null allele was not present.

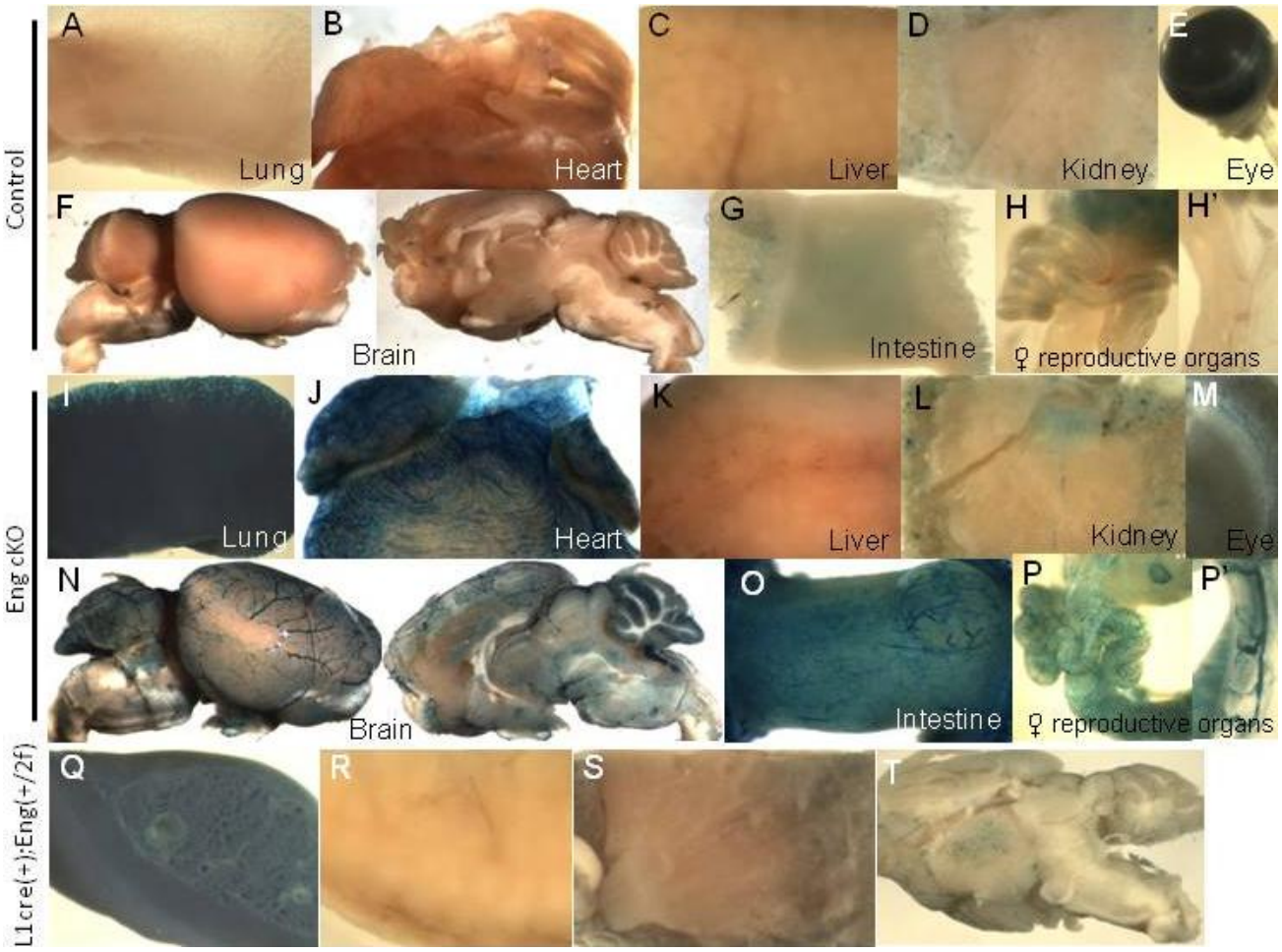

Figure 3-7. As the mice also contained the ROSA26 gene, X-gal staining of various organs was performed to confirm L1cre was active in expected organs. Control A) lung, B) heart, C) liver, D) kidney, E) eye, F) brain, G) intestine, and H) female reproductive organ were not stained by X-gal, confirming the absence of cre. Cre activity was visualized in *Eng* cKO as I) lung, J) heart, M) eye, N) brain, O) intestine, and P) female reproductive organs were stained blue with X-gal. As expected the K) liver and L) kidney were not stained. X-gal staining of select L1cre(+);$Eng^{+/2f}$ organs show the same expected X-gal staining trend. The Q) lung and T) brain stained blue, but not the R) liver or S) kidney.

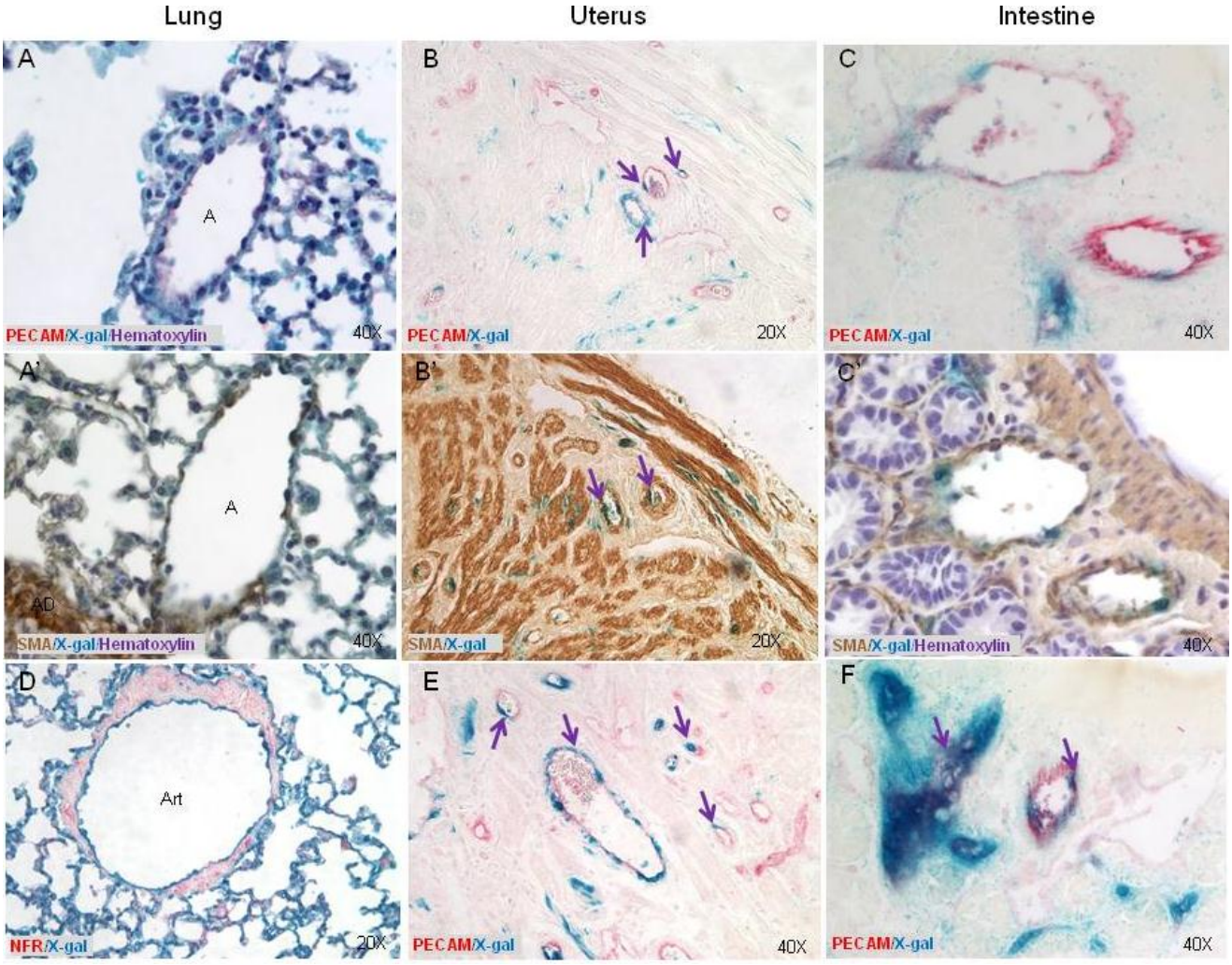

Figure 3-8. Histological evaluation of X-gal stained *Eng* cKO organs confirm cre was active specifically in ECs. The strong X-gal staining indicates that L1cre is highly active in the lung. As this is an uninflated lung section and the X-gal staining is so strong in the lung, it is difficult to differentiate between EC (A) and SMC (A') layers. D) X-gal is specific to the endothelium as the SMCs are not stained blue in the represented arteriole vessel. B, B') PECAM-1 and SMA staining of uterine vessels show L1cre is active in ECs. E) Another view of a uterine vessel reveals EC-specific X-gal staining. C,C') PECAM-1 and SMA staining of intestinal vessels reveal EC-specific X-gal staining. F) Another example of the *Eng* cKO intestinal vessel. A, artery; Art, arteriole.

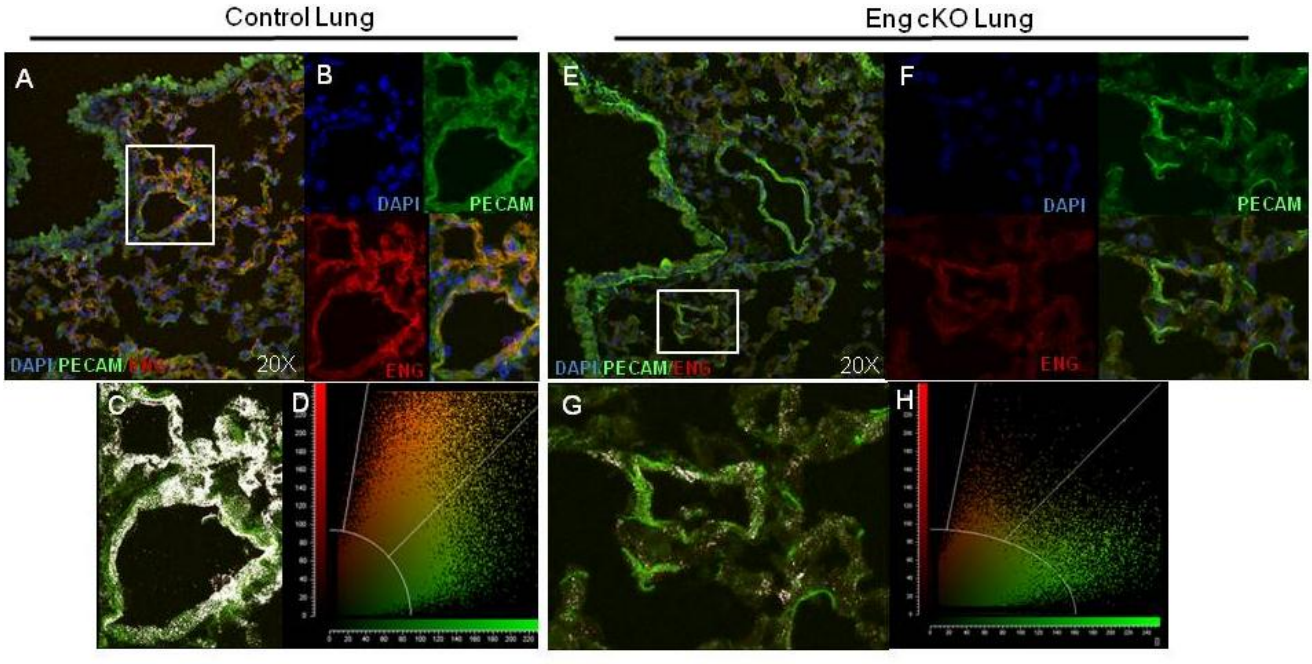

I

	Colocalization	
	Control	Eng cKO
Pearson's Correlation	0.7003	0.6312
Overlap Coefficient	0.86	0.8297
Colocalization Rate	61.07%	28.61%

Figure 3-9. Colocalization staining of PECAM-1 and ENG. The number of ECS expressing ENG were reduced in adult *Eng* cKO lungs. Overview of a lung cross section shows αENG expression was reduced in *Eng* cKO mice (E) compared to Control littermates (A). An arterial vessel was selected from the Control (B) and *Eng* cKO (F) lungs and magnified. Colocalization between PECAM-1 and ENG were compared (denoted by white pixels, C, G) and quantitated. D,H) graphical representation of colocalization rate (area between two straight lines) confirmed that the number ECs expressing ENG was reduced in *Eng* cKO. I) Numerical representation show there was ~50% colocalization in the *Eng* cKO mice.

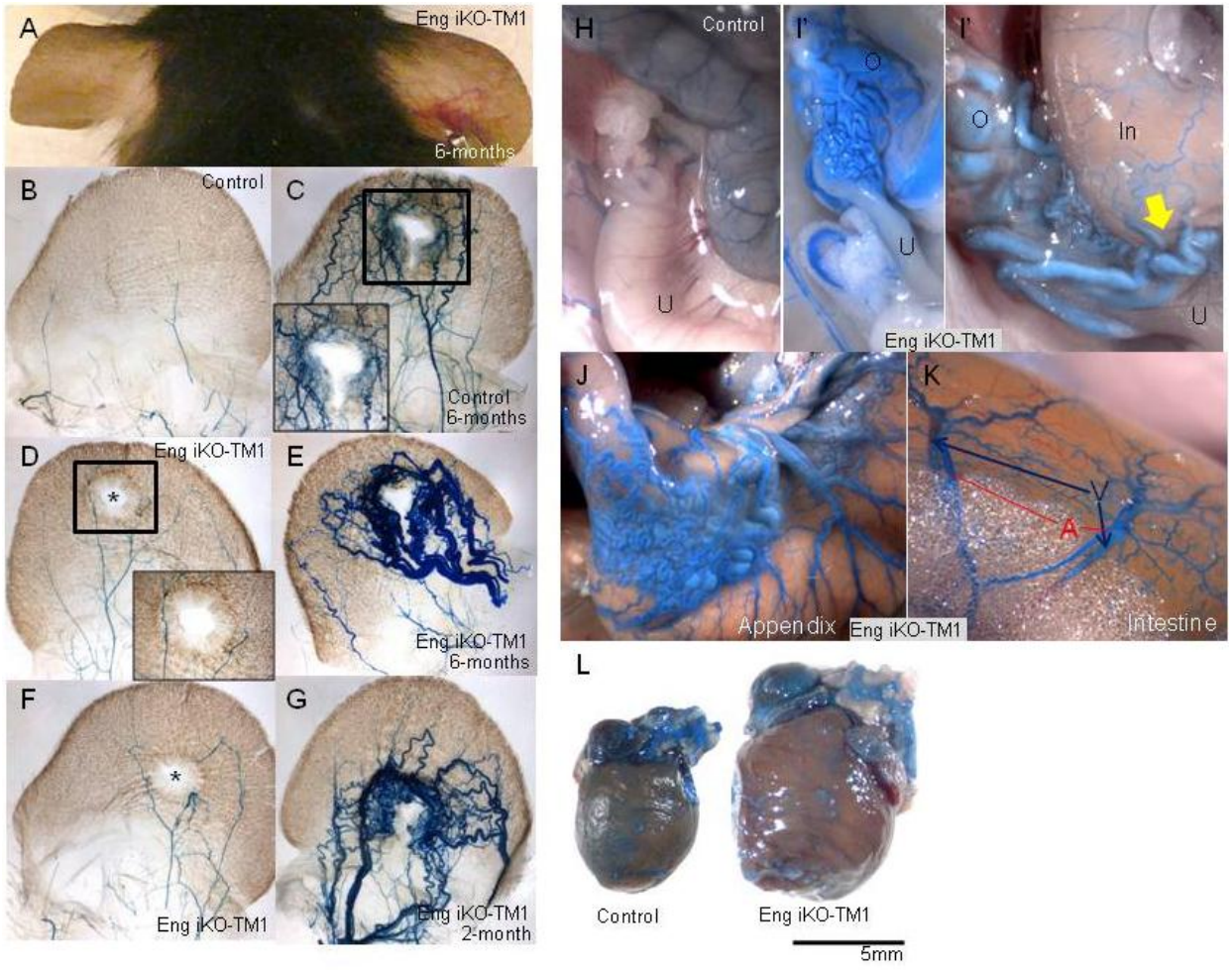

Figure 3-10. *Eng* iKO mice given a single IP injection of high dose TM were viable and phenotypes developed much more slowly than *Alk1* iKO mice. A) The only obvious phenotype was the development of telangiectases in ear tissue surrounding the ear ID tag, shown here 6-months after tamoxifen treatment. B) Latex injection of control uninjured ears act as control of how the latex dye does not readily enter the microvasculature of the ear. C) Vascular latex casting of the systemic vessels after 6 months demonstrates many defined microvessels in the ear tissue surrounding the ear tag. E) Conversely, dilated, tortuous vessels and AVMs were seen in *Eng* iKO-TM1/high dose mice. G) A noticeable dilation of vessels surrounding the tagged-ear tissue was slow to progress, with the abnormal vessels visible by 2-months. D) Control and F) *Eng* iKO-TM1/high dose mice given a 2-mm wound in the untagged ear did not develop AVMs. H) Control female reproductive organ after latex. Latex casting displayed gross vascular defects in the ovaries and fallopian tubes, but not uterus, in females 5-months (I) and 6-months (I') after TM. Though AV-shunting was commonly seen in the appendix (J) and intestine (K), there were two *Eng* iKO-TM1/high dose mice that demonstrated severe AVMs in the appendix. *Eng* iKO-TM1/high dose collected more than 2-months after TM displayed cardiomegaly (L).

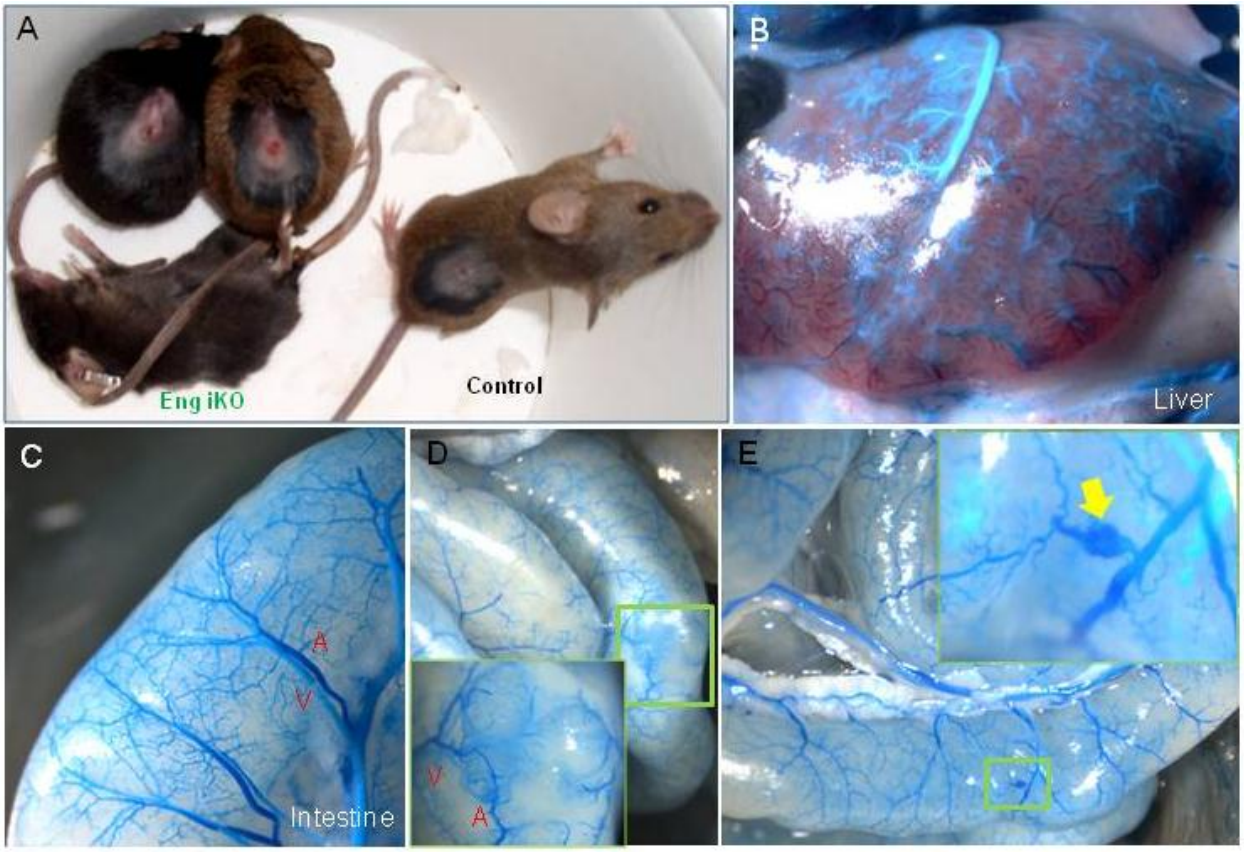

Figure 3-11. *Eng* iKO-TM2 or 3/high dose died within seven days of treatment. A) *Eng* iKO-TM3/high dose mice were lethargic, hunched, and in some cases close to death by day seven after TM. B) 3/17 *Eng* iKO-TM3/high dose mice had abnormal livers. C,D,E) *Eng* iKO-TM3/high dose mice often displayed distended intestines, and in some case, not all, hemorrhaging and AV shunting. (inset of D) Magnified view of vessels revealed dilated arteries and veins, in addition to massive AV-shunting, but no obvious vascular malformations. E) A small AVM in the intestine was found in one mouse.

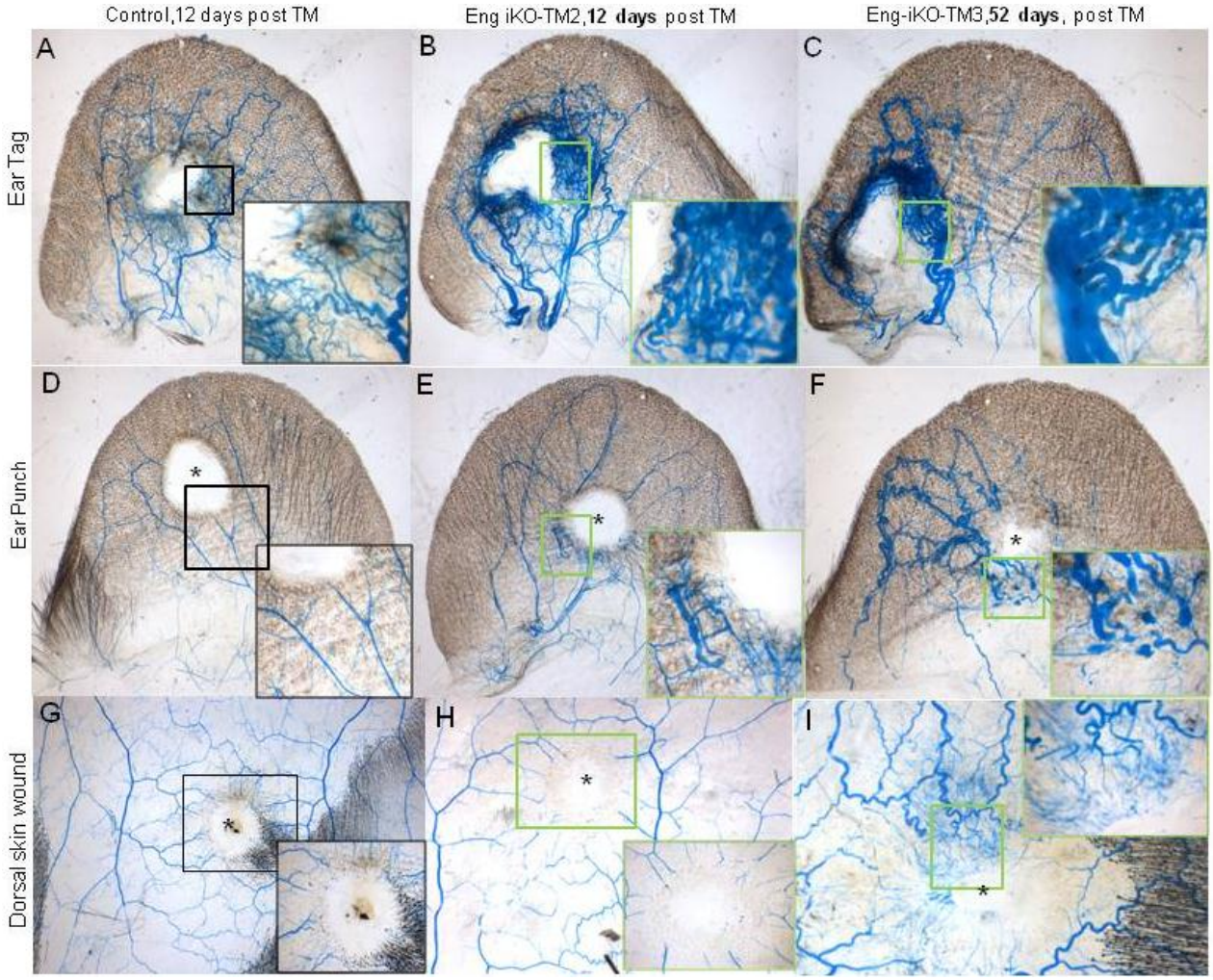

Figure 3-12. *Eng* iKO mice given two to three low doses of TM developed the same pattern of vascular lesions in a shorter time period. A) Fine microvessels properly form in control ID-tagged ear tissue. B) *Eng* iKO-TM2, low dose mice were capable of developing dilated, tortuous vessels by twelve days after TM treatment. C) *Eng* iKO-TM3/low dose mice displayed gross AVMs in 52 days in a similar manner of *Eng* iKO-TM1/high dose mice. No AVMs developed in control ear punch (D) nor skin wound (G), *Eng* iKO-TM2, low dose ear punch (E) nor skin wound (H), or *Eng* iKO-TM3/low dose ear punch (F) nor skin wound (I). Although, there appears to be mild telangiectases in the *Eng* iKO-TM3/low dose ear punch (magnification of F). It should be noted that images are representations of the most extreme phenotypes. Other *Eng* iKO, low dose do not show this phenotype. * Asterisks denote wound site.

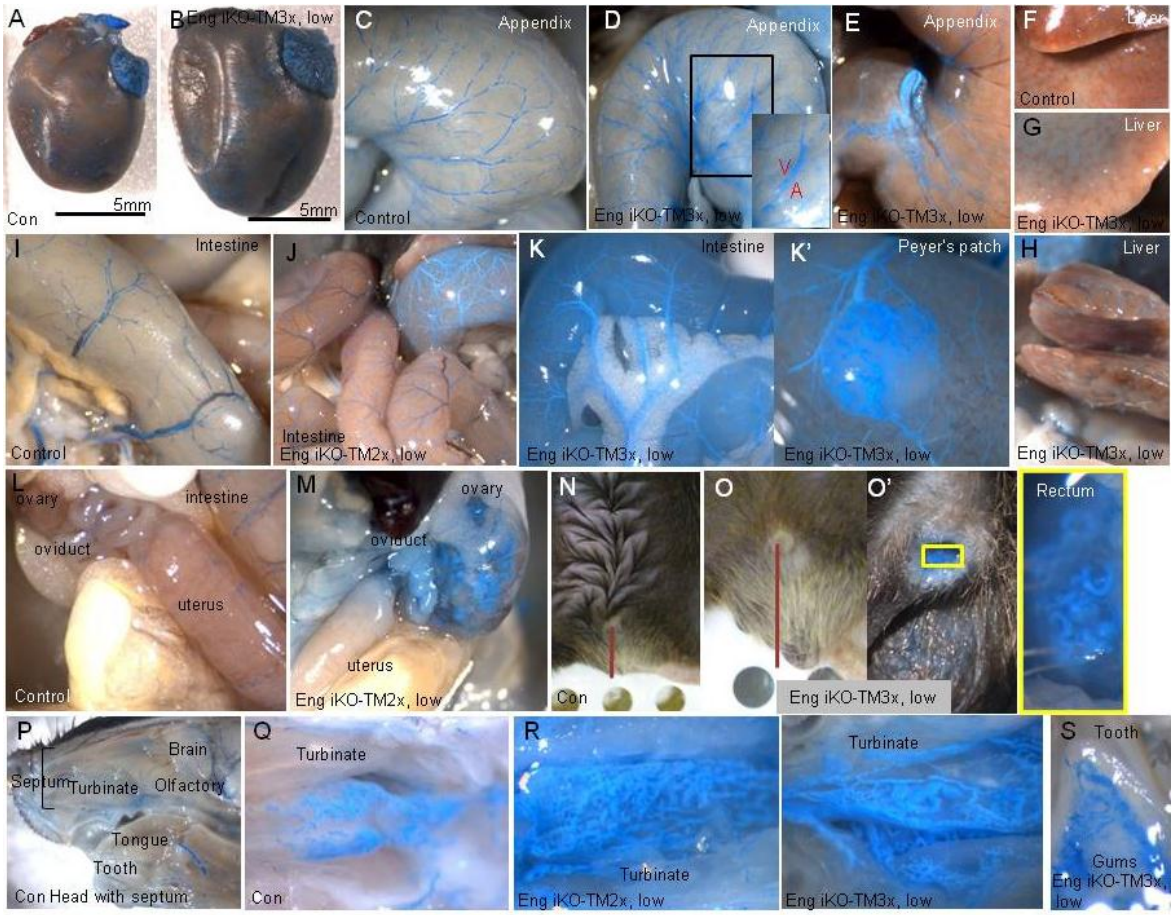

Figure 3-13. *Eng* iKO-TM2 or 3/low *dose* developed vascular phenotypes in more consistent manner but with variable severity. *Eng* iKO/low dose mice developed cardiomegaly (B), as compared to A) control littermates. The appendix (C-E), liver (F-H), GI tract (I-K), female (L-M) and male (N-O) reproductive organs, and head vessels (O-S) were affected in *Eng* iKO/low dose mice. C) Control appendix. D) In many cases, there was mild AV shunting in the appendix of *Eng* iKO/low dose mice. E) 1/17 *Eng* iKO-TM3, low dose mice developed an AVM 3-months after tamoxifen. In many cases, the G) iKO-TM2/3/low dose livers were similar to F) controls. H) However, 2/17 iKO-TM3, low dose livers were regressed. I) Control liver, with peyer's patch present. J-K) Varying degrees of multifocal AV-shunting was found in all *Eng* iKO/low dose mice intestines. K) In 2/17 *Eng* iKO-TM3/low dose mice, AVMs developed specifically within the peyer's patch. L) Control female reproductive organ. M) AVMs developed specifically in ovarian, not uterine vessels of all *Eng* iKO/low dose females. N) Control scrotum, with measurement from penis to anus. O) *Eng* iKO-TM3/low dose scrotum is visibly larger. O') Latex vascular casting revealed AVMs in the rectum (magnified view in yellow box). P) Anatomy of the control head. Q) Control turbinate has picked up some latex. R) Two examples of *Eng* iKO/low dose mice that developed AVMs within the turbinate. S) 1/17 *Eng* iKO-TM3/low dose mouse developed vascular malformations in gums.

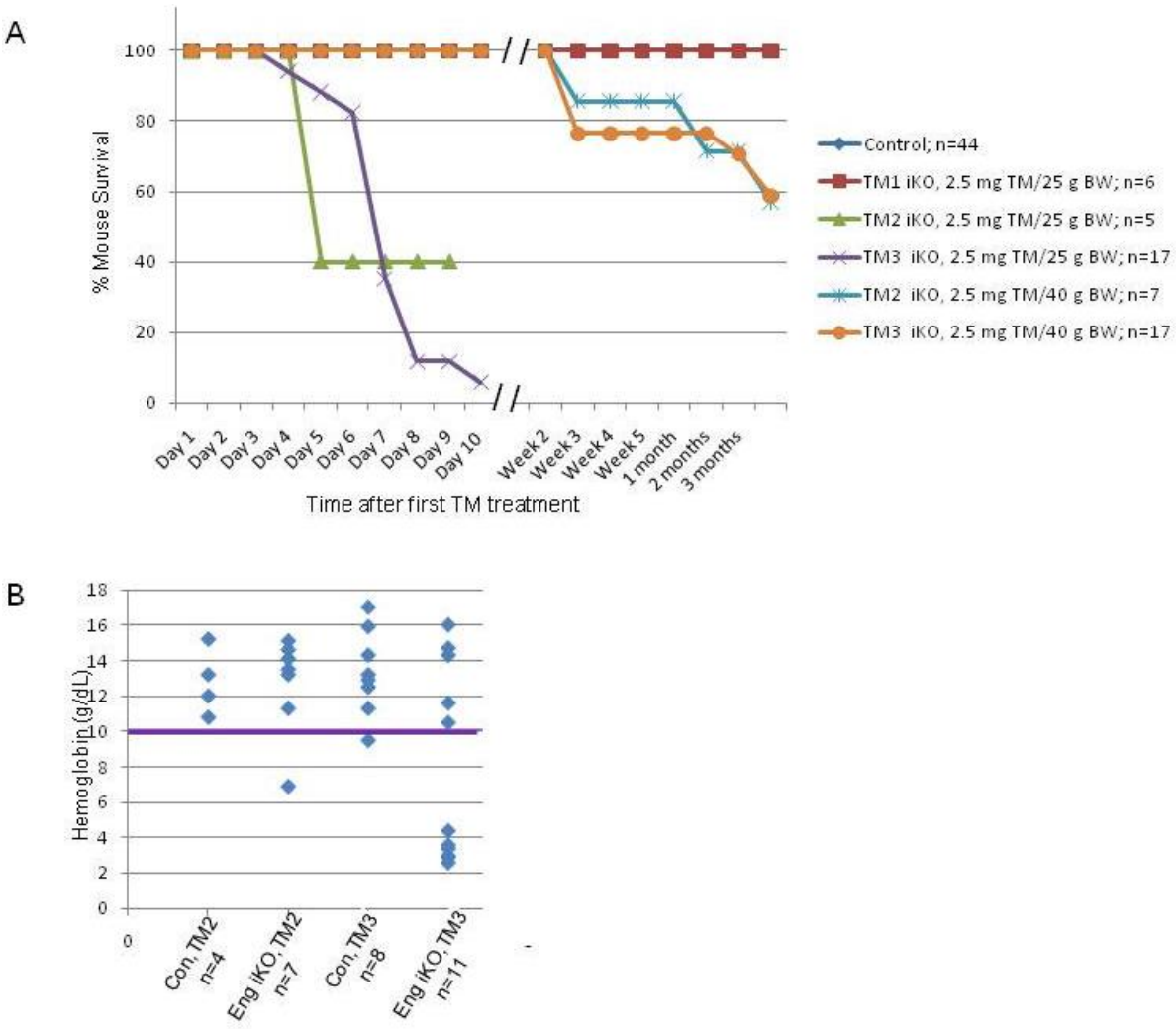

Figure 3-14. Kaplan-Meier survival curve for each *Eng* iKO treatment and Hgb measurement of *Eng* iKO/low dose mice. A) A summary Kaplan-Meier survival curve for each *Eng* iKO treatment. Controls were pooled together as there was no difference in longevity in response to TM among the Control groups. B) Hgb levels in *Eng* iKO-TM2 or 3/low dose and Controls were compared 2 to 3 months after TM treatment. Interestingly, it was observed that despite having low Hgb counts in a few *Eng* iKO-TM3/low dose mice, not all presented any overt health concerns besides the appearance of white paws.

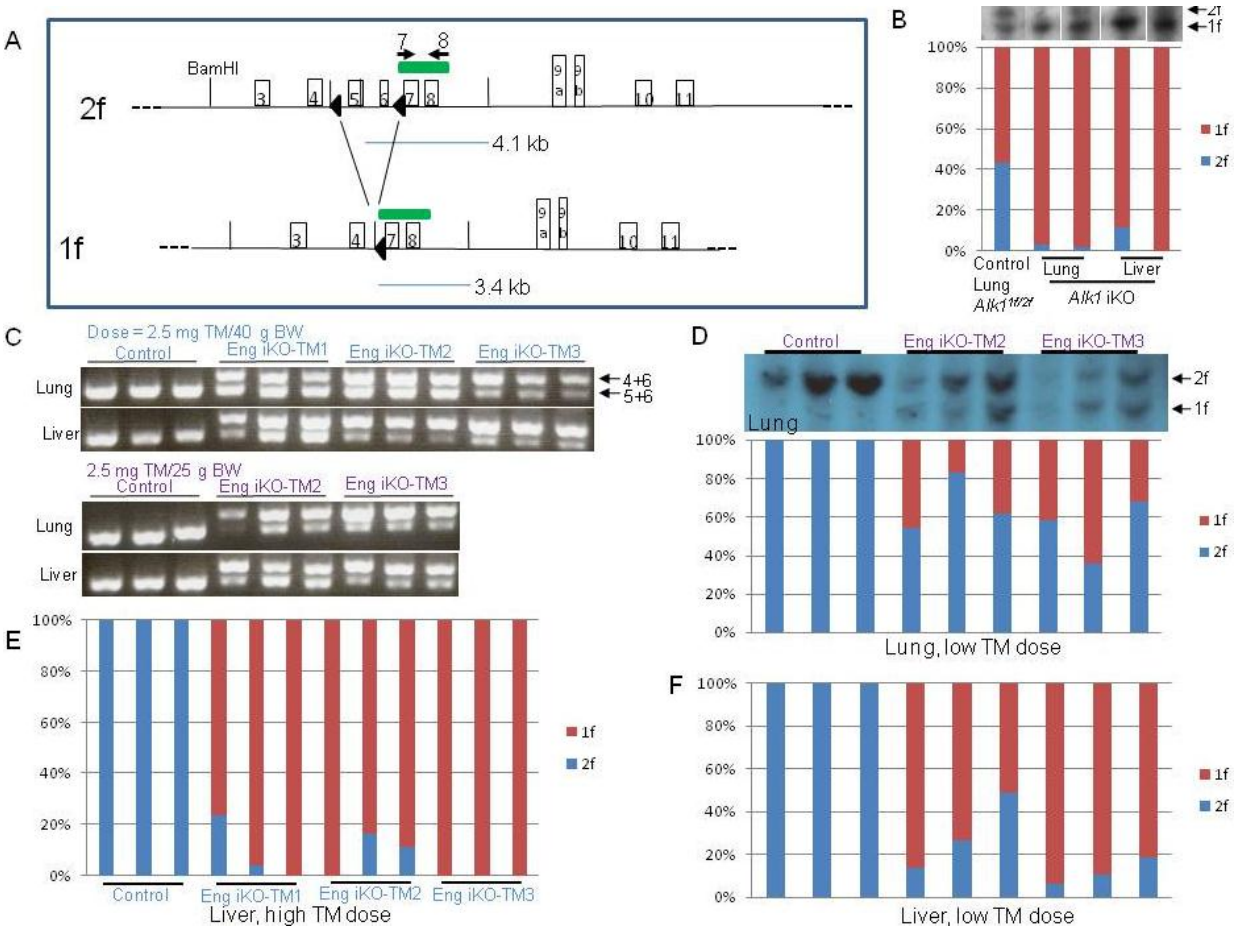

Figure 3-15. Testing efficiency of conversion of the 2f to 1f allele conversion between the different TM treatments in *Eng* iKO mice to *Alk1* iKO mice. A) Schematic for genomic southern blot of Eng. The gDNA was digested with BamHI (denoted by black lines). A probe was generated that would recognize any fragments containing exons 7-8. For the 2f allele, the probe would recognize a 4.1-kb fragment. For the 1f allele, a 3.4-kb fragment would be detected. B) Southern blot of *Alk1* iKO lung and liver samples provides a comparison point of the efficiency of the *Alk1* 2f to 1f conversion with the single high dose of TM. C) Genomic PCR using primers 5+6 (floxed allele) and 4+6 (1f allele) was done to confirm the genotype of each sample used. At least three samples each of Controls and each TM treatments were collected. The lung and liver were tested. D) Southern blot of Eng iKO/low dose lungs with graphical representation of quantification of the 2f to 1f allele from each sample. Multiple injections of the low dose do not appear to effective convert the 2f to 1f allele, which may explain the lack of pulmonary phenotype. E) The use of the higher dose of TM leads to >75% conversion to the 1f allele in the liver. F) TM appears to be much more effective in the liver overall as there is a higher 2f to 1f conversion rate in liver samples taken from the same Eng iKO/low dose mice as in C. Additionally, increasing the number of injections lead to higher conversion rates.

CHAPTER 4
SPATIOTEMPORAL ROLE OF ENDOTHELIAL TGF-β SIGNALING DURING DEVELOPMENT

In early studies and for a long time, investigations on the TGF-β signaling mechanism in ECs have focused on the interaction between the type I receptors, ALK1 and ALK5 [148, 155]. This relationship is of interest to those in the HHT field, despite there never being a connection between ALK5 and HHT, because there was a belief that an aberrant balancing act between ALK1 and ALK5 within ECs contributed to the development of HHT lesions. However, we previously provided evidence that ALK1 signaling is independent of ALK5 and, more surprisingly, TGFBR2 as mice in which *Tgfbr2* and *Alk5* were ablated using the EC-specific L1cre line were viable [64]. The indication that ALK1 signaling is separate from the TGFBR2, and instead prefers BMP signaling [65, 66], raises the question of whether TGF-β superfamily ligands are the physiological ligands for ALK,1 as previously believed. It was quite curious that the cKO mice were seemingly completely unaffected by the loss of *Alk5* and *Tgfbr2* within the ECs. Thus, another question that arises is whether different TGF-β signaling members actually have spatiotemporal roles during embryogenesis, particularly in the endothelium. To examine this we investigated the mechanism of cerebrovascular development.

Neurovascular Development

Along with the vasculature, the neural system is one of the first organ systems to develop *in vivo* [173]. The development of the neurovasculature is driven solely through angiogenesis. It was initially believed that angiogenesis in the central nervous system (CNS) was a passive process, in which vessels develop in response to the needs of the developing brain. However, there is mounting evidence suggesting that CNS

angiogenesis is indeed a dynamic process [173]. Additionally, although it is accepted that there are overlapping transcription factors that regulate both neurogenesis and CNS angiogenesis, it is still unknown whether neuronal development and cerebral angiogenesis occurs independently. There are two categories of brain vessels: the pial vessels (which develop into the venous sinuses) and the periventricular vessels (the arterial networks). Pial vessels are present more widely throughout the brain at E9, whilst periventricular vessels are the dominant vessels within in the telencephalon/forebrain region [174]. For this study the periventricular region is of interest. Within the telencephalon, EC migration of periventricular vessels begins directionally from dorsal to ventral then lateral to medial (Figure 4-7D, top image). This mechanism is still largely unknown, thus we sought to see whether endothelial TGF-β signaling pathway may be involved.

Nishimura reported from *in vitro* studies that paracrine astrocyte-EC signaling was essential in maintaining vascular integrity. Specifically, they found that the integrin αvβ8 expressed on astrocytes were responsible for activating the latent TGF-β ligand, which then induce TGF-β signaling on ECs in order to regulate various angiogenic downstream targets [175]. However, this has yet to be confirmed *in vivo*.

Integrin Activation of TGF-β Subfamily Ligands

Synthesis and activation of the TGF-β subfamily of ligands is a tightly regulated process [176, 177] (Described in detail in Figure 4-1). As mentioned, TGF-β are initially secreted as latent proteins bound by the LAP that may be deposited in the ECM until released, typically in a context and tissue dependent manner. There are several modes by which the TGF-β may be freed. Environmental changes, such as heat and pH changes, have been shown as examples [178]. Thrombospondin-1 (Tsp-1) is a major

proteolytic activator of the ligand. Tsp-1 acts by binding the LAP, causing a conformational change in the LAP that forces it to lose its hold of the TGF-β ligand. Integrins are also well known TGF-β ligand activators [178].

Integrins are heterodimeric receptors that contain noncovalently associated α-subunit and β-subunits. In mammals, the combinations of eighteen identified α-subunits (α1-9, IIb, D, E, L, M, R, V, X) with eight different β-subunits (β1-8) make up at least 24 different integrins [179]. Integrins activate the ligands by recognizing and binding to specific Arginine-Glycine-Aspartate acid (RGD) sequences found within the LAP. With the integrin bound, the LAP is removed from the TGF-β ligand by cleavage or a conformational change [179, 180]. TGF-β2 lacks the RGD sequence, thus integrin-mediated activation is relevant only for TGF-β1 and TGF-β3 [178].

Functionally, integrins are involved in a variety of cellular processes, most notably cell adhesion, but has been found to be important in angiogenesis as some are found, particularly *α*v, to be upregulated during angiogenesis *in vivo*. Of the 24 types of integrins identified, eight have been associated with endothelial cells [180, 181]. Two classes of embryos were found from conventional knockout models of αv (*itgav*$^{-/-}$) and of integrin αvβ8 (*itgb8*$^{-/-}$) [182, 183]. The majority (~80%) of Class I embryos from each knockout model died at midgestation. The remaining 20-30% of embryos developed cerebral hemorrhaging starting around E10-12. These mice were born with brain hemorrhages and cleft palates (as previously reported in *Tgfb3*$^{-/-}$ mice [184]) and died shortly after birth. A double knockout of the TGF-β1 and β3 (*Tgfb1*$^{RDE/RDE}$/*Tgfb3*$^{-/-}$) ligands resulted in similar cerebral hemorrhaging within the forebrain at midgestation. In this model the aspartic acid of the TGF-β1-LAP RGD sequence was changed to

glutamic acid and the TGF-β3 was a conventional KO. The recurrent cerebral hemorrhaging seen in the general knockouts suggests TGF-β signaling via integrin-mediated activation of the TGF-β1 and TGF-β3 ligands is vital for proper neurovascular development, particularly in the periventricular vessels [185]. Additionally, the period when the phenotype was seen in the various models from E10.5-13.5, indicates this action occurs specifically during midgestation. Furthermore, conditional knockout models of *itgav* and *itgb8* showed αvβ8 expressed on the neuroepithelium (deleted using *Nestin*-cre and *GFAP-cre*), not ECs (deleted using *Tie2*-cre), are required [186, 187]. More recently, a conditional murine knockout model of *Tgfb3*-cre;*Alk5*$^{fl/fl}$ was characterized in which the authors reported cerebral hemorrhaging in embryos. However, is not clear when the cerebral hemorrhaging first appeared in the *Tgfb3*-cre;*Alk5*$^{fl/fl}$ as E14.5 was the earliest reported stage [188]. Though, the phenotype correlation among the models strongly indicates that neural αvβ8 is involved in establishment of cerebral vasculature by activating the TGF-β ligands, it is not clear if the mechanism continues onto another neuroepithelial cell or another cell type. Furthermore, the consistent and close timing of the specific phenotype occurring during late-mid gestation also suggests that this establishment is essential during a specific time period.

Thus, we tested *in vivo* whether paracrine astrocytic integrin activation of TGF-β signaling on ECs during midgestation is essential for proper cerebral vessel development. We focus more downstream of the TGF-β pathway, on TGFBR2 and ALK5, and expect that deleting each from ECs at midgestation would result in the same cerebral hemorrhaging.

Results

Characterization of an Endothelial-Specific Alk1-*cre Knock-in Line*

TGFBR2 and ALK5 are involved in a variety of cellular processes and expressed on many cell types. There have been previous reports of conditional murine knockouts wherein each receptor has been ablated from ECs using different EC-specific cre deleter lines. *Tie1*-cre*;Alk5*$^{fl/fl}$ and *Tie1*-cre*;Tgfbr2*$^{fl/fl}$ recaptitulated the null phenotypes [55, 177]. Although, these models may not reflect the true role of ALK5 and TGFBR2 in ECs or angiogenesis because cre activity in the *Tie1*-cre line begins around E8 [189], which is before any embryonic vascular events commence at E8-9. We previously described mouse models in which *Alk5* and *Tgfbr2* were deleted in ECs using the L1cre line, in which cre is driven by a 9.2-kb region of the *Alk1* promoter. In this line cre is active beginning at late gestation, at E13.5. The knockout mice were viable and seemingly unaffected by the loss of either receptor in the ECs, but the lack of phenotype could be due to the late cre activity. The use of *Tie2*-cre, in which cre begins by E8.5 [190], yielded variable results. *Tie2*-cre(+);*Alk5*$^{fl/fl}$ mice were able to survive past midgestation; however, the *Tie2-cre;Alk5*$^{fl/fl}$ mice displayed cardiac edema that resulted in cardiac failure and death by E13.5 [191]. As for *Tie2*cre-*Tgfbr2*$^{fl/fl}$ embryos, 65% mimicked the conventional KOs, and the remaining ~35% that survived past midgestation were phenotypically indistinct from control littermate up to E12.5, but by were embryonic lethal by E13.5. The authors reported, but did not show, that mutant embryos were edemic and hemorrhagic, and stated the cause of death was presumably “cardiovascular insufficiency” [192]. More recently, the tamoxifen-inducible endothelial-specific VE-Cadherin (Cdh5(PAC)-Cre^{ERT2}) line was used to delete *Tgfbr2*$^{fl/fl}$ at E11.5, which resulted in embryonic lethality between E15-18 due to cardiac defects [193].

Interestingly, the authors of the *Tie2-cre* and Cdh5(PAC)-Cre^{ERT2}-mediated ablation models discussed cerebral hemorrhaging, however, did not further elaborate on the phenotype as the studies focused more on cardiac development [151, 191, 193].

To assess the importance of TGFBR2 and ALK5 on ECs during midgestation as well as resolve timing issues related to the activation of cre, we generated and used a novel EC-specific cre knockin line (*Alk1*^{GFPcre}*),* in which a GFPCre fusion gene was inserted into the *Alk1* locus (Figure 4-2A). The GFPcre cassette is inserted into intron 3 and replaces exons 4-8. Cre is still expressed in *Alk1*-expressing endothelial cells because a 9.2-kb region of the *Alk1* promoter, up to exon 2, is sufficient to drive *Alk1* expression. In the *Alk1*^{GFPcre} line, cre is expressed beginning at E9.5 in a patchy manner throughout the embryo (Figure 4-1B), including the head (Figure 4-2B'). Cre expression is drastically increased at E10.5 and active in ECs of all organs (Figure 4-1C), in a similar fashion to previously reported *Alk1* expression studies. Further analysis of transverse sections of the X-gal stained head revealed *Alk1*^{GFPcre} revealed cre was active in ECs invading the neuroepithelium (Figure 4-1D and D').

Endothelial-Specific Deletion of Tgfbr2 *and* Alk5 *Resulted in Cerebral Hemorrhaging Beginning at E11.5 and Embryonic Lethality by E15.5 and E14.5, Respectively*

It has been reported that *itgb8*$^{-/-}$ embryos that survived to birth, *Tgfb*1$^{RDE/RDE}$;*Tgfb*3$^{-/-}$ embryos and surviving *itgav*$^{-/-}$ embryos exhibited specific cerebral hemorrhaging within the ganglionic eminence (GE) during late-mid gestation, indicating a vital role of TGF-β signaling in proper development of the neurovasculature. Furthermore, it was shown that specifically deleting *Itgb8* and *itgav* in ECs, using *Tie2*-cre, did not result in any vascular defects, but doing so in the neuroepithelium, using *Nestin*-cre, did. This suggests that αvβ8 and *αv*-integrins within ECs are not essential in cerebrovasular

development. However, it is not clear whether the activated ligand binds to another neuronal or a vascular cell. When our collaborators, the McCarty lab in Texas, used Nestin-cre to ablate *Tgfbr2* in neuroepithelial cells, Nestin-cre(+);*Tgfbr2*$^{fl/fl}$ mice survived with no obvious phenotypes or other developmental defects, forgoing the possibility that another neuronal cell is involved (Data not shown). Conversely, when *Tgfbr2* or *Alk5* was silenced in ECs, there were no live *Alk1*^{GFPcre}*;Alk5*$^{fl/fl}$*(Alk5* cKO*)* nor *Alk1*^{GFPcre}*; Tgfbr2*$^{fl/fl}$ *(Tgfbr2* cKO*)* pups were born, indicating these were embryonic lethal. Embryos were collected at embryonic day (E)10.5, E11.5, E13.5, E14.5, E15.5, and E18.5 to determine whether the cerebral hemorrhaging occurred and when, as well of time and possible causes of death.

At E10.5, *Tgfbr2 and Alk5* cKO *embryos* were indisintguishable from control littermates (Figure 4-3A,B). It should be noted that controls were littermates that lack the *Alk1*^{GFPcre}*;Alk5*$^{+/fl}$ or *Alk1*^{GFPcre}*;Tgfbr2*$^{+/fl}$. At E11.5 all *Alk1*^{GFPcre}*;Tgfbr2*$^{fl/fl}$ and *Alk1*^{GFPcre}*;Alk5*$^{fl/fl}$ exhibited cerebral bleeding within the forebrain region (Figure 4-3C,D). The hemorrhaging remained largely within defined areas of the brain likely the GE and midbrain then progressively worsened during gestation. Interestingly, hemorrhages were only seen in the central nervous system (CNS), and no other organs appeared to be affected. By E13.5 the head of *Alk1*^{GFPcre}*;Tgfbr2*$^{fl/fl}$ embryos were edemic (Figure 4-3E). *Alk1*^{GFPcre}*;Alk5*$^{fl/fl}$ mice died a day earlier but did not exhibit the same level of edema *as Alk1*^{GFPcre}*;Tgfbr2*$^{fl/fl}$ embryos (Figure 4-3F). Additionally, the chest cavity of *Alk1*^{GFPcre}*;Alk5*$^{fl/fl}$ embryos appeared distended, suggesting *Alk1*^{GFPcre}*;Alk5*$^{fl/fl}$ may have had cardiac defects. *Alk1*^{GFPcre}*;Tgfbr2*$^{fl/fl}$embryos died by E14.5, with littermates undergoing various stages of death, from having very faintly beating hearts and close to

death or already dead and undergoing desorption (Figure 4-3G). There was bilateral cerebral bleeding in the cKO models starting at E11.5 (Figure 4-3H) and the bilateral bleeding also worsened over time, represented here at E13.5 (Figure 4-3I). In some, not all, *Alk1*^{GFPcre}*;Tgfbr2*$^{fl/fl}$ *and Alk1*^{GFPcre}*;Alk5*$^{fl/fl}$ embryos, hemorrhages were seen along the spinal cord (Figure 4-3J and K).

Alk1^{GFPCre};Tgfbr2$^{fl/fl}$ *and Alk1*^{GFPcre}*;Alk5*$^{fl/fl}$ *Embryos Form Glomeruloid-like Vascular Structures in the Ganglionic Eminence*

H&E staining and PECAM-1 (red) staining for ECs of transverse sections of the E10.5 embryonic head revealed that *Tgfbr2*$^{fl/fl}$ and *Alk5*$^{fl/fl}$ cKO embryos (a representative cKO section shown in Figure 4-4B and B') developed proper vessels comparably to control littermates (Figure 4-4A and A'). By E11.5 H&E staining shows the heads of *Alk1*^{GFPcre}*;Tgfbr2*$^{fl/fl}$ *and Alk1*^{GFPcre}*;Alk5*$^{fl/fl}$ *have* perforations within the GE (Figure 4-4G and K), as compared to the control (Figure 4-4C). Interestingly, PECAM-1-staining revealed that vascular endothelial cells were clumped into glomeruloid-like structures, which are not seen in control littermates (Figure 4-4D) in both *Alk1*^{GFPcre}*;Tgfbr2*$^{fl/fl}$ and *Alk1*^{GFPcre}*;Alk5*$^{fl/fl}$ *models (Figure 4-4H and L)*. The aggregate of EC cells suggest the lack of proper EC migration. The aberrant vessel development appears to be specific to the neuroepithelium as the vessels lying just outside the neuroepithelial tissue are not dilated (Figure 4-4I and M) and are comparable to the control vessels (Figure 4-4E). At E11.5 the neurovasculature appears to be the only organ system to be affected as the heart and lungs develop as control littermates (Figure 4-4F, J, and N).

Alk1^{GFPCre};Tgfbr2$^{fl/fl}$ *Embryos Die by E14.5 with CNS-Specific Vascular Defects, but all Other Organ Systems are Largely Unaffected*

H&E stained sections of E13.5 heads confirmed much of the hemorrhages within *Alk1^{GFPCre};Tgfbr2$^{fl/fl}$ embryos* were around the abnormal GE and telencephalon. The fourth and third ventricles of the brain were grossly distended (Figure 4-5B). Further examination of the vascular ECs of the GE and telencephalon reveal the vessels to be disorganized, tortuous and disassociated with surrounding neural tissues as in the control. Vessels of the dicephalon are dilated and irregular, which made the vessels more vulnerable to rupturing and leaking out. Nucleated blood cells were found within the tissue and cavities, not contained within the vessels.

Phenotypically, the brain appeared to be the only organ affected in *Alk1^{GFPCre}; Tgfbr2$^{fl/fl}$* embryos. Further examination of the heart and lung development showed these did not seem affected by loss of endothelial TGFBR2 (Figure 4-5C and F). To analyze proper blood vessel formation, the smooth muscle layer was additionally stained with smooth muscle actin (SMA). The vessels of *Alk1^{GPFCre};Tgfbr2$^{fl/fl}$* lungs were similar to control vessels in terms of the development of the smooth muscle and endothelial layer layers (Figure 4-5D and G) being unaffected. Likewise, SMA staining of the dorsal aorta was similar in both the *Tgfbr2* cKO and controls (Figure 4-5E and H). These findings suggest that deleting *Tgfbr2* in ECs specifically during midgestation has a grave impact on brain development, particular angiogenesis, but not as much on cardiac and lung development.

Alk1^{GFPCre}; Alk5$^{fl/fl}$ *Embryos Die by E13.5 with Evidence of Gross Cerebral Vessel and Cardiac Defects*

In the *Alk1^{GFPCre};Alk5$^{fl/fl}$* the GE is perforated, as seen in the *Alk1^{GFPCre};Tgfbr2$^{fl/fl}$* and blood cells are seen within the third ventricle and tissue (Figure 4-6A and B).

However, a magnified view shows that the GE nor diencephalon is as severely damaged in *Alk1*^{GFPCre};*Alk5*$^{fl/fl}$ embryos as in the *Alk1*^{GFPCre};*Tgfbr2*$^{fl/fl}$ embryos (Figure 4-6A and B, panels two and three). There is no evidence of edema of the head as in the *Tgfbr2* cKO. PECAM-1 staining of ECs presents vessels that are disorganized in the GE, but the diencephalon vessels are not as impacted by the endothelial loss of *Alk5* (Figure 4-6A and B).

The development of the pulmonary vasculature was also not affected, but the *Alk1*^{GFPCre};*Alk5*$^{fl/fl}$ heart appears undeveloped *(Figure 4-6C and E)*. The ventricles are trabeculated, but the ventricular septum does not appropriately fuse at the atrioventricular cushions. The dorsal aorta is not round but irregular in shape (Figure 4-6D and E).The endothelial layer of the dorsal aorta is developed as in the control (data not shown), however, SMA staining reveals the smooth muscle layer was diffused, compared to the control, suggesting a failure in the resolution phase of establishing the vessel. Thus, the vSMCs are more diffuse around the aorta instead of established around the vessel.

Discussion

The angiogenic processes involving TGF-β signaling are still poorly understood. In many cases *in vivo* models did not correlate to *in vitro* finding, nor are conditional KO models phenotypes in agreement. For one example, endothelial-specific *Tie1*-mediated ablation of the generally expressed receptors *Tgfbr2* and *Alk5* and the majority of *Tie2*-cre(+);*Tgfbr2*$^{fl/fl}$ are embryonic lethal, like conventional knockouts, at E10-10.5 due to aberrant yolk sac vasculogenesis and angiogenesis [55, 192]. In contrast, *Tie2*-cre;*Alk5*$^{fl/fl}$, 35% *Tie2*-cre;*Tgfbr2*$^{fl/fl}$, and Cdh5(PAC)-Cre^{ERT2};*Tgfbr2*$^{fl/fl}$ embryos survive past midgestation, however, these died of cardiac defects during late gestation [191].

Contradictory, still, our lab reported that conditional knockouts of both receptors using another endothelial-specific transgenic line, L1cre, were not developmentally affected [64]. The timing of cre activity could be a contributing factor in the contrasting phenotypes. In the *Tie1*-cre line, Cre activity begins at E8, around the same time the vasculature forms (E8-9), and slightly before the reported first expression of TGFBR2 [194]. Hence, the null nor *Tie1-cre* deletion models would reflect the true function of these receptors in angiogenesis at midgestation. As for the L1cre line, Cre is not initiated until late gestation, at E13.5 [64]. The *Tie2*-cre (E8.5) and Cdh5(PAC)-Cre^{ERT2} (induced at E11.5) models have slightly later cre expression [190], however, the phenotypes were variable or, as in the case of the *Tie2*-cre(+);*Tgfbr2*$^{fl/fl}$, the authors' descriptions were vague [192, 193]. The differing phenotypes imply a temporal role for ALK5 and TGFBR2 in ECs. Thus, we generated a novel *Alk1*-cre knock-in line, *Alk1*^{GFPCre}. The slight delay in the initiation of *cre* activity at E9.5 provided an opportunity to more accurately examine the roles endothelial TGFBR2 and ALK5 play in angiogenesis during midgestation than previous models.

To test specifically examine the spatiotemporal role of TGFBR2 and ALK5 during embryogenesis, we focused on the development of the cerebral vessels. Nishimura et al postulated from *in vitro* findings that integrin αvβ8 on astroctyes interacted with the LAP of a secreted TGF-β ligand, consequently activating TGF-β signaling within ECs [175]. Several independent knockout models, such as the *itgav*$^{-/-}$ [182], *itgb8*$^{-/-}$ [183], *Tgfb1*$^{RDE/RDE}$*/Tgfb3*$^{-/-}$ [185], *Tgfb3-cre;Alk5*$^{fl/fl}$ *[188] and Id1/3*$^{-/-}$ [TGF-β transcription downstream targets] [195], strongly support this hypothesis and all develop the same cerebral hemorrhaging within the forebrain region. Conditional KO of *itgav*$^{-/-}$ and *itgb8*$^{-/-}$

in neuroepithelial, but not endothelial, cells also result in the hemorrhagic phenotype, confirming neuronal derived αvβ8 is essential [186, 187]. However, it is not clear what type of cell may be the target cell. We present *in vivo* confirmation that endothelial TGFBR2 and ALK5 are the targets as each developed the same cerebral hemorrhaging. Further establishing TGF-β activation on ECs is involved, our collaborators found Nestin-cre(+);*Tgfbr2*$^{fl/fl}$ had no phenotype; though, the data was not shown here.

We show that EC-specific deletion of *Alk5* and *Tgfbr2* using the *Alk1*-cre knock-in resulted in a consistent and highly specific cerebral hemorrhage phenotype that initially manifested at E11-11.5. Though there has been previous endothelial-specific KOs of each receptor that reported cerebral hemorrhaging in some embryos, we are the first to show that the GE is perforated and vessels disorganized in *Alk1*^{GFPCre};*Tgfbr2*$^{fl/fl}$ and *Alk1*^{GFPCre};*Alk5*$^{fl/fl}$ embryos in a similar, consistent fashion as the *itgav*$^{-/-}$, *itgb8*$^{-/-}$, *Tgfb1*$^{RDE/RDE}$/*Tgfb3*$^{-/-}$ *models*. Interestingly, there was a slight delay in the appearance of the cerebral phenotype in the surviving *Tie2-cre*;*Alk5*$^{fl/fl}$ and *Tie2-cre;Tgfbr2*$^{fl/fl}$ compared to our *Alk1*^{GFPCre} lines, however, the results were still consistent in that a phenotype was seen in the *ALK5* cKO than the *TGFBR2* cKO. Additionally, the previous endothelial-specific knockout models report embryos died due to cardiac defects. We show that *Alk1*^{GFPCre};*Alk5*$^{fl/fl}$ display defects in the ventricular septum, but in a manner similar to the Cdh5(PAC)-Cre^{ERT2};*Tgfbr2*$^{fl/fl}$, instead of the *Tie2*-cre(+);*Alk5*$^{fl/fl}$. There was a failure of complete ventricular septation and failure to fuse with the atrioventricular cushions in our *Alk5* cKO and the Cdh5(PAC)-Cre^{ERT2};*Tgfbr2*$^{fl/fl}$ KOs. The *Tie2*-cre(+);*Alk5*$^{fl/fl}$ embryos did not properly form a ventricular septum. Interestingly, the only organ system

apparently affected in the *Alk1*^{GFPCre};*Tgfbr2*$^{fl/fl}$ embryos is the CNS, as no obvious developmental cardiac defects were seen. Considering deleting*Tgfbr2* with Cdh5(PAC)-Cre^{ERT2} two days later (at E11.5) than *Alk1*^{GFPCre} (at E9.5) resulted in a cardiac phenotype enforces the essential temporal role of endothelial TGFBR2 during development.

CNS angiogenesis heavily relies on the migration and sprouting of ECs, particularly in EC tip cells providing directionality in response to various factors in the microvascular environment [173, 174, 196]. Our data suggests that TGF-β signal activation within EC tip cells by the TGF-β1/3 ligands are essential for EC migration of periventricular vessels. However, downstream targets or interactions with other signaling pathways may be required for further sprouting and directionality. There are several murine KO models of other transcriptional factors (for example, ETS family member, Fli1) and members of other signaling family members (Wnt/β-catenin) important in angiogenesis of the brain in which cerebral hemorrhaging has been observed which may provide further insight into the mechanism underlying neurovascular development [197, 198]. The strongest candidate of an interacting signaling pathway (with the endothelial TGF-β signaling) involves the orphan G protein-coupled receptor GPR124/tumor endothelial marker 5 (TEM5) [199]. It was reported that GFR124 also appears to have spatial temporal role during neurovascular development, specifically in the ECs of vessels within the forebrain. GFR124 KO mice, particularly in the ECs, resulted in the same cerebral phenotypes as our *Tgfbr2* and *Alk5* cKO models, with other organ systems unaffected. Furthermore, GPR124 requires Cdc42-Par6 [196],

a transcription factor important for filipodia formation and determining cell polarity, in angiogenic migration and directionality to remain within the forebrain environment [200].

A more novel view of cerebral vessel development states that the ECs of periventricular vessels migrate (beginning at E10) from the ventral to dorsal forebrain to establish an angiogenic gradient, in which specific transcription factors are expressed in different regions of the forebrain [201]. Nkx2.1 and Dxl1/2 are expressed in the ventral region, while Pax6 is expressed in the dorsal region [201]. Loss of either of these factors results in reduced periventricular vessel migration, particularly in the dorsal forebrain. As *Pax6* is a morphogenetic factor important in patterning throughout the body but also in axonal guidance and neuronal guidance [202], it is tempting to speculate that the αvβ8 integrin of neuroepithelial cells within the dorsal forebrain may begin to activate the TGF-β1/3 ligand at E10. The migration of ECs is initiated by activation of TGF-β signaling in the tip cells, which regulate the ligand for GPR124 or interacts with the GPR124 signaling pathway. Sprouting and directionality of EC migration is then controlled by GPR124-Cdc42-Par6. This model explains how the cerebral phenotype was specific to the GE of the forebrain (which is in the ventral region). ECs are able to sprout and perhaps migrate within the GE, however, the loss of any components leads to failure of migration directionality into the dorsal forebrain. The periventricular vessels aggregate within GE, the vessel walls weaken/rupture, and the perforations in the ventral brain form due to apoptosis. However, the mechanisms will need to be further evaluated, for example, by examining the expression of GPR124 or Cdc42 in our cKO models. [Summarized in Figure 4-7]

We show that endothelial TGF-β signaling via the receptors TGFBR2 and ALK5 is indispensable for establishment of the neurovasculature and for cardiac development during midgestational embryogenesis, and the vascular beds of the rest of the body are largely unaffected. The results also suggest that TGF-β signaling play spatial and temporal roles during development, which correspond with previously reported expression patterns of TGFBR2. This finding helps rectify the seemingly opposing phenotypes seen in various conditional knockout models of various TGF-β signaling family members. It may also provide insight in maintenance of cerebral vessels in adult stages and help understand cerebral vessel defects, such as AVMs, that may appear.

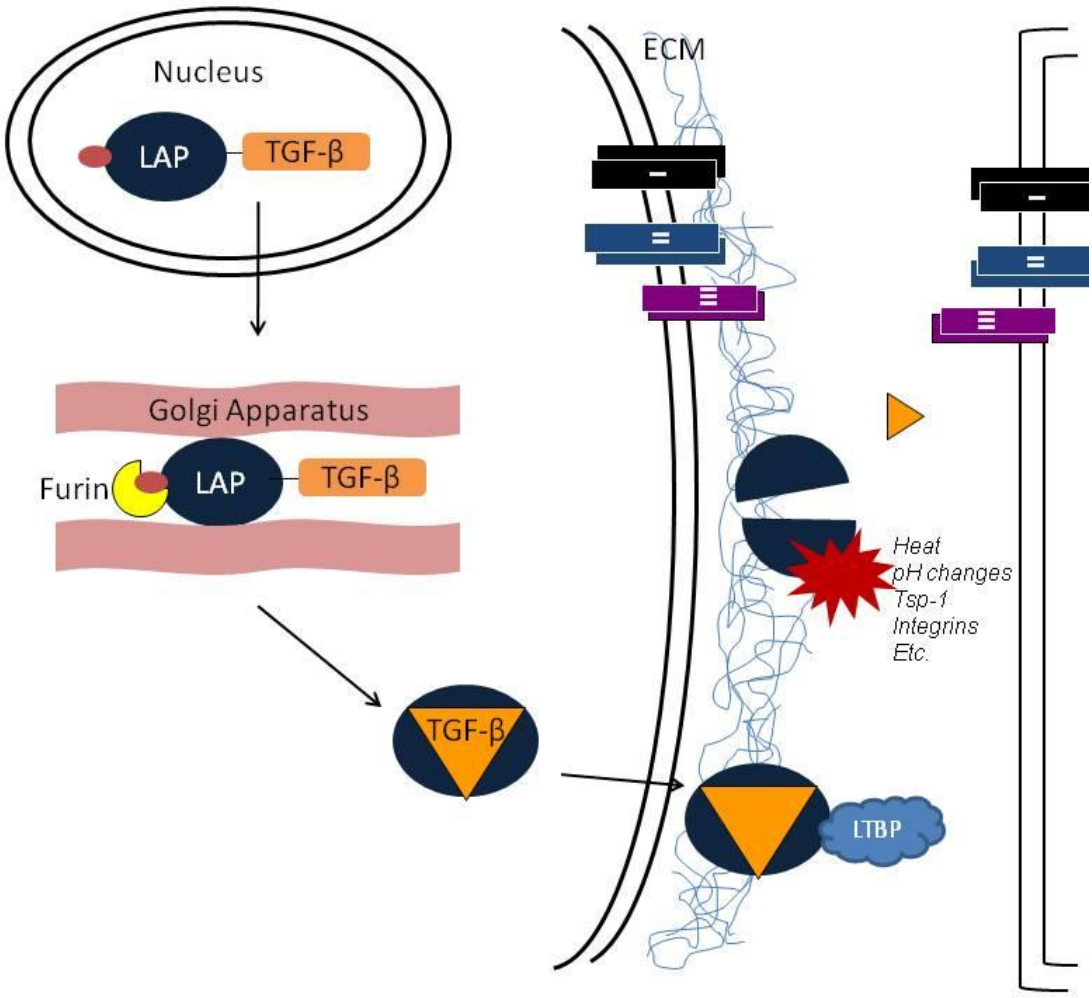

Figure 4-1. Synthesis and activation of the TGF-β ligand. The TGF-β ligand is initially synthesized in a precursor form that includes, starting from the 5' end, a prodomain signaling peptide, a latency-associated peptide (LAP), and the TGF-β ligand. After release from the nucleus, the proto-TGF-β enters the Golgi apparatus, where furin enzymatically cleaves the signaling peptide. As the ligand prepares to exit the cell, the LAP encompasses the TGF-β ligand and acts a chaperone. When secreted from the cell, the LAP still enclosed the TGF-β ligand as well as associate with the latent TGF-β binding protein (LTBP). This large complex is deposited in the extracellular matrix of a cell until it is activated by various means, such as pH change, heat, specific enzymes, or integrins. In these cases the TGF-β ligand is freed from the LAP and allowed to bind and activate TGF-β type II receptors. Tsp-1, Thrombospondin-1.

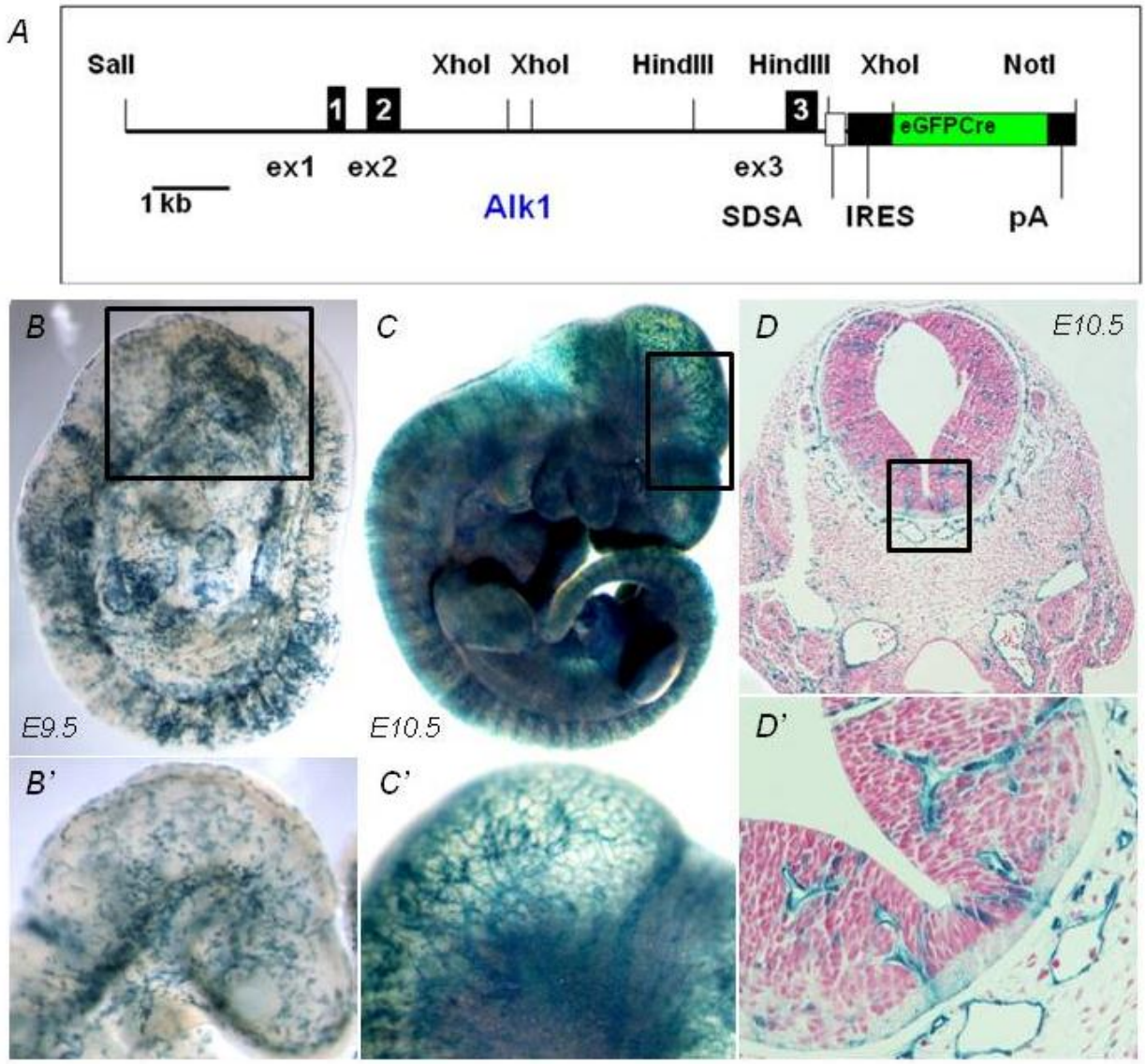

Figure 4-2. *Alk1*^{GFPcre} – a novel EC-specific cre deleter line. A) A GFPcre fusion construct was inserted into the endogenous *Alk1* gene, replacing exons 4-8. B) The cre in this knockin line is active beginning at E9.5 of mouse embryogenesis in all ECs expressing *Alk1, however, in a punctate fashion*. A closer view of the E9.5 head is seen in (B'). C) By E10.5 more uniform X-gal staining covers the entire embryo, in all organs. C') A magnified view of the head confirms more robust X-gal staining. D) A transverse section of the brain reveals strong endothelial-specific staining. D') *Alk1*^{GFPcre} is active in the ECs penetrating the neuroepithelium, thus should be appropriate to use in the study. SD/SA, SV40 splicing donor/acceptor signal; IRES, internal ribosomal entry sequence; pA, poly-A signal.

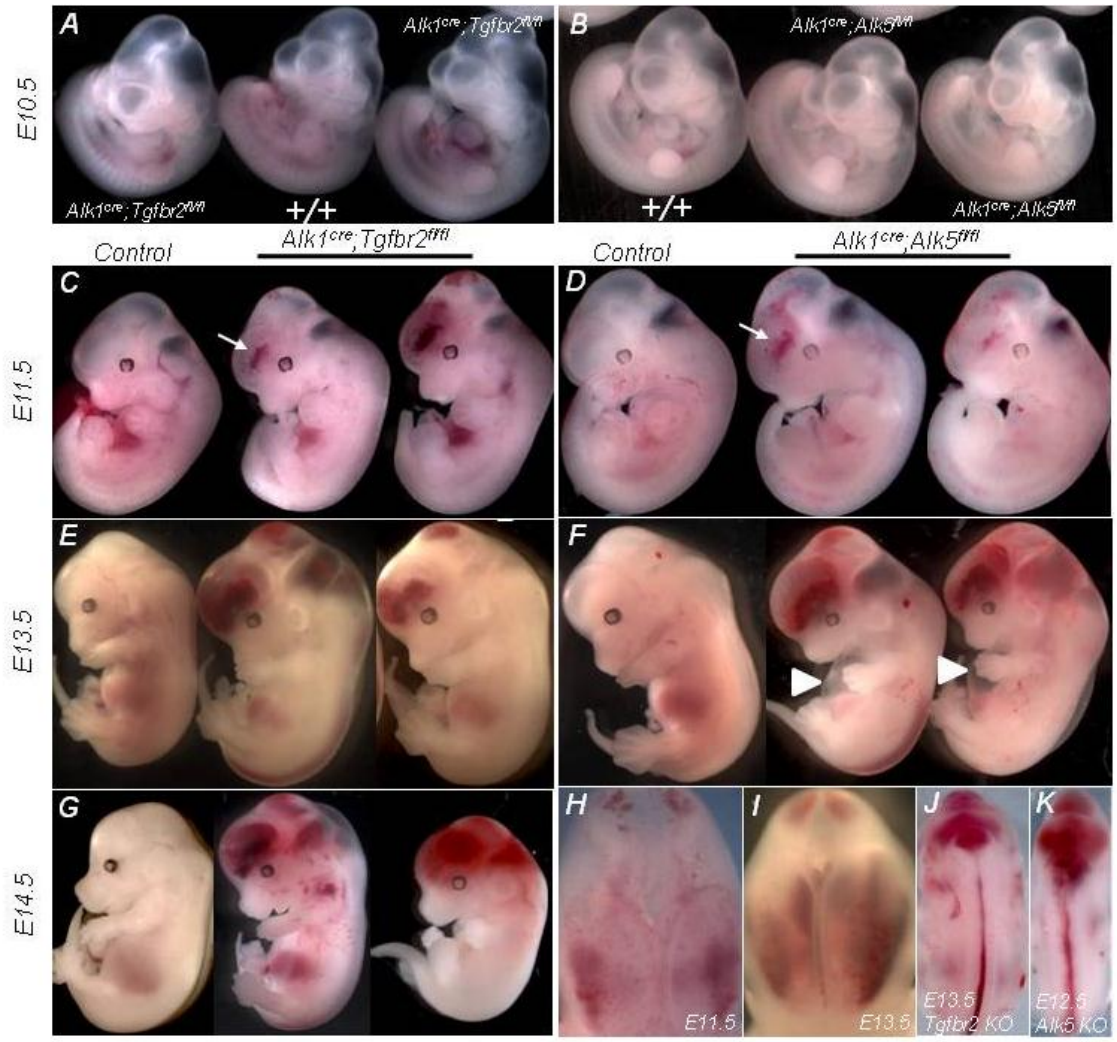

Figure 4-3. *Tgfbr2* and *Alk5* cKO embryos display specific cerebral hemorrhaging beginning at E11.5. *Tgfbr2* (A) and *Alk5* (B) mutant embryos are indistinguishable from control littermates at E10.5. Beginning at E11.5, both *Tgfbr2* and *Alk5* cKO embryos begin exhibiting the same hemorrhaging in the forebrain region, shown by the white arrows. The cerebral hemorrhaging worsened over time in both cKO models (C and D). E) The head region of the *Tgfbr2* cKO embryos becoming edemic, but with the same hemorrhages seen; however, there were no hemorrhages seen in any other organ system besides the central nervous system. F) *Alk5* cKO embryos died by E13.5. In addition to CNS hemorrhages, the chest area of *Alk5* cKO embryos were distended (white arrow head), indicating there may have been cardiac defects associated with the *Alk5* cKOs. G) *Tgfbr2* cKO embryos died a day later, at E14.5, with embryos presenting severe brain hemorrhaging and very faintly beating heart, or already dead and in the process of resorption. H) and I) the forebrain bleeding was seen in both hemispheres of the brain. In some, not all, *Tgfbr2* (J) and *Alk5* (K) embryos, there were hemorrhages in the spinal cord beginning at E12.5.

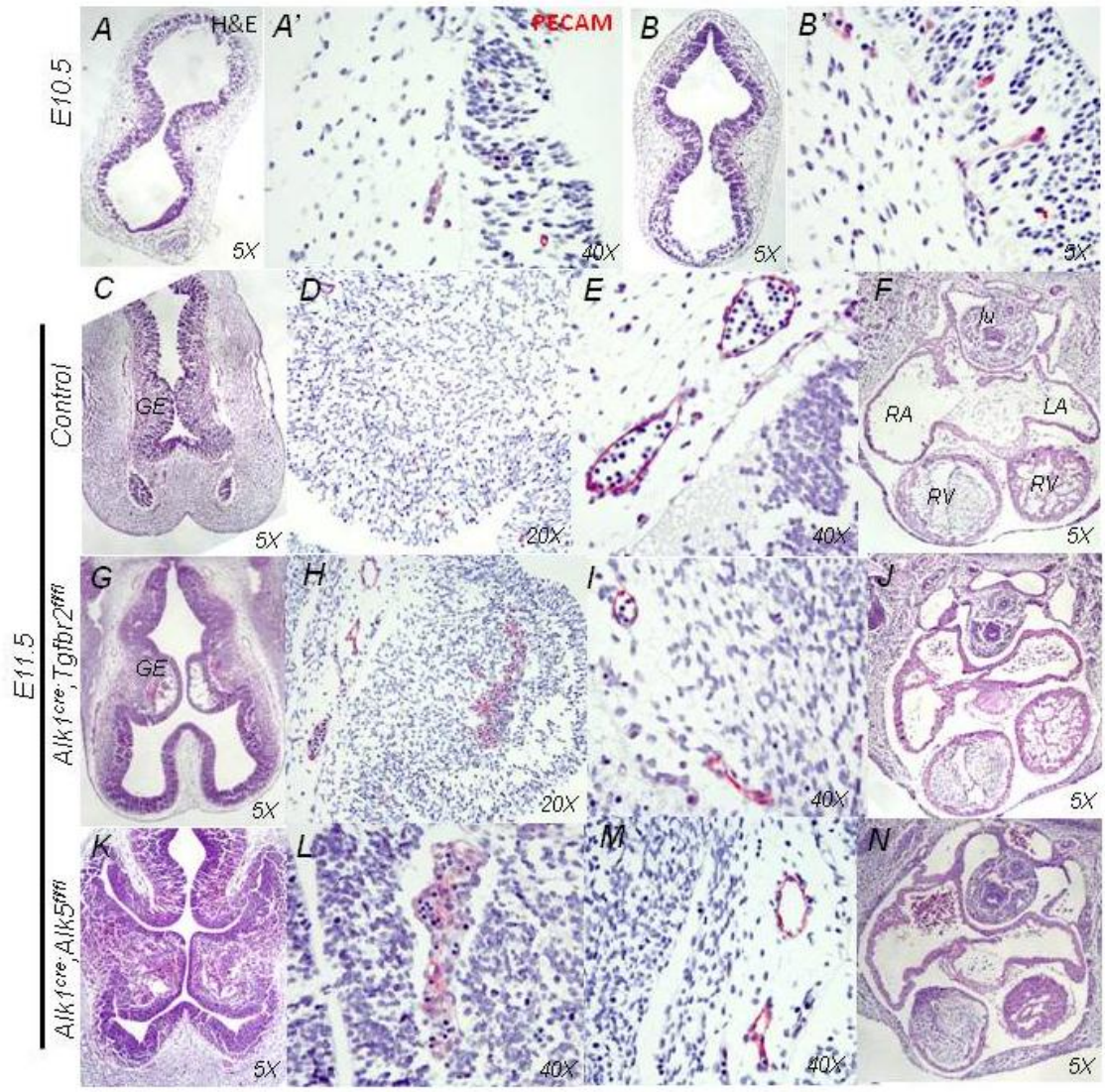

Figure 4-4. Histological Sections of E10.5 and E11.5 embryos. At E10.5, as compared to the control (A and A'), there is no evidence of any vascular defects in the brain vessels in the mutant mice, as seen in a representative section in (B) and an enlarged picture in (B'). C) At E11.5 all blood cells are confined to vessels that are closely associated with the surrounding cerebral tissue in the GE (closer view in D). E) Vessels in the tissue outside of the forebrain region. Conversely, *Tgfbr2* (G) and *Alk5* (K) cKO embryos begin displaying cavitations in the GE, specifically at E11.5. A closer view of PECAM-1-stained sections revealed that ECs clustered into glomeruloid-like structures (H and L). However, it appears that only vessels within the neuroepithelium were affected as vessels lying outside of the GE were normal, as compared to the control, and blood cells were confined to the vessels. There does not seem to be any cardiac defects in the *Tgfbr2* (J) or *Alk5* (N) cKO embryos, as mutant hearts were comparable to control hearts (F). GE, ganglionic eminence; lu, lung; RA, right atrium; RV, right ventricle; LA, left atrium; LV, left ventricle.

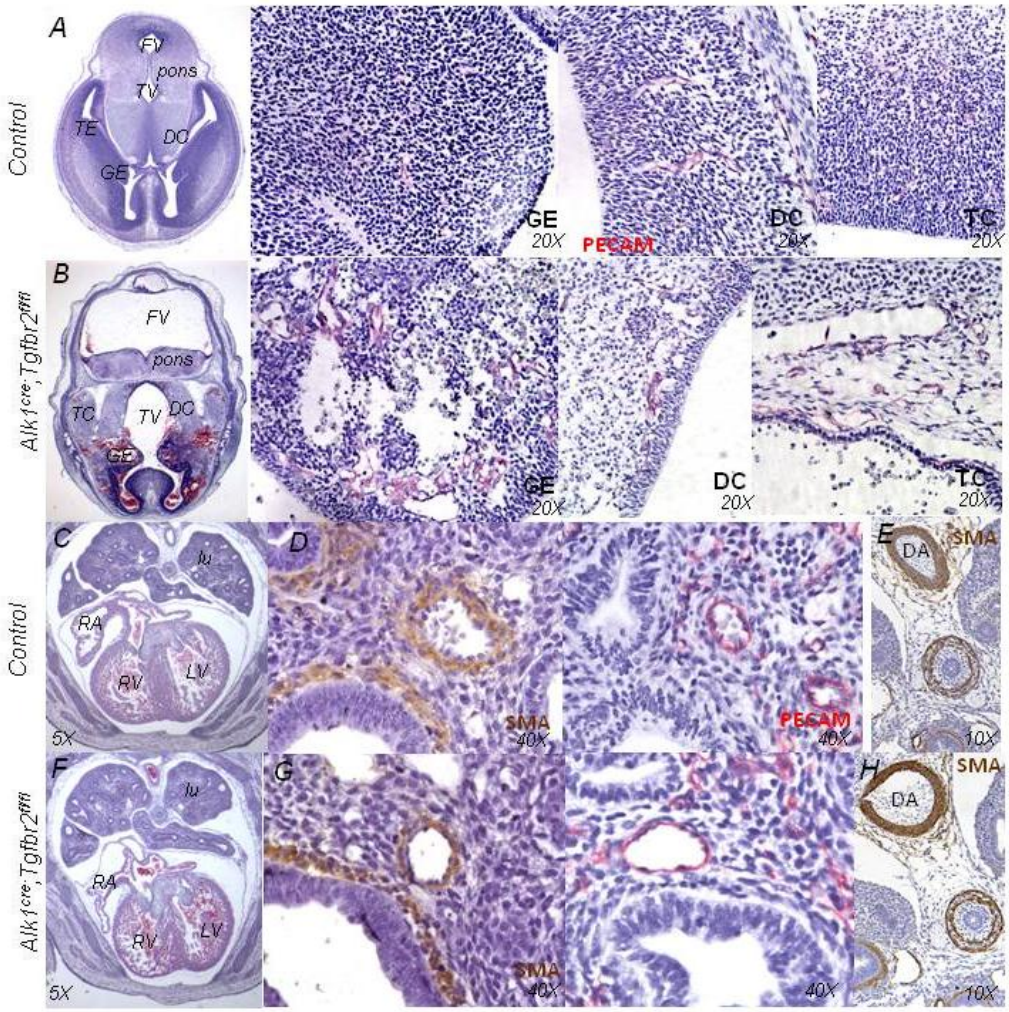

Figure 4-5. Endothelial-specific deletion of *Tgfbr2* during midgestation specifically affected cerebral vessel formation at E13.5. Overall transverse view of the E13.5 control head (A) shows a properly developed head with various parts of the head labeled. A closer view of the GE, DC, and TC show EC layers of vessels (PECAM-1-stained red) are closely associated with the surrounding tissue. However, the *Tgfbr2* mutant head (B) displays hemorrhages in the forebrain region and the fourth ventricle and third ventricles are enlarged. A closer view of the GE shows large cavitations and disorganized, poorly formed vessels. The vessels within the DC are dilated and there are some cavitations. In the TE, vessels are dilated. Development of the lungs and heart of the *Tgfbr2* cKO (F) did not appear to be affected and were comparable to control controls (C). PECAM-1 and SMA (brown) staining of the *Tgfbr2* mutant revealed that proper endothelial (G') and smooth muscle (G) layers developed in the lungs as in the control (D and D'). SMA staining confirms no developmental differences between control (E) and *Tgfbr2* mutant (H) dorsal aortas. FV, fourth ventricle; TV, third ventricle; TE, telancephalon; DC, dicephalon; GE, ganglion eminence; lu, lung; RA, right atrium; RV, right ventricle; LA, left atrium; LV, left ventricle. DA, dorsa aorta.

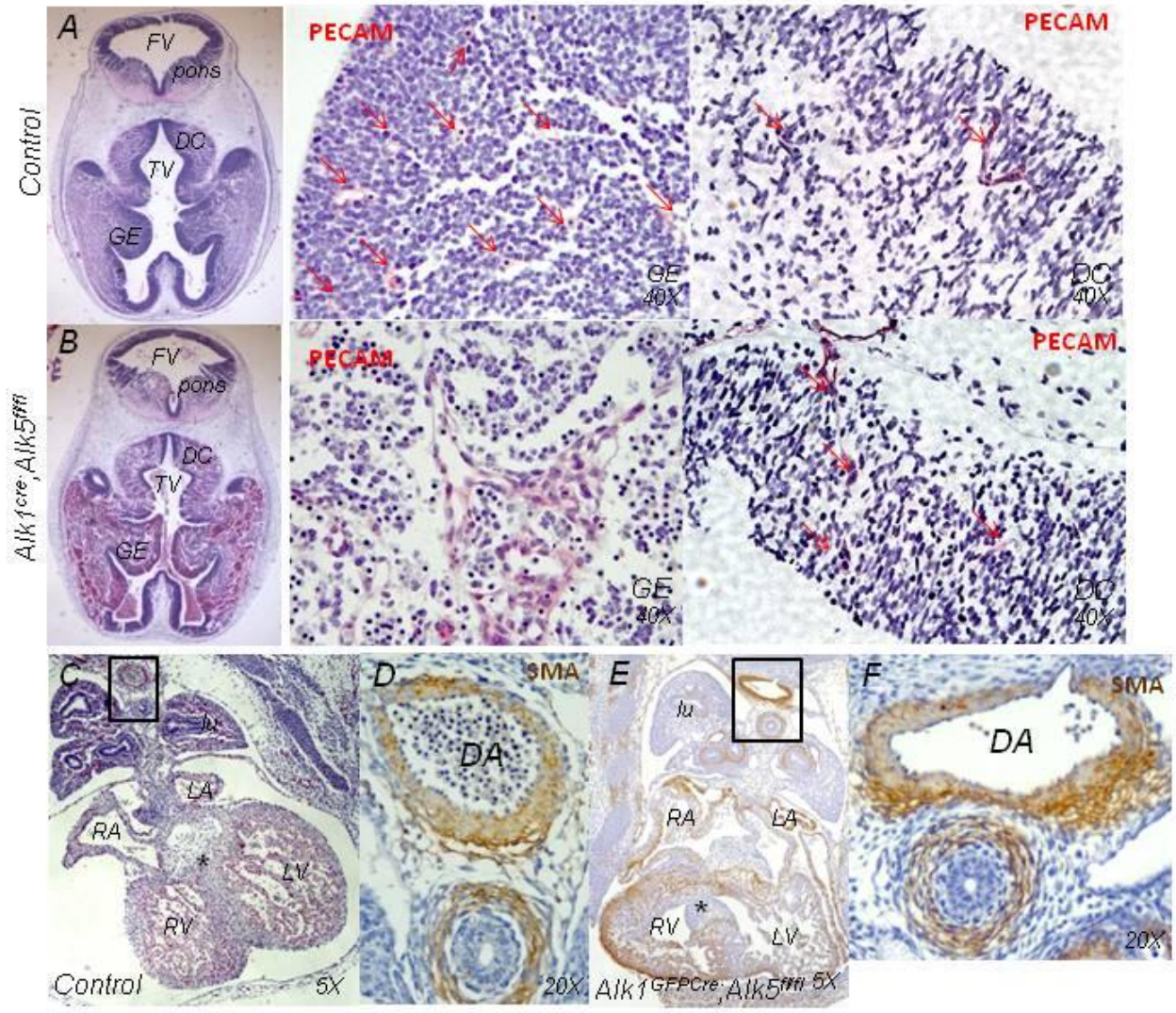

Figure 4-6. *Alk5* cKO embryos exhibited abnormal cerebral vasculature in the GE and cardiac defects. A) H&E stain of a transverse view of the control head. Panels two (GE) and three (DC) show PECAM-1-stained ECs (red arrows) of the neuroepithelial vessels. These vessels are fine and closely associated with the surrounding tissue. B) H&E stain of *Alk5* cKO head reveals the GE is perforated and there is free blood cells within the tissue. The ECs of the GE are still clumped in glomeruloid-like structures, as in E11.5 brains, in the GE (B, panel one). In panel two, the vessels within the DC is similar to control heads. C) Control E12.5 heart. D) A magnified view of the SMA-stained control dorsal aorta. E) The *Alk5* cKO heart is underdeveloped and the ventricular septum does not properly fuse in the atrioventricular cushion (*). F) The *Alk5* cKO dorsal aorta is irregularly shaped and the smooth muscle layer appears diffuse. FV, fourth ventricle; TV, third ventricle; TE, telancephalon; DC, dicephalon; GE, ganglion eminence; lu, lung; RA, right atrium; RV, right ventricle; LA, left atrium; LV, left ventricle. DA, dorsa aorta.

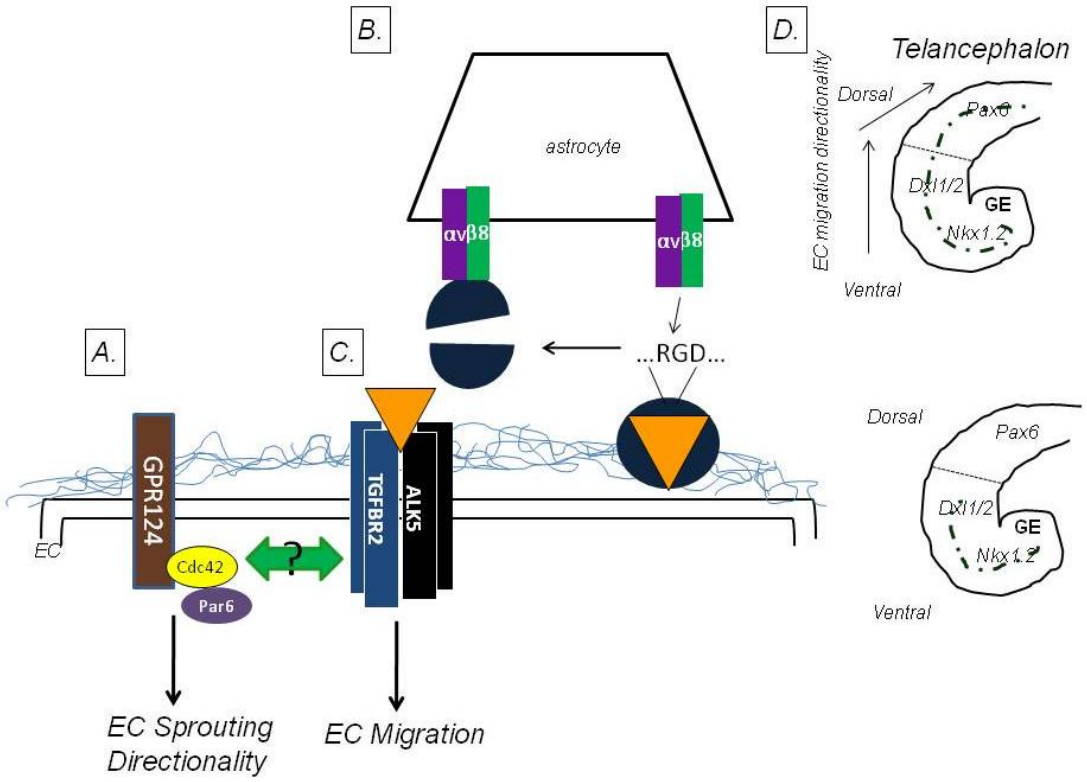

Figure 4-7. Proposed mechanism of cerebrovascular development in the telencephalon. A) GPR124 is active before E10 and involved in EC sprouting in the ventral telencephalon. Other factors, such as Nkx2.1 may facilitate in EC migration within this region. B) At E10, the ECs begin to migrate from the ventral to dorsal telencephalon. This is initiated by the activation of the latent TGF-β1/3 ligand by neural αvβ8 recognizing and binding to a RGD sequence within the LAP of the ligand. C) A conformational change in the LAP causes it to release the ligand, which subsequently activates TGF-β signaling within ECs (most likely tip cells), specifically through the receptor pair TGFBR2 and ALK5. This leads to downstream regulation migration. Cdc42-Par6 is required for GPR124 migration directionality, however, it is unclear whether Cdc42-Par6 would associate before or after TGF-β induction. D) A recent model of CNS angiogenesis suggests that periventricular vessels migrate from the ventral to dorsal telancephalon to establish an angiogenic gradient by which specific transcription factors are expressed (top image). Pax6 is an axon guidance factor, hence it seems that that vessel would migrate to the dorsal region if driven or enticed by a neuronal cell. Thus, if this model is implicated in our proposed mechanism, the loss of TGFBR2 or ALK5 means there is no active migration in the EC tip cells. The consequence is the sprouting ECs remain in the dorsal telancephalon, which includes the GE. The ECs accumulate and aggregate. The cells begin to under apoptosis and cause cavitations in the tissue (bottom panel). Dotted green lines denote EC migration path.

CHAPTER 5
CONCLUSIONS AND PERSPECTIVES

In the present study, the focus was to elucidate the role various TGF-β signaling superfamily members play in ECs to determine pathogenetic etiology underlying the formation of vascular malformations, such as those exemplified in HHT. The focus was specifically on the *in vivo* roles of the Type III receptor Endoglin, Type II receptor TGFBR2, and Type I receptor ALK5. The functions of these receptors in vascular endothelial biology are still largely unknown and debated, as previous findings have been contradictory or unclear.

In Chapter 3, the interaction between the two major genetic causes of the vascular disorder HHT were examined by generating two different *Eng* cKO models using the same two cre deleter lines (L1cre and R26-Cre^{ER}) previously used in *Alk1* cKO models, then comparing the phenotypes. Then in Chapter 4, we sought to determine whether TGFBR2 and ALK5 have spatiotemporal roles during embryogenesis by selectively silencing each receptor in endothelial cells using a novel transgenic *Alk1* cre-knockin line (*Alk1*^{GFPCre}).

Endothelial and Global *Eng* cKO Mice Suggest Divergent Pathogenetic Mechanisms Underlying HHT1 and HHT2

It is assumed in the HHT field that ALK1 and ENG are intimately involved in ECs, likely transducing signals via the BMP signaling pathway (Figure 1-1), thus it would be expected that deletion of either gene would lead to the HHT vascular malformations (e.g. AV-shunting, AVMs, etc). The Oh lab had previously generated and characterized the first *Alk1* cKO murine models that featured AVMs, as seen in HHT, at high, consistent frequencies. This was achieved using the endothelial-specific cre-deleter line, L1cre, and the tamoxifen-inducible, globally expressed R26-Cre^{ER} line. It was quite

surprising that neither the Eng cKO mice nor the *Eng* iKO mice given the same treatment as the *Alk1* iKO model were severely impacted by the loss of *Eng*. Though it appeared that there may be a technical issue responsible (the efficiency at which the 2f allele is converted to the null 1f allele by different tamoxifen treatments) for the more varied phenotypes seen in the *Eng* iKO model, there were common phenotypes seen in similar organs in both models that prove these were true phenotypes.

Many of the same organ systems were affected in the *Eng* and *Alk1* ablation models, but there were few shared patterns of pathology. Necroscopies of the *Eng* and *Alk1* iKO model revealed local hemorrhaging, AV-shunting, and AVMs in the intestine. The AVMs usually formed in the peyer's patch. The heart was also commonly enlarged, a secondary response to the hemorrhages, in cKO models of each receptor. Many more distinct differences were observed in the two models. Death occurred early in both endothelial-specific and global deletion of *Alk1* (by E17.5/PN5 or 3 weeks, respectively), while *Eng* cKO and *Eng* iKO are viable, with only a quarter of *Eng* iKO dying by 21 days. It was previously published that *Alk1* iKO mice exhibited *de novo* AVMs in response to acute wounds given in the ear and dorsal skin. However, we found that the *Eng* iKO mice rarely do; instead, AVMs always appeared in tissue surrounding the ear ID tag, which can be considered a chronic injury. Also, AVMs formed specifically in the uterine vessels of the female reproductive organs of *Alk1* iKO, while *Eng* iKO mice exhibited ovarian AVMs. More surprising is that the pulmonary vasculature was not obviously affected in either *Eng* deletion model even though the lungs presented phenotypes at high frequencies in *Alk1* deletion models. These distinct phenotypes

bring unanticipated evidence that there are separate pathogenetic mechanisms underlying HHT1 and HHT2.

This seems plausible considering the expression pattern of ENG versus ALK1. ALK1 is more restricted to arterial ECs, while ENG is more pan-endothelial. ENG expression has also been found in other cell types, such as the smooth muscle layer (in low levels) and several types of circulating cells, such as monocytes, HSCs, and stromal cells. Additionally, it was reported in the pulmonary vasculature that ENG and ALK1 expression overlaps only in the distal vessels. In the Eng cKO mice, as *Eng* is silenced in arterial ECs, venous *Eng* is still present. The lack of phenotype in this model could be explained in that circulating cells expressing *Eng* could be compensating for the loss of vascular *Eng*. Future studies examining the bone marrow or circulating endothelial cells (CECs) must be performed to confirm this possibility. As for the *Eng* iKO model, quantification of the genomic copy of the 1f allele suggests that the dosage and number of tamoxifen affects how much *Eng* is deleted. In contrast to the endothelial-specific cKO models or the *Alk1* iKO models, it is less predictable which vessel and cell type *Eng* is actually silenced in the *Eng* iKO mice. This can account for the variable phenotype. For example, for the mice in which there was overlap in the phenotype, such as AVMs in the peyer's patch, between *Alk1* and *Eng* iKO mice, it could mean that more arterial ENG was silenced. More comprehensive expression studies in the *Eng* iKO model should be conducted either by isolating ECs and CECs and quantifying expression of *Eng* or histological analysis by immunofluorescence to determine whether one vessel type or cell type (other than ECs) may be more impacted.

Endothelial TGF-β Signaling has Spatiotemporal Roles in Cerebrovascular Development

The understanding of the *in vivo* mechanisms of TGF-β signaling in ECs during angiogenesis has been complicated by contradictory phenotypes in conventional and conditional knockout mouse models. Because it was believed that a balance between TGFBR2-ALK1 and TGFBR2-ALK5 was essential in maintaining vascular homeostasis, ALK1 involvement with TGFBR2 and ALK5 has been of interest in the HHT field. In Chapter 4 we tested the hypothesis that endothelial TGF-β signaling has spatial and temporal roles in vascular development, focusing on the tightly regulated mechanism of cerebrovascular development. Using a novel cre deleter line (*Alk1*^{GFPCre}) to silence *Alk5* and *Tgfbr2* in ECs at E9.5, we provide *in vivo evidence that* astrocytic integrin αvβ8 was responsible for activating latent ligands TGF-β1/3, which bind and activate TGFBR2 and ALK5 within ECs. *Alk1*^{GFPCre};*Tgfbr2*$^{fl/fl}$ and *Alk1*^{GFPCre};*Alk5*$^{fl/fl}$ displayed the similar specific cerebral hemorrhaging in the forebrain region , particularly in the GE, as seen in *GPR124*$^{-/-}$*, itgav*$^{-/-}$*, itgb8*$^{-/-}$*,* and *Tgfb1*$^{RDE/RDE}$*;Tgfb3*$^{-/-}$ mice. The only organ system affected in the *Alk1*^{GFPCre};*Tgfbr2*$^{fl/fl}$ mice was the CNS, particularly the cerebral vessels. This differs slightly from the Cdh5(PAC)-Cre^{ERT2};*Tgfbr2*$^{fl/fl}$ by which *Tgfbr2* was deleted 48 hrs later, but developed ventricular septal defects. This delay seemingly accentuates the temporal aspect of TGF-β signaling. The CNS manifestation was less severe in *Alk1*^{GFPCre};*Alk5*$^{fl/fl}$ embryos. However, mutants also had cardiac development defects and died sooner. A potential mechanism is that during midgestation EC sprouting may be activated by the GPR124; at E10 αvβ8 may begin to activate TGF-β signaling in EC to regulate migration. Because TGF-β was activated by the astrocyte, this may influence the Cdc42 to direct migration towards the dorsal region of the telencephalon. It is

probable that the loss of ALK5 and TGFBR2 lead to a defect in the activation of EC migration. Thus, EC sprouting is taking place, but the lack of proper migration out of the GE occur results in the glomeruloid-like vascular aggregates. It would be interesting to see whether this mechanism would be important in maintenance of the cerebral vasculature in adult tissue and whether it may contribute to BAVMs. It should be noted that the study confirms that ALK5 is in fact expressed and essential in ECs, in contrast to expression studies stating it is expressed only in SMCs. The earlier results can be clarified in that ALK5 is typically expressed at such low levels in ECs that it was not detectable by that study's X-gal staining.

Perspectives

The use of the murine models has the advantage over *in vitro* models in that the signal transduction can be examined in a physiological mammalian model that is similar to humans, without the bias of conditional or artificially supplemented medium. A drawback to our models is that the mice were mixed genetic background (containing 129Sv/J, C57BL/6, and FVB), which may influence the frequency by which a phenotype may be seen due to modifier genes. This was an issue that was addressed in the currently used *Eng*$^{+/-}$HHT1 mouse model, by which the C57BL/6 backbred line is now often used. Backcrossing the *Eng* cKO mice to either a pure C57BL/6 or 129Sv/J background may resolve the problem.

As the three known genes associated with HHT as part of the TGF-β signaling pathway, it is strongly believed that ALK1, ENG, and SMAD4 signal in a linear pathway. However, the findings here that the *Eng* cKOs, behaved distinctly from *Alk1* cKO mice, in addition to findings that L1cre(+);*Smad4*$^{fl/fl}$ mice were also viable (personal observations), have proven the HHT mechanism may be much more complicated than

anticipated. To rectify potentially independent signaling pathways indicated from the findings in the three (*Alk1, Eng, Smad4*) EC-cKO models, a double L1cre-mediated endothelial-specific knockout mouse (L1cre(+);*Smad4*$^{fl/fl}$;*Eng*$^{fl/fl}$) may need to be generated to determine how essential ENG and SMAD4 truly are for ALK1 signaling. As mentioned earlier in this chapter, the mild phenotype in *Eng* cKO mice may be due to the wider expression of ENG in vascular endothelial cells in addition to compensation of the loss of arterial ENG with ENG-expressing CECs. The same phenomena may be relevant for SMAD4, although SMAD4 is expressed on other tissue and cells types, not only ECs. It would be expected that if ENG and SMAD4 were essential for ALK1, the double KO would likely recapitulate the L1cre(+);*Alk1*$^{2f/2f}$ mice. Thus, settle whether there are differing mechanisms underlying HHT.

The goal of generating the HHT murine models and understanding the physiological and pathological signal transduction in the endothelium is to ultimately create and test therapeutic treatments for patients. Although, the current models provided some interesting insight into the *in vivo* mechanisms of the different TGF-β receptors in ECs and potential mechanisms in AVM formation, the *Eng* cKO studies seem to raise even more questions. For example, do the disparate mechanisms of HHT1 and HHT2 (or even HHT3, HHT4, and JP-HHT when more information arises) conclude that the various types of HHT must be approached or treated separately in the clinical setting? One way to decipher this is to perform a microarray analysis of different tissues taken from each *Eng* cKO model and compare the gene expression profile derived from the *Alk1* cKO models, such as those we previously accumulated from lung samples. As the finding from Chapter 4 suggests it may be essential to evaluate each

organ separately as there are time- and organ-specific expression of different TGF-β signaling members during angiogenesis. Additionally, there are potential organ-specific molecules, such as the orphan GPR124, that should be given more attention because they may contribute to vascular malformations.

The differences in response to chronic and acute injuries between the *Alk1* iKO and *Eng* iKO were an interesting finding. As *Eng* iKO mice constantly developed AVMs because of the ear ID tag, it may be possible that AVMs in the *Eng* deficient vessels may be a response to the recruitment of inflammatory cytokines, such as tumor necrosis factor-α (TNF-α), to the irritated site. There is previous evidence that inducing inflammation in $Eng^{+/-}$, for example by dextran sulfate, lead to aberrant angiogenesis. A future study in the *Eng* iKO mice would be to infuse a nanoparticle with TNF-α and embed the infused nanoparticle into the dorsal skin of the mouse. The potential formation of AVMs to the nanoparticle would be observed.

In conclusion, we generated several cKO models that provided interesting *in vivo* insight into TGF-β signaling in ECs. Though the phenotype severity varied in the *Eng* iKO, the appearance of vascular malformations was consistent, making it a valuable tool in studying HHT. Additionally, the *Tgfbr2* and *Alk5* cKO models indicated TGF-β signaling have essential spatial and temporal roles in angiogenesis. Finally, a novel transgenic $Alk1^{GFPCre}$ was introduced and has proven to be an effective and useful line to study and evaluate the specific functions of angiogenic molecules at midgestation. Overall, our mouse models produced more consistent phenotypes than currently available mouse models and will be vital to future studies in HHT.

Table 5-1. Comparison of *Eng* vs *Alk1* cKO mouse models

cKO Genotype	Lethality	Time of visible phenotype	Affected organs
L1cre(+);*Eng*$^{2f/2f}$	Survived	Aged 15-months	GI tract Liver
1) L1cre(+);*Alk1*$^{2f/2f}$ 2) L1cre(+);*Alk1*$^{3f/3f}$	1) PN5 2) E17.5	E15.5	Lung GI tract Liver Brain
R26-Cre$^{ER(+)}$;*Eng*$^{2f/2f}$ +TM (5 treatments): 1) 2.5 mg/25 g BW x 1 2) 2.5 mg/25 g BW x 2 3) 2.5 mg/25 g BW x 3 4) 2.5 mg/40 g BW x 2 5) 2.5 mg/40 g BW x 3	[Time after TM given] 1) Survived 2) 10 days 3) 10 days 4) ¼ at 3 wks, variable 5) ¼ at 3 wks, variable	1) 2 months 2) 4 days 3) 4 days 4) 4 days 5) 4 days *	Ear (ID-tag) GI tract ♀: ovarian vessels Liver
1) R26-Cre$^{ER(+)}$; *Alk1*$^{2f/2f}$ 2) R26-Cre$^{ER(+)}$; *Alk1*$^{3f/3f}$ + 2.5 mg TM/25 g BW x1	By 21 days	7 days	Lungs GI tract ♀: uterine vessels Liver (*Alk1*$^{3f/3f}$ iKO) Acute wound Ear Dorsal skin

Table 5-2. Summary of *Alk5* and *Tgfbr2* cKO models

cKO Genotype	Lethality	Time of visible phenotype	Affected organs
Alk1^{GFPCre};*Tgfbr2*$^{fl/fl}$	E14.5	E11.5	Brain (edemic), Ganglionic eminence Diencephalon Telencephalon Spine (variable)
Alk1^{GFPCre};*Alk5*$^{fl/fl}$	E13.5	E11	Forebrain, Ganglionic eminence Spine (variable) Heart

LIST OF REFERENCES

1. Aird WC. Phenotypic heterogeneity of the endothelium: I. Structure, function, and mechanisms. *Circ Res.* 2007;100(2):158-73.

2. Jain RK. Molecular regulation of vessel maturation*. Nat Med*. 2003;9(6):685-93.

3. Rocha, SF, Adams RH. Molecular differentiation and specialization of vascular beds. *Angiogenesis.* 2009*;12(2):139-47.*

4. Flamme I, Frolich T, Risau W. Molecular mechanisms of vasculogenesis and embryonic angiogenesis. *J Cell Physiol*. 1997;173(2):206-10.

5. Risau W, Flamme I. Vasculogenesis*. Annu Rev Cell Dev Biol* 1995;11:73-91.

6. Hirashima M, Suda T. Differentiation of arterial and venous endothelial cells and vascular morphogenesis*. Endothelium*. 2006;13(2):137-45.

7. LaRue AC, Lansford R, Drake C.J. Circulating blood island-derived cells contribute to vasculogenesis in the embryo proper*. Dev Biol*. 2003;262(1):162-72.

8. Kovacic JC, Moore J, Herbert A, Ma D, Boehm M, Graham RM. Endothelial progenitor cells, angioblasts, and angiogenesis--old terms reconsidered from a current perspective*. Trends Cardiovasc Med*. 2008;18(2):45-51.

9. Risau W. Mechanisms of angiogenesis*. Nature*. 1997;386(6626):671-4.

10. Drake CJ. Embryonic and adult vasculogenesis*. Birth Defects Res C Embryo Today*. 2003;69(1):73-82.

11. Baldwin HS. Early embryonic vascular development*. Cardiovasc Res*. 1996;31 Spec No:E34-45.

12. Aird WC. Endothelium in health and disease*. Pharmacol Rep*. 2008;60(1):139-43.

13. Adams RH, Alitalo K. Molecular regulation of angiogenesis and lymphangiogenesis. *Nat Rev Mol Cell Biol*. 2007;8(6):464-78.

14. Adams RH. Molecular control of arterial-venous blood vessel identity*. J Anat*. 2003;202(1):105-12.

15. Buschmann I, Schaper W. Arteriogenesis Versus Angiogenesis: Two Mechanisms of Vessel Growth*. News Physiol Sci.* 1999;14:121-125.

16. Cai W, Schaper W. Mechanisms of arteriogenesis*. Acta Biochim Biophys Sin (Shanghai)*. 2008;40(8):681-92.

17. Boon LM, Ballieux F, Vikkula M. Pathogenesis of vascular anomalies. *Clin Plast Surg*. 2011;38(1):7-19.

18. Brouillard P, Vikkula M. Vascular malformations: localized defects in vascular morphogenesis. *Clin Genet*. 2003;63(5):340-51.

19. Brouillard P, Vikkula M. Genetic causes of vascular malformations. *Hum Mol Genet*. 2007;16 Spec No. 2:R140-9.

20. Marchuk DA, Srinivasan S, Squire TL, Zawistowski JS. Vascular morphogenesis: tales of two syndromes. *Hum Mol Genet*. 2003;12 Spec No 1:R97-112.

21. Cleaver O, Melton DA. Endothelial signaling during development. *Nat Med*. 2003;9(6):661-8.

22. Adams RH, Wilkinson GA, Weiss C, Diella F, Gale NW, Deutsch U, Risau W, Klein R. Roles of ephrinB ligands and EphB receptors in cardiovascular development: demarcation of arterial/venous domains, vascular morphogenesis, and sprouting angiogenesis. *Genes Dev*. 1999;13(3):295-306.

23. Aird WC. Phenotypic heterogeneity of the endothelium: II. Representative vascular beds. *Circ Res*, 2007;100(2):174-90.

24. Pardali E, Goumans MJ, ten Dijke P. Signaling by members of the TGF-beta family in vascular morphogenesis and disease. *Trends Cell Biol*. 2010;20(9):556-67.

25. Breier G, Risau W. *T*he role of vascular endothelial growth factor in blood vessel formation. *Trends Cell Biol*. 1996;6(12):454-6.

26. Sato TN, Tozawa Y, Deutsch U, Wolburg-Buchholz K, Fujiwara Y, Gendron-Maguire M, Gridley T, Wolburg H, Risau W, Qin Y. Distinct roles of the receptor tyrosine kinases Tie-1 and Tie-2 in blood vessel formation. *Nature*. 1995;376(6535):70-4.

27. Augustin HG, Koh GY, Thurston G, Alitalo K. Control of vascular morphogenesis and homeostasis through the angiopoietin-Tie system. *Nat Rev Mol Cell Biol*. 2009;10(3):165-77.

28. Carmeliet P, Ferreira V, Breier G, Pollefeyt S, Kieckens L, Gertsenstein M, Fahrig M, Vandenhoeck A, Harpal K, Eberhardt C, Declercq C, Pawling J, Moons L, Collen D, Risau W, Nagy A. Abnormal blood vessel development and lethality in embryos lacking a single VEGF allele. *Nature*. 1996;380(6573):435-9.

29. Hofmann JJ, Iruela-Arispe ML. Notch signaling in blood vessels: who is talking to whom about what? *Circ Res*. 2007;100(11):1556-68.

30. Rossant J, Howard L. Signaling pathways in vascular development. *Annu Rev Cell Dev Biol*. 2002;18:541-73.

31. Moustakas A, Heldin CH. The regulation of TGFbeta signal transduction. *Development*. 2009;136(22):3699-714.

32. Zhu HJ, Burgess AW. Regulation of transforming growth factor-beta signaling. *Mol Cell Biol Res Commun*. 2001;4(6):321-30.

33. Shi Y, Massague J. Mechanisms of TGF-beta signaling from cell membrane to the nucleus. *Cell*. 2003;113(6):685-700.

34. Bobik A. Transforming growth factor-betas and vascular disorders. *Arterioscler Thromb Vasc Biol*. 2006;26(8):1712-20.

35. Derynck R, Feng XH. TGF-beta receptor signaling. *Biochim Biophys Acta*. 1997;1333(2):F105-50.

36. ten Dijke P, Hill CS. New insights into TGF-beta-Smad signalling. *Trends Biochem Sci*. 2004;29(5):265-73.

37. Massague J. The TGF-beta family of growth and differentiation factors. *Cell*.1987;49(4):437-8.

38. Wrana JL, Attisano L, Cárcamo J, Zentella A, Doody J, Laiho M, Wang XF, Massagué J. TGF beta signals through a heteromeric protein kinase receptor complex. *Cell*. 1992;71(6):1003-14.

39. Persson U. Izumi H, Souchelnytskyi S, Itoh S, Grimsby S, Engström U, Heldin CH, Funa K, ten Dijke P. The L45 loop in type I receptors for TGF-beta family members is a critical determinant in specifying Smad isoform activation. *FEBS Lett*. 1998;434(1-2):83-7.

40. Walshe TE. TGF-beta and microvessel homeostasis. *Microvasc Res*. 2010;80(1):166-73.

41. Gatza CE, Oh SY, Blobe GC. Roles for the type III TGF-beta receptor in human cancer. *Cell Signal.* 2010;22(8):1163-74.

42. Bernabeu C, Lopez-Novoa JM, Quintanilla M. The emerging role of TGF-beta superfamily coreceptors in cancer. *Biochim Biophys Acta*. 2009;1792(10):954-73.

43. Jovine L, Qi H, Williams Z, Litscher E, Wassarman PM. The ZP domain is a conserved module for polymerization of extracellular proteins. *Nat Cell Biol*. 2002;4(6):457-61.

44. Barbara NP, Wrana JL, Letarte M. Endoglin is an accessory protein that interacts with the signaling receptor complex of multiple members of the transforming growth factor-beta superfamily. *J Biol Chem*. 1999;274(2):584-94.

45. Lin H, Wang H, Zhu C. The Smad pathway in transforming growth factor-beta signaling. *Sci China C Life Sci*. 2003;46(5):449-63.

46. Feng XH, Derynck R. Specificity and versatility in tgf-beta signaling through Smads. *Annu Rev Cell Dev Biol*. 2005;21:659-93.

47. Moustakas A, Heldin CH. From mono- to oligo-Smads: the heart of the matter in TGF-beta signal transduction. *Genes Dev*. 2002;16(15):1867-71.

48. Itoh S, ten Dijke P. Negative regulation of TGF-beta receptor/Smad signal transduction. *Curr Opin Cell Biol*. 2007;19(2):176-84.

49. Zhang YE. Non-Smad pathways in TGF-beta signaling. *Cell Res*. 2009;19(1):128-39.

50. Lowery JW, de Caestecker MP. BMP signaling in vascular development and disease. *Cytokine Growth Factor Rev*. 2010;21(4):287-98.

51. Judge DP, Dietz HC. Marfan's syndrome. *Lancet*. 2005;366(9501):1965-76.

52. Loeys BL, Chen J, Neptune ER, Judge DP, Podowski M, Holm T, Meyers J, Leitch CC, Katsanis N, Sharifi N, Xu FL, Myers LA, Spevak PJ, Cameron DE, De Backer J, Hellemans J, Chen Y, Davis EC, Webb CL, Kress W, Coucke P, Rifkin DB, De Paepe AM, Dietz HC. A syndrome of altered cardiovascular, craniofacial, neurocognitive and skeletal development caused by mutations in TGFBR1 or TGFBR2. *Nat Genet*. 2005;37(3):275-81.

53. Dickson MC, Martin JS, Cousins FM, Kulkarni AB, Karlsson S, Akhurst RJ. Defective haematopoiesis and vasculogenesis in transforming growth factor-beta 1 knock out mice. *Development.* 1995;121(6):1845-54.

54. Martin JS, Dickson MC, Cousins FM, Kulkarni AB, Karlsson S, Akhurst RJ. Analysis of homozygous TGF beta 1 null mouse embryos demonstrates defects in yolk sac vasculogenesis and hematopoiesis. *Ann N Y Acad Sci*. 1995;752:300-8.

55. Larsson J, Goumans MJ, Sjöstrand LJ, van Rooijen MA, Ward D, Levéen P, Xu X, ten Dijke P, Mummery CL, Karlsson S. Abnormal angiogenesis but intact hematopoietic potential in TGF-beta type I receptor-deficient mice. *EMBO J*. 2001;20(7):1663-73.

56. Li DY, Sorensen LK, Brooke BS, Urness LD, Davis EC, Taylor DG, Boak BB, Wendel DP. Defective angiogenesis in mice lacking endoglin. *Science*. 1999;284(5419):1534-7.

57. Bourdeau A, Dumont DJ, Letarte M. A murine model of hereditary hemorrhagic telangiectasia. *J Clin Invest*. 1999;104(10):1343-51.

58. Oshima M, Oshima H, Taketo MM. TGF-beta receptor type II deficiency results in defects of yolk sac hematopoiesis and vasculogenesis. *Dev Biol*. 1996;179(1):297-302.

59. Chang H, Huylebroeck D, Verschueren K, Guo Q, Matzuk MM, Zwijsen A. Smad5 knockout mice die at mid-gestation due to multiple embryonic and extraembryonic defects. *Development*. 1999;126(8):1631-42.

60. Goumans MJ, Valdimarsdottir G, Itoh S, Rosendahl A, Sideras P, ten Dijke P. Balancing the activation state of the endothelium via two distinct TGF-beta type I receptors. *EMBO J*. 2002;21(7):1743-53.

61. Goumans MJ, Valdimarsdottir G, Itoh S, Lebrin F, Larsson J, Mummery C, Karlsson S, ten Dijke P. Activin receptor-like kinase (ALK)1 is an antagonistic mediator of lateral TGFbeta/ALK5 signaling. *Mol Cell*. 2003;12(4):817-28.

62. Lamouille S, Mallet C, Feige JJ, Bailly S. Activin receptor-like kinase 1 is implicated in the maturation phase of angiogenesis. *Blood*. 2002;100(13):4495-501.

63. Seki T, Hong KH, Oh SP. Nonoverlapping expression patterns of ALK1 and ALK5 reveal distinct roles of each receptor in vascular development. *Lab Invest*. 2006;86(2):116-29.

64. Park SO, Lee YJ, Seki T, Hong KH, Fliess N, Jiang Z, Park A, Wu X, Kaartinen V, Roman BL, Oh SP. ALK5- and TGFBR2-independent role of ALK1 in the pathogenesis of hereditary hemorrhagic telangiectasia type 2. *Blood*. 2008;111(2):633-42.

65. Scharpfenecker M, van Dinther M, Liu Z, van Bezooijen RL, Zhao Q, Pukac L, Löwik CW, ten Dijke P. BMP-9 signals via ALK1 and inhibits bFGF-induced endothelial cell proliferation and VEGF-stimulated angiogenesis. *J Cell Sci*. 2007;120(Pt 6):964-72.

66. David L, Mallet C, Mazerbourg S, Feige JJ, Bailly S. Identification of BMP9 and BMP10 as functional activators of the orphan activin receptor-like kinase 1 (ALK1) in endothelial cells. *Blood*. 2007;109(5):1953-61.

67. Luo J, Tang M, Huang J, He BC, Gao JL, Chen L, Zuo GW, Zhang W, Luo Q, Shi Q, Zhang BQ, Bi Y, Luo X, Jiang W, Su Y, Shen J, Kim SH, Huang E, Gao Y, Zhou JZ, Yang K, Luu HH, Pan X, Haydon RC, Deng ZL, He TC. TGFbeta/BMP type I receptors ALK1 and ALK2 are essential for BMP9-induced osteogenic signaling in mesenchymal stem cells. *J Biol Chem*. 2010;285(38):29588-98.

68. Daina E, D'Ovidio F, Sabba C. Introduction: hereditary hemorrhagic telangiectasia as a rare disease. *Curr Pharm Des*. 2006;12(10):1171-2.

69. Sabba C, Pasculli G, Cirulli A, Gallitelli M, Virgilio G, Resta F, Guastamacchia E, Palasciano G. Hereditary hemorrhagic teleangiectasia (Rendu-Osler-Weber disease). *Minerva Cardioangiol*. 2002;50(3):221-38.

70. Geisthoff UW, Hille K, Ruprecht KW, Verse T, Plinkert PK. Prevalence of ocular manifestations in hereditary hemorrhagic telangiectasia. *Graefes Arch Clin Exp Ophthalmol*. 2007;245(8):1141-4.

71. Lenato GM, Guanti G. Hereditary Haemorrhagic Telangiectasia (HHT): genetic and molecular aspects. *Curr Pharm Des*. 2006;12(10):1173-93.

72. Shovlin CL. Hereditary haemorrhagic telangiectasia: pathophysiology, diagnosis and treatment. *Blood Rev*. 2010;24(6):203-19.

73. McAllister KA, Grogg KM, Johnson DW, Gallione CJ, Baldwin MA, Jackson CE, Helmbold EA, Markel DS, McKinnon WC, Murrell J, et al. Endoglin, a TGF-beta binding protein of endothelial cells, is the gene for hereditary haemorrhagic telangiectasia type 1. *Nat Genet*. 1994;8(4):345-51.

74. Shovlin CL, Hughes JM, Tuddenham EG, Temperley I, Perembelon YF, Scott J, Seidman CE, Seidman JG. A gene for hereditary haemorrhagic telangiectasia maps to chromosome 9q3. *Nat Genet*. 1994;6(2):205-9.

75. Gallione CJ, Repetto GM, Legius E, Rustgi AK, Schelley SL, Tejpar S, Mitchell G, Drouin E, Westermann CJ, Marchuk DA. A combined syndrome of juvenile polyposis and hereditary haemorrhagic telangiectasia associated with mutations in MADH4 (SMAD4). *Lancet*. 2004;363(9412):852-9.

76. Gallione C, Aylsworth AS, Beis J, Berk T, Bernhardt B, Clark RD, Clericuzio C, Danesino C, Drautz J, Fahl J, Fan Z, Faughnan ME, Ganguly A, Garvie J, Henderson K, Kini U, Leedom T, Ludman M, Lux A, Maisenbacher M, Mazzucco S, Olivieri C, Ploos van Amstel JK, Prigoda-Lee N, Pyeritz RE, Reardon W, Vandezande K, Waldman JD, White RI Jr, Williams CA, Marchuk DA. Overlapping spectra of SMAD4 mutations in juvenile polyposis (JP) and JP-HHT syndrome. Am J Med Genet A. 2010 Feb;152A(2):333-9.

77. Cole SG, Begbie ME, Wallace GM, Shovlin CL. A new locus for hereditary haemorrhagic telangiectasia (HHT3) maps to chromosome 5. *J Med Genet*. 2005;42(7):577-82.

78. Bayrak-Toydemir P, McDonald J, Akarsu N, Toydemir RM, Calderon F, Tuncali T, Tang W, Miller F, Mao R. A fourth locus for hereditary hemorrhagic telangiectasia maps to chromosome 7. *Am J Med Genet A*. 2006;140(20):2155-62.

79. Govani FS, Shovlin CL. Fine mapping of the hereditary haemorrhagic telangiectasia (HHT)3 locus on chromosome 5 excludes VE-Cadherin-2, Sprouty4 and other interval genes. *J Angiogenes Res*. 2010;2:15.

80. Pece-Barbara N, Cymerman U, Vera S, Marchuk DA, Letarte M. Expression analysis of four endoglin missense mutations suggests that haploinsufficiency is the predominant mechanism for hereditary hemorrhagic telangiectasia type 1. *Hum Mol Genet*. 1999;8(12):2171-81.

81. Pece N, Vera S, Cymerman U, White RI Jr, Wrana JL, Letarte M. Mutant endoglin in hereditary hemorrhagic telangiectasia type 1 is transiently expressed intracellularly and is not a dominant negative. *J Clin Invest*. 1997;100(10):2568-79.

82. Hoag JB, Terry P, Mitchell S, Reh D, Merlo CA. An epistaxis severity score for hereditary hemorrhagic telangiectasia. *Laryngoscope*. 2010;120(4):838-43.

83. Braverman IM, Keh A, Jacobson BS. Ultrastructure and three-dimensional organization of the telangiectases of hereditary hemorrhagic telangiectasia. *J Invest Dermatol*. 1990;95(4):422-7.

84. Pasculli G, Resta F, Guastamacchia E, Di Gennaro L, Suppressa P, Sabbà C. Health-related quality of life in a rare disease: hereditary hemorrhagic telangiectasia (HHT) or Rendu-Osler-Weber disease. *Qual Life Res*. 2004;13(10):1715-23.

85. Jacobson BS. Hereditary hemorrhagic telangiectasia: A model for blood vessel growth and enlargement. *Am J Pathol*. 2000;156(3):737-42.

86. Faughnan ME, Palda VA, Garcia-Tsao G, Geisthoff UW, McDonald J, Proctor DD, Spears J, Brown DH, Buscarini E, Chesnutt MS, Cottin V, et al. International guidelines for the diagnosis and management of hereditary haemorrhagic telangiectasia. *J Med Genet*. 2011;48(2):73-87. Epub 2009.

87. Brady AP, Murphy MM, O'Connor TM. Hereditary haemorrhagic telangiectasia: a cause of preventable morbidity and mortality. *Ir J Med Sci*. 2009;178(2):135-46.

88. Sabba C, Pompili M. Review article: the hepatic manifestations of hereditary haemorrhagic telangiectasia. *Aliment Pharmacol Ther*. 2008;28(5):523-33.

89. Dupuis-Girod S, Chesnais AL, Ginon I, Dumortier J, Saurin JC, Finet G, Decullier E, Marion D, Plauchu H, Boillot O. Long-term outcome of patients with hereditary hemorrhagic telangiectasia and severe hepatic involvement after orthotopic liver transplantation: a single-center study. *Liver Transpl*. 2010;16(3):340-7.

90. Abdalla SA, Gallione CJ, Barst RJ, Horn EM, Knowles JA, Marchuk DA, Letarte M, Morse JH. Primary pulmonary hypertension in families with hereditary haemorrhagic telangiectasia. *Eur Respir J*. 2004;23(3):373-7.

91. Stringham R, Shah NR. Pulmonary arterial hypertension: an update on diagnosis and treatment. *Am Fam Physician*. 2010;82(4):370-7.

92. Girerd B, Montani D, Coulet F, Sztrymf B, Yaici A, Jaïs X, Tregouet D, Reis A, Drouin-Garraud V, Fraisse A, Sitbon O, O'Callaghan DS, Simonneau G, Soubrier F, Humbert M. Clinical outcomes of pulmonary arterial hypertension in patients carrying an ACVRL1 (ALK1) mutation. *Am J Respir Crit Care Med*. 2010;181(8):851-61.

93. Chen ST, Karnezis T, Davidson TM. Safety of intranasal Bevacizumab (avastin) treatment in patients with hereditary hemorrhagic telangiectasia-associated epistaxis. *Laryngoscope*. 2010 Nov 11. [Epub ahead of print]

94. Davidson TM, Olitsky SE, Wei JL. Hereditary hemorrhagic telangiectasia/avastin. *Laryngoscope*. 2010;120(2):432-5.

95. Lebrin F, Srun S, Raymond K, Martin S, van den Brink S, Freitas C, Bréant C, Mathivet T, Larrivée B, Thomas JL, Arthur HM, Westermann CJ, Disch F, Mager JJ, Snijder RJ, Eichmann A, Mummery CL. Thalidomide stimulates vessel maturation and reduces epistaxis in individuals with hereditary hemorrhagic telangiectasia. *Nat Med.* 2010;16(4):420-8.

96. Fernandez-L A, Garrido-Martin EM, Sanz-Rodriguez F, Ramirez JR, Morales-Angulo C, Zarrabeitia R, Perez-Molino A, Bernabéu C, Botella LM. Therapeutic action of tranexamic acid in hereditary haemorrhagic telangiectasia (HHT): regulation of ALK-1/endoglin pathway in endothelial cells. *Thromb Haemost*. 2007;97(2):254-62.

97. Jameson JJ, Cave DR. Hormonal and antihormonal therapy for epistaxis in hereditary hemorrhagic telangiectasia. *Laryngoscope*. 2004;114(4):705-9.

98. Gluckman JL, Portugal LG. Modified Young's procedure for refractory epistaxis due to hereditary hemorrhagic telangiectasia. *Laryngoscope*. 1994;104(9):1174-7.

99. Illum P, Bjerring P. Hereditary hemorrhagic telangiectasia treated by laser surgery. *Rhinology*. 1988;26(1):19-24.

100. Geisthoff UW, Fiorella ML, Fiorella R. Treatment of recurrent epistaxis in HHT. *Curr Pharm Des*. 2006;12(10):1237-42.

101. Velasco B, Ramírez JR, Relloso M, Li C, Kumar S, Lopez-Bote JP, Pérez-Barriocanal F, López-Novoa JM, Cowan PJ, d'Apice AJ, Bernabéu C. Vascular gene transfer driven by endoglin and ICAM-2 endothelial-specific promoters. *Gene Ther*. 2001;8(12):897-904.

102. Fernandez-L A, Sanz-Rodriguez F, Zarrabeitia R, Pérez-Molino A, Hebbel RP, Nguyen J, Bernabéu C, Botella LM. Blood outgrowth endothelial cells from Hereditary Haemorrhagic Telangiectasia patients reveal abnormalities compatible with vascular lesions. *Cardiovasc Res*. 2005;68(2):235-48.

103. Allinson KR, Carvalho RL, van den Brink S, Mummery CL, Arthur HM. Generation of a floxed allele of the mouse Endoglin gene. *Genesis*. 2007;45(6):391-5.

104. Chytil A, Magnuson MA, Wright CV, Moses HL. Conditional inactivation of the TGF-beta type II receptor using Cre:Lox. *Genesis*. 2002;32(2):73-5.

105. Johnson DW, Berg JN, Baldwin MA, Gallione CJ, Marondel I, Yoon SJ, Stenzel TT, Speer M, Pericak-Vance MA, Diamond A, Guttmacher AE, Jackson CE, Attisano L, Kucherlapati R, Porteous ME, Marchuk DA. Mutations in the activin receptor-like kinase 1 gene in hereditary haemorrhagic telangiectasia type 2. *Nat Genet.* 1996;13(2):189-95.

106. Lesca G, Genin E, Blachier C, Olivieri C, Coulet F, Brunet G, Dupuis-Girod S, Buscarini E, Soubrier F, Calender A, Danesino C, Giraud S, Plauchu H; French-Italian HHT Network. Hereditary hemorrhagic telangiectasia: evidence for regional founder effects of ACVRL1 mutations in French and Italian patients. *Eur J Hum Genet*. 2008;16(6):742-9.

107. Olivieri C, Pagella F, Semino L, Lanzarini L, Valacca C, Pilotto A, Corno S, Scappaticci S, Manfredi G, Buscarini E, Danesino C. Analysis of ENG and ACVRL1 genes in 137 HHT Italian families identifies 76 different mutations (24 novel). Comparison with other European studies. *J Hum Genet*. 2007;52(10):820-9.

108. Sadick H, Hage J, Goessler U, Stern-Straeter J, Riedel F, Hoermann K, Bugert P. Mutation analysis of "Endoglin" and "Activin receptor-like kinase" genes in German patients with hereditary hemorrhagic telangiectasia and the value of rapid genotyping using an allele-specific PCR-technique. *BMC Med Genet*. 2009;10:53.

109. Fernandez LA, Sanz-Rodriguez F, Zarrabeitia R, Perez-Molino A, Morales C, Restrepo CM, Ramirez JR, Coto E, Lenato GM, Bernabeu C, Botella LM. Mutation study of Spanish patients with hereditary hemorrhagic telangiectasia and expression analysis of Endoglin and ALK1. *Hum Mutat*. 2006;27(3):295.

110. Bayrak-Toydemir P, McDonald J, Markewitz B, Lewin S, Miller F, Chou LS, Gedge F, Tang W, Coon H, Mao R. Genotype-phenotype correlation in hereditary hemorrhagic telangiectasia: mutations and manifestations. *Am J Med Genet A*. 2006;140(5):463-70.

111. Thomas B, Eyries M, Montagne K, Martin S, Agrapart M, Simerman-François R, Letarte M, Soubrier F. Altered endothelial gene expression associated with hereditary haemorrhagic telangiectasia. *Eur J Clin Invest*. 2007;37(7):580-8.

112. Seki T, Yun J, Oh SP. Arterial endothelium-specific activin receptor-like kinase 1 expression suggests its role in arterialization and vascular remodeling. *Circ Res*. 2003;93(7):682-9.

113. Fernandez-Ruiz E, St-Jacques S, Bellón T, Letarte M, Bernabéu C. Assignment of the human endoglin gene (END) to 9q34-->qter. *Cytogenet Cell Genet*. 1993;64(3-4):204-7.

114. Qureshi ST, Gros P, Letarte M, Malo D. The murine endoglin gene (Eng) maps to chromosome 2. *Genomics*. 1995;26(1):165-6.

115. Bernabeu C, Conley BA, Vary CP. Novel biochemical pathways of endoglin in vascular cell physiology. J *Cell Biochem*. 2007;102(6):1375-88.

116. Koleva RI, Conley BA, Romero D, Riley KS, Marto JA, Lux A, Vary CP. Endoglin structure and function: Determinants of endoglin phosphorylation by transforming growth factor-beta receptors. *J Biol Chem*. 2006;281(35):25110-23.

117. Gougos A, Letarte M. Primary structure of endoglin, an RGD-containing glycoprotein of human endothelial cells. *J Biol Chem*. 1990;265(15):8361-4.

118. Bellon T, Corbí A, Lastres P, Calés C, Cebrián M, Vera S, Cheifetz S, Massague J, Letarte M, Bernabéu C. Identification and expression of two forms of the human transforming growth factor-beta-binding protein endoglin with distinct cytoplasmic regions. *Eur J Immunol*. 1993;23(9):2340-5.

119. ten Dijke P, Goumans MJ, Pardali E. Endoglin in angiogenesis and vascular diseases. *Angiogenesis*. 2008;11(1):79-89.

120. Buhring HJ, Müller CA, Letarte M, Gougos A, Saalmüller A, van Agthoven AJ, Busch FW. Endoglin is expressed on a subpopulation of immature erythroid cells of normal human bone marrow. *Leukemia*. 1991;5(10):841-7.

121. Gougos A, St Jacques S, Greaves A, O'Connell PJ, d'Apice AJ, Bühring HJ, Bernabeu C, van Mourik JA, Letarte M. Identification of distinct epitopes of endoglin, an RGD-containing glycoprotein of endothelial cells, leukemic cells, and syncytiotrophoblasts. *Int Immunol*. 1992;4(1):83-92.

122. Rokhlin OW, Cohen MB, Kubagawa H, Letarte M, Cooper MD. Differential expression of endoglin on fetal and adult hematopoietic cells in human bone marrow. *J Immunol*. 1995;154(9):4456-65.

123. Jonker L, Arthur HM. Endoglin expression in early development is associated with vasculogenesis and angiogenesis. *Mech Dev*. 2002;110(1-2):193-6.

124. Ma X, Labinaz M, Goldstein J, Miller H, Keon WJ, Letarte M, O'Brien E. Endoglin is overexpressed after arterial injury and is required for transforming growth factor-beta-induced inhibition of smooth muscle cell migration. *Arterioscler Thromb Vasc Biol*. 2000;20(12):2546-52.

125. Piao M, Tokunaga O. Significant expression of endoglin (CD105), TGFbeta-1 and TGFbeta R-2 in the atherosclerotic aorta: an immunohistological study. *J Atheroscler Thromb*. 2006;13(2):82-9.

126. Torsney E, Charlton R, Parums D, Collis M, Arthur HM. Inducible expression of human endoglin during inflammation and wound healing in vivo. *Inflamm Res*. 2002;51(9):464-70.

127. Velasco S, Alvarez-Muñoz P, Pericacho M, Dijke PT, Bernabéu C, López-Novoa JM, Rodríguez-Barbero A. L- and S-endoglin differentially modulate TGFbeta1 signaling mediated by ALK1 and ALK5 in L6E9 myoblasts. *J Cell Sci*. 2008;121(Pt 6):913-9.

128. Blanco FJ, Grande MT, Langa C, Oujo B, Velasco S, Rodriguez-Barbero A, Perez-Gomez E, Quintanilla M, López-Novoa JM, Bernabeu C. S-endoglin expression is induced in senescent endothelial cells and contributes to vascular pathology. *Circ Res*. 2008;103(12):1383-92.

129. Perez-Gomez E, Eleno N, López-Novoa JM, Ramirez JR, Velasco B, Letarte M, Bernabéu C, Quintanilla M. Characterization of murine S-endoglin isoform and its effects on tumor development. *Oncogene*. 2005;24(27):4450-61.

130. Stepan H, Geipel A, Schwarz F, Krämer T, Wessel N, Faber R. Circulatory soluble endoglin and its predictive value for preeclampsia in second-trimester pregnancies with abnormal uterine perfusion. *Am J Obstet Gynecol*. 2008;198(2):175 e1-6.

131. Young BC, Levine RJ, Karumanchi SA. Pathogenesis of preeclampsia. *Annu Rev Pathol*. 2010;5:173-92.

132. Hladunewich M, Karumanchi SA, Lafayette R. Pathophysiology of the clinical manifestations of preeclampsia. *Clin J Am Soc Nephrol*. 2007;2(3):543-9.

133. Grill S, Rusterholz C, Zanetti-Dällenbach R, Tercanli S, Holzgreve W, Hahn S, Lapaire O. Potential markers of preeclampsia--a review. *Reprod Biol Endocrinol*. 2009;7:70.

134. Luft FC. Soluble endoglin (sEng) joins the soluble fms-like tyrosine kinase (sFlt) receptor as a pre-eclampsia molecule. *Nephrol Dial Transplant*. 2006;21(11):3052-4.

135. Levine RJ, Lam C, Qian C, Yu KF, Maynard SE, Sachs BP, Sibai BM, Epstein FH, Romero R, Thadhani R, Karumanchi SA; CPEP Study Group. Soluble endoglin and other circulating antiangiogenic factors in preeclampsia. *N Engl J Med*. 2006;355(10):992-1005.

136. Salahuddin S, Lee Y, Vadnais M, Sachs BP, Karumanchi SA, Lim KH. Diagnostic utility of soluble fms-like tyrosine kinase 1 and soluble endoglin in hypertensive diseases of pregnancy. *Am J Obstet Gynecol*. 2007;197(1):28 e1-6.

137. Lopez-Novoa JM. Soluble endoglin is an accurate predictor and a pathogenic molecule in pre-eclampsia. *Nephrol Dial Transplant*. 2007;22(3):712-4.

138. Venkatesha S, Toporsian M, Lam C, Hanai J, Mammoto T, Kim YM, Bdolah Y, Lim KH, Yuan HT, Libermann TA, Stillman IE, Roberts D, D'Amore PA, Epstein FH, Sellke FW, Romero R, Sukhatme VP, Letarte M, Karumanchi SA. Soluble endoglin contributes to the pathogenesis of preeclampsia. *Nat Med*. 2006;12(6):642-9.

139. Wipff J, Avouac J, Borderie D, Zerkak D, Lemarechal H, Kahan A, Boileau C, Allanore Y. Disturbed angiogenesis in systemic sclerosis: high levels of soluble endoglin. *Rheumatology (Oxford)*. 2008;47(7):972-5.

140. Calabro L, Fonsatti E, Bellomo G, Alonci A, Colizzi F, Sigalotti L, Altomonte M, Musolino C, Maio M. Differential levels of soluble endoglin (CD105) in myeloid malignancies. *J Cell Physiol*. 2003;194(2):171-5.

141. Lastres P, Letamendía A, Zhang H, Rius C, Almendro N, Raab U, López LA, Langa C, Fabra A, Letarte M, Bernabéu C. Endoglin modulates cellular responses to TGF-beta 1. *J Cell Biol*. 1996;133(5):1109-21.

142. Lebrin F, Goumans MJ, Jonker L, Carvalho RL, Valdimarsdottir G, Thorikay M, Mummery C, Arthur HM, ten Dijke P. Endoglin promotes endothelial cell proliferation and TGF-beta/ALK1 signal transduction. *EMBO J*. 2004;23(20):4018-28.

143. Lee NY, Ray B, How T, Blobe GC. Endoglin promotes transforming growth factor beta-mediated Smad 1/5/8 signaling and inhibits endothelial cell migration through its association with GIPC. *J Biol Chem*. 2008;283(47):32527-33.

144. Dallas NA, Samuel S, Xia L, Fan F, Gray MJ, Lim SJ, Ellis LM. Endoglin (CD105): a marker of tumor vasculature and potential target for therapy. *Clin Cancer Res*. 2008;14(7):1931-7.

145. Abdalla SA, Pece-Barbara N, Vera S, Tapia E, Paez E, Bernabeu C, Letarte M. Analysis of ALK-1 and endoglin in newborns from families with hereditary hemorrhagic telangiectasia type 2. *Hum Mol Genet*. 2000;9(8):1227-37.

146. Ota T, Fujii M, Sugizaki T, Ishii M, Miyazawa K, Aburatani H, Miyazono K. Targets of transcriptional regulation by two distinct type I receptors for transforming growth factor-beta in human umbilical vein endothelial cells. *J Cell Physiol*. 2002;193(3):299-318.

147. Abdalla SA, Letarte M. Hereditary haemorrhagic telangiectasia: current views on genetics and mechanisms of disease. *J Med Genet*. 2006;43(2):97-110.

148. Arthur HM, Ure J, Smith AJ, Renforth G, Wilson DI, Torsney E, Charlton R, Parums DV, Jowett T, Marchuk DA, Burn J, Diamond AG. Endoglin, an ancillary TGFbeta receptor, is required for extraembryonic angiogenesis and plays a key role in heart development. *Dev Biol*. 2000;217(1):42-53.

149. Perlingeiro, RC. Endoglin is required for hemangioblast and early hematopoietic development. *Development*. 2007;134(16):3041-8.

150. Mancini ML, Terzic A, Conley BA, Oxburgh LH, Nicola T, Vary CP. Endoglin plays distinct roles in vascular smooth muscle cell recruitment and regulation of arteriovenous identity during angiogenesis. *Dev Dyn*. 2009;238(10):2479-93.

151. Mahmoud M, Allinson KR, Zhai Z, Oakenfull R, Ghandi P, Adams RH, Fruttiger M, Arthur HM. Pathogenesis of arteriovenous malformations in the absence of endoglin. *Circ Res*. 2010;106(8):1425-33.

152. Fernandez LA, Sanz-Rodriguez F, Blanco FJ, Bernabéu C, Botella LM. Hereditary hemorrhagic telangiectasia, a vascular dysplasia affecting the TGF-beta signaling pathway. *Clin Med Res*. 2006;4(1):66-78.

153. Sanz-Rodriguez F, Fernandez-L A, Zarrabeitia R, Perez-Molino A, Ramírez JR, Coto E, Bernabeu C, Botella LM. Mutation analysis in Spanish patients with hereditary hemorrhagic telangiectasia: deficient endoglin up-regulation in activated monocytes. *Clin Chem*. 2004;50(11):2003-11.

154. Urness LD, Sorensen LK, Li DY. Arteriovenous malformations in mice lacking activin receptor-like kinase-1. *Nat Genet.* 2000;26(3):328-31.

155. Oh SP, Seki T, Goss KA, Imamura T, Yi Y, Donahoe PK, Li L, Miyazono K, ten Dijke P, Kim S, Li E. Activin receptor-like kinase 1 modulates transforming growth factor-beta 1 signaling in the regulation of angiogenesis. *Proc Natl Acad Sci U S A*. 2000;97(6):2626-31.

156. Roman BL, Pham VN, Lawson ND, Kulik M, Childs S, Lekven AC, Garrity DM, Moon RT, Fishman MC, Lechleider RJ, Weinstein BM. Disruption of acvrl1 increases endothelial cell number in zebrafish cranial vessels. *Development*. 2002;129(12):3009-19.

157. Sorensen LK, Brooke BS, Li DY, Urness LD. Loss of distinct arterial and venous boundaries in mice lacking endoglin, a vascular-specific TGFbeta coreceptor. *Dev Biol*. 2003;261(1):235-50.

158. Srinivasan S, Hanes MA, Dickens T, Porteous ME, Oh SP, Hale LP, Marchuk DA. A mouse model for hereditary hemorrhagic telangiectasia (HHT) type 2. *Hum Mol Genet.* 2003;12(5):473-82.

159. Bourdeau A, Faughnan ME, Letarte M. Endoglin-deficient mice, a unique model to study hereditary hemorrhagic telangiectasia. *Trends Cardiovasc Med*. 2000;10(7):279-85.

160. Bourdeau A, Faughnan ME, McDonald ML, Paterson AD, Wanless IR, Letarte M. Potential role of modifier genes influencing transforming growth factor-beta1 levels in the development of vascular defects in endoglin heterozygous mice with hereditary hemorrhagic telangiectasia. *Am J Pathol*. 2001;158(6):2011-20.

161. Seki T, Hong KH, Yun J, Kim SJ, Oh SP. Isolation of a regulatory region of activin receptor-like kinase 1 gene sufficient for arterial endothelium-specific expression. *Circ Res*. 2004;94(8):e72-7.

162. Park SO, Wankhede M, Lee YJ, Choi EJ, Fliess N, Choe SW, Oh SH, Walter G, Raizada MK, Sorg BS, Oh SP. Real-time imaging of de novo arteriovenous malformation in a mouse model of hereditary hemorrhagic telangiectasia. *J Clin Invest*. 2009;119(11):3487-96.

163. Sohal DS, Nghiem M, Crackower MA, Witt SA, Kimball TR, Tymitz KM, Penninger JM, Molkentin JD. Temporally regulated and tissue-specific gene manipulations in the adult and embryonic heart using a tamoxifen-inducible Cre protein. *Circ Res*. 2001;89(1):20-5.

164. Sabba C, Cirulli A, Rizzi R, Pasculli G, Gallitelli M, Specchia G, Liso V. Angiogenesis and hereditary hemorrhagic telangiectasia. Rendu-Osler-Weber disease. *Acta Haematol*. 2001;106(4):214-9.

165. Mahmoud M, Borthwick GM, Hislop AA, Arthur HM. Endoglin and activin receptor-like-kinase 1 are co-expressed in the distal vessels of the lung: implications for two familial vascular dysplasias, HHT and PAH. *Lab Invest*. 2009;89(1):15-25.

166. van Laake LW, van den Driesche S, Post S, Feijen A, Jansen MA, Driessens MH, Mager JJ, Snijder RJ, Westermann CJ, Doevendans PA, van Echteld CJ, ten Dijke P, Arthur HM, Goumans MJ, Lebrin F, Mummery CL. Endoglin has a crucial role in blood cell-mediated vascular repair. *Circulation*. 2006;114(21):2288-97.

167. Hao Q, Zhu Y, Su H, Shen F, Yang GY, Kim H, Young WL. VEGF Induces More Severe Cerebrovascular Dysplasia in Endoglin than in *Alk1* Mice. *Transl Stroke Res*. 2010;1(3):197-201.

168. Hao Q, Su H, Marchuk DA, Rola R, Wang Y, Liu W, Young WL, Yang GY. Increased tissue perfusion promotes capillary dysplasia in the ALK1-deficient mouse brain following VEGF stimulation. *Am J Physiol Heart Circ Physiol*. 2008;295(6):H2250-6.

169. Jerkic M, Peter M, Ardelean D, Fine M, Konerding MA, Letarte M. Dextran sulfate sodium leads to chronic colitis and pathological angiogenesis in Endoglin heterozygous mice. *Inflamm Bowel Dis*. 2010;16(11):1859-70.

170. Xu B, Wu YQ, Huey M, Arthur HM, Marchuk DA, Hashimoto T, Young WL, Yang GY. Vascular endothelial growth factor induces abnormal microvasculature in the endoglin heterozygous mouse brain. *J Cereb Blood Flow Metab*. 2004;24(2):237-44.

171. Torsney E, Charlton R, Diamond AG, Burn J, Soames JV, Arthur HM. Mouse model for hereditary hemorrhagic telangiectasia has a generalized vascular abnormality. *Circulation*. 2003;107(12):1653-7.

172. Toporsian M, Gros R, Kabir MG, Vera S, Govindaraju K, Eidelman DH, Husain M, Letarte M. A role for endoglin in coupling eNOS activity and regulating vascular tone revealed in hereditary hemorrhagic telangiectasia. *Circ Res*. 2005;96(6):684-92.

173. Vasudevan A, Bhide PG. Angiogenesis in the embryonic CNS: a new twist on an old tale. *Cell Adh Migr*. 2008;2(3):167-9.

174. Gerhardt H, Betsholtz C. How do endothelial cells orientate? *EXS*. 2005;94:3-15.

175. Cambier S, Gline S, Mu D, Collins R, Araya J, Dolganov G, Einheber S, Boudreau N, Nishimura SL. Integrin alpha(v)beta8-mediated activation of transforming growth factor-beta by perivascular astrocytes: an angiogenic control switch. *Am J Pathol*. 2005;166(6):1883-94.

176. ten Dijke P, Arthur HM. Extracellular control of TGFbeta signalling in vascular development and disease. *Nat Rev Mol Cell Biol*. 2007;8(11):857-69.

177. Leveen P, Larsson J, Ehinger M, Cilio CM, Sundler M, Sjöstrand LJ, Holmdahl R, Karlsson S. Induced disruption of the transforming growth factor beta type II receptor gene in mice causes a lethal inflammatory disorder that is transplantable. *Blood*. 2002;100(2):560-8.

178. Worthington JJ, Klementowicz JE, Travis MA. TGFbeta: a sleeping giant awoken by integrins. *Trends Biochem Sci*. 2010;36(1):47-54.

179. Hodivala-Dilke KM, Reynolds AR, Reynolds LE. Integrins in angiogenesis: multitalented molecules in a balancing act. *Cell Tissue Res*. 2003;314(1):131-44.

180. Sheppard D. Endothelial integrins and angiogenesis: not so simple anymore. *J Clin Invest*. 2002;110(7):913-4.

181. Silva R, D'Amico G, Hodivala-Dilke KM, Reynolds LE. Integrins: the keys to unlocking angiogenesis. *Arterioscler Thromb Vasc Biol*. 2008;28(10):1703-13.

182. Bader BL, Rayburn H, Crowley D, Hynes RO. Extensive vasculogenesis, angiogenesis, and organogenesis precede lethality in mice lacking all alpha v integrins. *Cell*. 1998;95(4):507-19.

183. Zhu J, Motejlek K, Wang D, Zang K, Schmidt A, Reichardt LF. beta8 integrins are required for vascular morphogenesis in mouse embryos. *Development*. 2002;129(12):2891-903.

184. Taya Y, O'Kane S, Ferguson MW. Pathogenesis of cleft palate in TGF-beta3 knockout mice. *Development*. 1999;126(17):3869-79.

185. Mu Z, Yang Z, Yu D, Zhao Z, Munger JS. TGFbeta1 and TGFbeta3 are partially redundant effectors in brain vascular morphogenesis. *Mech Dev*. 2008;125(5-6):508-16.

186. McCarty JH, Lacy-Hulbert A, Charest A, Bronson RT, Crowley D, Housman D, Savill J, Roes J, Hynes RO. Selective ablation of alphav integrins in the central nervous system leads to cerebral hemorrhage, seizures, axonal degeneration and premature death. *Development*. 2005;132(1):165-76.

187. Proctor JM, Zang K, Wang D, Wang R, Reichardt LF. Vascular development of the brain requires beta8 integrin expression in the neuroepithelium. *J Neurosci*. 2005;25(43):9940-8.

188. Li WY, Dudas M, Kaartinen V. Signaling through Tgf-beta type I receptor Alk5 is required for upper lip fusion. *Mech Dev*. 2008;125(9-10):874-82.

189. Gustafsson E, Brakebusch C, Hietanen K, Fässler R. Tie-1-directed expression of Cre recombinase in endothelial cells of embryoid bodies and transgenic mice. *J Cell Sci*. 2001;114(Pt 4):671-6.

190. Kisanuki YY, Hammer RE, Miyazaki J, Williams SC, Richardson JA, Yanagisawa M. Tie2-Cre transgenic mice: a new model for endothelial cell-lineage analysis in vivo. *Dev Biol*. 2001;230(2):230-42.

191. Sridurongrit S, Larsson J, Schwartz R, Ruiz-Lozano P, Kaartinen V. Signaling via the Tgf-beta type I receptor Alk5 in heart development. *Dev Biol*. 2008;322(1):208-18.

192. Jiao K, Langworthy M, Batts L, Brown CB, Moses HL, Baldwin HS. Tgfbeta signaling is required for atrioventricular cushion mesenchyme remodeling during in vivo cardiac development. *Development*. 2006;133(22):4585-93.

193. Robson A, Allinson KR, Anderson RH, Henderson DJ, Arthur HM. The TGFbeta type II receptor plays a critical role in the endothelial cells during cardiac development. *Dev Dyn*. 2010;239(9):2435-42.

194. Wang YQ, Sizeland A, Wang XF, Sassoon D. Restricted expression of type-II TGF beta receptor in murine embryonic development suggests a central role in tissue modeling and CNS patterning. *Mech Dev*. 1995;52(2-3):275-89.

195. Lyden D, Young AZ, Zagzag D, Yan W, Gerald W, O'Reilly R, Bader BL, Hynes RO, Zhuang Y, Manova K, Benezra R. Id1 and Id3 are required for neurogenesis, angiogenesis and vascularization of tumour xenografts. *Nature*. 1999;401(6754):670-7.

196. Dejana E, Nyqvist D. News from the brain: the GPR124 orphan receptor directs brain-specific angiogenesis. *Sci Transl Med*. 2010;2(58):58ps53.

197. Tanaka Y, Naruse I, Hongo T, Xu M, Nakahata T, Maekawa T, Ishii S. Extensive brain hemorrhage and embryonic lethality in a mouse null mutant of CREB-binding protein. *Mech Dev*. 2000;95(1-2):133-45.

198. Daneman R, Agalliu D, Zhou L, Kuhnert F, Kuo CJ, Barres BA. Wnt/beta-catenin signaling is required for CNS, but not non-CNS, angiogenesis. *Proc Natl Acad Sci U S A*. 2009;106(2):641-6.

199. Kuhnert F, Mancuso MR, Shamloo A, Wang HT, Choksi V, Florek M, Su H, Fruttiger M, Young WL, Heilshorn SC, Kuo CJ. Essential regulation of CNS angiogenesis by the orphan G protein-coupled receptor GPR124. *Science*. 2010;330(6006):985-9.

200. Johansson A, Driessens M, Aspenstrom P. The mammalian homologue of the Caenorhabditis elegans polarity protein PAR-6 is a binding partner for the Rho GTPases Cdc42 and Rac1. *J Cell Sci*. 2000;113 (Pt 18):3267-75.

201. Vasudevan A, Long JE, Crandall JE, Rubenstein JL, Bhide PG. Compartment-specific transcription factors orchestrate angiogenesis gradients in the embryonic brain. *Nat Neurosci*. 2008;11(4):429-39.

202. Simpson TI, Pratt T, Mason JO, Price DJ. Normal ventral telencephalic expression of Pax6 is required for normal development of thalamocortical axons in embryonic mice. *Neural Dev.* 2009;4:19.

BIOGRAPHICAL SKETCH

Ha-Long Nguyen, the youngest of five children, was born and raised in Clearwater, Florida. After graduating from Clearwater High School in 2001, she attended the University of Central Florida in Orlando, FL, where she majored in molecular biology and microbiology. During summer 2003, her first scientific research experience was in the laboratory of Dr. My Lien Dao at the University of South Florida, looking at the role of *Streptococcus mutans* in tooth decay. During her junior and senior years she joined the laboratory of Dr. Antonis Zervos and researched apoptotic processes in cardiovascular disease, including screening for apoptotic inhibitors from natural extracts. After receiving her Bachelor of Science in 2005, she worked for Dr. Steven Ebert and studied the role of catecholamines in cardiac development. In 2006 she entered the Interdisciplinary Program in Biomedical Sciences at the University of Florida. In spring 2007, she joined the laboratory of Dr. S. Paul Oh, where her dissertation research involved the generation and characterization of conditional knockout mouse models of different TGF-β signaling members to elucidate their roles in endothelial cells.